EXAMINATIONS INTO THE CALCIUM HYPOTHESIS OF ALZHEIMER'S DISEASE

Dustin J. Shilling

A DISSERTATION

in

Neuroscience

Presented to the Faculties of the University of Pennsylvania

in

Partial Fulfillment of the Requirements for the

Degree of Doctor of Philosophy

2013

Supervisor of Dissertation

Signature _____

Dr. J. Kevin Foskett, Professor of Physiology, Perelman School of Medicine

Graduate Group Chairperson

Signature _____

Dr. Joshua I. Gold, Associate Professor, Department of Neuroscience, Perelman School of Medicine

Dissertation Committee

Dr. Douglas Coulter (Chair), Professor of Pediatrics, Children's Hospital of Philadelphia

Dr. Steven Arnold, Professor of Psychiatry, Perelman School of Medicine

Dr. Ted Abel, Professor of Biology, School of Arts and Sciences

Dr. Frank LaFerla, Professor of Neurobiology, School of Biological Sciences

ACKNOWLEDGMENTS

My graduate career has provided an extremely rewarding learning experience, and I have many people to thank for that. To start, I would like to thank my mentor, Kevin Foskett, for his expertise, advice and guidance. His willingness to invest his time, resources, and to let me explore my interests was invaluable to my development as a scientist. For that I am extremely grateful.

I would like to thank the members of the Foskett laboratory who provided important technical training, advice, and were always willing to discuss my data. Many thanks to Marioly Muller, Adam Siebert, Daniel Mak, King-Ho Cheung, Rob Lee, Cesar Cardenas, Jung Yang, Horia Vais, Zhongming Ma, and Akiyuki Taruno.

I am extremely grateful to Ted Abel and Doug Coulter who were willing to collaborate with me on my thesis work. The expertise, training and access to experimental hardware they provided were critical in accomplishing this work. I am indebted to all those in their laboratories who were so willing to selfishness allow me to work on their rigs. Special thanks to Hajime Takano, Morgan Bridi, and Alan Park, all of whom spent an enormous amount of time providing technical support and training. I would also like to thank the University of Pennsylvania Behavioral Core, specifically Tim O'Brien for providing training in behavioral assays.

Thank you to Doug Coulter for Chairing my thesis committee and the other members, Ted Abel, Steven Arnold, Robert Neumar and Frank LaFerla. These individuals have dedicated time to support my growth as a scientist, and their comments have guided my project and allowed for its success. I would also like to thank the

Neuroscience Graduate Group and the countless faculty and staff members that contributed to my training during my graduate career. In combination their efforts have provided me with a strong foundation in neuroscience.

Lastly, I would like to thank my family and friends for their support and understanding during my time in graduate school. Their encouragement and distraction allowed me to make it through the roughest times during my training. Special thanks to Sheena Baratono for her willingness to counsel, sympathize, and celebrate with me through the ups-and-downs of graduate school.

My thesis training was supported in part by a National Institutes of Health Grant AG038240.

ABSTRACT

EXAMINATIONS INTO THE CALCIUM HYPOTHESIS OF ALZHEIMER'S DISEASE

Dustin J. Shilling

J. Kevin Foskett, Ph.D.

Alzheimer's disease (AD) is devastating to the patient, their family and friends, and represents a significant fiscal burden to our society. Currently available therapeutics provide only mild symptomatic relief and do not alter the course of the disease. Developing the next generation of disease modifying therapies requires an understanding of the early cellular changes responsible for AD. A hindrance to progress is the fact that most patients develop AD sporadically. However, mutations in the presenilin (PS) homologs cause dominantly inherited, early-onset AD. These mutations provide an important tool for understanding the cellular changes that cause AD. One consequence of PS mutations is exaggerated intracellular Ca^{2+} ($[Ca^{2+}]_i$) signaling. However, the mechanisms underlying this phenomenon remain controversial and its role in AD pathogenesis is unknown. Presented here are data indicating that exaggerated $[Ca^{2+}]_i$ signaling is dependent upon the inositol 1,4,5-trisphosphate receptor ($InsP_3R$) and contributes to AD pathogenesis *in vivo*. We began our studies by testing multiple proposed mechanisms for exaggerated $[Ca^{2+}]_i$ signaling. To do this we employed multiple Ca^{2+} imaging protocols and Ca^{2+} indicators to directly measure ER Ca^{2+} dynamics in

several cell systems. We found that decreasing $InsP_3R$ protein levels rescues exaggerated $[Ca^{2+}]_i$ signaling in primary cortical neurons and hippocampal slices from mice expressing mutant PS1. We then determined the contribution of exaggerated $[Ca^{2+}]_i$ signaling to AD pathogenesis. Using a combination of genetic, biochemical, electrophysiological and behavioral techniques, we found that rescue of exaggerated $[Ca^{2+}]_i$ signaling attenuates mild cognitive impairment and AD-like phenotypes in mouse models. Reduction of $InsP_3R1$ protein level in the PS1M146V knock-in AD mouse rescued enhanced hippocampal ryanodine receptor protein level, enhanced hippocampal synaptic potentiation, and constitutive activation of the CaMKIV-CREB transcriptional pathway. In 3xTg AD mice, reduced $InsP_3R1$ protein level attenuated Aβ and phospho-tau accumulation and hippocampal electrophysiology and memory impairments. Together, these results reveal that mutant PS-associated exaggerated $[Ca^{2+}]_i$ signaling is $InsP_3R1$-dependent, a proximal event, and contributes to the development of AD *in vivo*. These findings advance our understanding of the pathological role of exaggerated $[Ca^{2+}]_i$ signaling in AD and identify several novel targets for the development of disease modifying therapeutics.

TABLE OF CONTENTS

LIST OF FIGURES

CHAPTER 2

CHAPTER 3

Chapter 1: Introduction

The long-term goals of this project are to understand the mechanisms and contributions of exaggerated intracellular Ca^{2+} ($[Ca^{2+}]_i$) signaling to the pathogenesis of Alzheimer's disease (AD). Ca^{2+} homeostasis is disrupted by familial Alzheimer's disease (FAD) presenilin (PS) mutations and potentially influences the pathological processes of the disease. This dissertation focuses on understanding how FAD mutations in PS1 influence $[Ca^{2+}]_i$ homeostasis and how exaggerated $[Ca^{2+}]_i$ signaling influences the development of AD. Prior studies, in combination with the data presented in this dissertation, suggest that FAD mutations in PS result in a gain-of-function enhancement of inositol 1,4,5-trisphosphate receptor ($InsP_3R$) gating as the underlying mechanism of exaggerated $[Ca^{2+}]_i$ signaling, and that this dysregulation contributes to AD pathogenesis *in vivo*. These findings suggest that disruption of $InsP_3R$-mediated $[Ca^{2+}]_i$ signaling plays an important role in FAD and may contribute to the more prevalent sporadic form of Alzheimer's disease. This dissertation provides novel insights into the mechanisms by which FAD mutant PS causes AD.

Alzheimer's Disease

AD is the most common form of dementia, estimated to affect 5.4 million US citizens in 2012 and results in an estimated cost of $200 billion dollars (Alzheimer's Association, 2012). Because the largest known risk factor for developing AD is advanced age, the prevalence of the disease will increase as the average life expectancy increases. In fact, it is projected that by 2050 the number of US citizens with AD will triple to 16 million (Alzheimer's Association, 2012). AD patients are commonly cared for by family

members, so this increase in prevalence will cause a significant social burden as well as fiscal costs.

Alois Alzheimer first described AD in 1906 as a progressive neurodegenerative disease that results in death. It is characterized by specific end-stage histopathological brain lesions, which are located primarily in the hippocampus and neocortex. These lesions consist of intracellular neurofibrillary tangles (NFT), composed of hyperphosphorylated aggregates of the microtubule-associated tau protein, and extracellular plaques composed of amyloid-β (Aβ).

Although the disease affects everyone differently, there are several common symptoms. In the earliest stages of the disease, individuals demonstrate anterograde long-term episodic amnesia - impairments in recalling new facts (declarative memory) and recent events (episodic memory). These memory functions are dependent on the temporal and neocortical brain regions, the first areas affected in the disease. As AD progresses, patients commonly display confusion, irritability, mood swings and some may act out aggressively.

Diagnosis of AD is based on performance on memory and cognitive tests, brain scans, apolipoprotein E (APOE) genotyping (discussed below) and cerebral spinal fluid analysis. Average life expectancy following diagnosis is approximately seven years (Molsa et al., 1986). There is no cure or preventative therapeutics available to treat AD, and current drugs only provide limited symptomatic relief. Clearly, further research is needed to develop disease-modifying therapies.

Alzheimer's Disease Genetics

Two types of AD have been identified, sporadic and familial. Sporadic AD (SAD) has a late age of onset (>60 yr of age), slow progression, and accounts for the vast majority of AD cases. In contrast, FAD is inherited in an autosomal dominant pattern and characterized by an early age of onset - patients typically develop symptoms between 30-60 yr of age - and rapid mental decline. FAD comprises less than 1% of all AD cases.

Sporadic Alzheimer's disease genetics

Although called sporadic, SAD does have a strong genetic component. However, the genetics underlying this form of AD are very complex, with several less penetrate genetic factors, epigenetic influences, and environmental factors conferring susceptibility. The only well established susceptibility gene is the one encoding the APOE protein. This gene is located on chromosome 19 and exists in three alleles, with APOE4 being a risk factor for AD. A single copy of the APOE4 allele confer a 2-3 fold increase in an individual's chance of developing AD, whereas two copies (homozygote APOE4) confer an 8-12 fold increase, compared to non-carriers (Myers et al., 1996; Slooter et al., 2004). APOE4 decreases the age of AD onset (Goldstein et al., 2001; Hsiung et al., 2004; Olarte et al., 2006), influences the severity of the disease by causing faster cognitive decline (Martins et al., 2005), increases hippocampal atrophy (Geroldi et al., 2000; Mori et al., 2002) and increases pathology at autopsy (Tiraboschi et al., 2004; Drzezga et al., 2009), and decreases survival time (Dal Forno et al., 2002). However, 40% of SAD patients do not carry an APOE4 allele indicating that other genetic factors must also contribute to the disease (Myers et al., 1996). In fact, genome-wide association studies have identified other susceptibility genes, but the effects they observe are

minimal, ranging from a 1.1 to 1.5 fold increase in the chance of developing AD (Harold et al., 2009; Lambert et al., 2009; Ertekin-Taner, 2010; Seshadri et al., 2010; Hollingworth et al., 2011).

Familial Alzheimer's disease genetics

In comparison to SAD, the genetics underlying FAD are much less complex and relatively well understood. The autosomal dominant inheritance pattern has allowed for the genes involved to be identified as those encoding the amyloid precursor protein (APP) (Goate et al., 1991) and the two PS homologs (Levy-Lahad et al., 1995; Sherrington et al., 1995), which share approximately 60% sequence identity.

The gene encoding APP is located on chromosome 21. Over 30 mostly missense mutations in the APP gene have been identified, accounting for 10-15% of all FAD pedigrees (Campion et al., 1999; Janssen et al., 2003). Nearly all APP mutations cluster around the three major processing sites that are relevant to the generation of Aβ (see below) and result in an increase in Aβ generation or alter the ratio of the more amyloidogenic $A\beta_{42}$ to the less hydrophobic $A\beta_{40}$ (Eckman et al., 1997; Tsubuki et al., 2003; Sahlin et al., 2007). Mutations in APP are fully penetrant, but different mutations do have varying ages of disease onset (Campion et al., 1999). In addition to mutations, duplication of the APP gene is observed in FAD pedigrees. Trisomy of chromosome 21 (Down's Syndrome) also results in early-onset AD (Rovelet-Lecrux et al., 2006; Sleegers et al., 2006).

The gene encoding PS1 is located on chromosome 14, and the gene encoding PS2 is located on chromosome 1. More than 150 fully penetrant mutations have been identified in the gene encoding PS1 and account for approximately 50% of FAD, whereas

fewer than 20 FAD causing mutations have been found in the gene encoding PS2 (Campion et al., 1999). PS2 mutations confer the widest range of disease onset and are not fully penetrant (Sherrington et al., 1996; Finckh et al., 2000; Tedde et al., 2003). PS mutations tend to be located in the transmembrane regions of the proteins and are located throughout the proteins' lengths. The majority of these are missense mutations but small deletions and insertions have been described (Bettens et al., 2010). PS FAD mutations cause a loss of catalytic activity and/or cleavage site specificity, which alters the ratio of the more amyloidogenic $A\beta_{42}$ to the less hydrophobic $A\beta_{40}$ (Chavez-Gutierrez et al., 2012).

The Cellular Functions of Familial Alzheimer's Disease Proteins

The initiating events in SAD are unknown, and tools to study this form of AD are lacking. Although FAD presents earlier in life than SAD, the two forms of AD share hallmark features, suggesting overlapping pathogenic mechanisms. Therefore, researchers have turned to FAD genetics to understand the molecular events causing AD. Over two decades of researcher has provided insights into the normal cellular functions of PSs and APP and how FAD mutations cause AD.

Amyloid precursor protein

The APP holoprotein is a type 1 transmembrane protein and appears to have several cellular functions, but genetic ablation in mice does not lead to a strong phenotype (Zheng et al., 1996). This is most likely due to compensation by the amyloid precursor-like proteins, APLP1 and APLP2 (Heber et al., 2000). Studies have suggested that the APP holoprotein may act as an axonal transport receptor by binding to the light

chain subunit of the kinesin 1 microtubule motor protein (Kamal et al., 2000), function in modulating signal transduction via an association with the G-protein, G_o (Nishimoto et al., 1993; Okamoto et al., 1996; Mbebi et al., 2002), or function as a cell surface receptor or as a synaptic adhesion molecule (Soba et al., 2005; Young-Pearse et al., 2007; Wang et al., 2009; Dahms et al., 2010; Zheng and Koo, 2011).

The cleavage products of APP may also have physiological functions. APP metabolism is a two-step proteolytic process commencing with either α-secretase or β-secretase cleavage. Both cleavage pathways result in a soluble APP product. The truncated membrane-bound APP is then subjected to an intramembrane cleavage by γ-secretase, causing the release of a peptide fragment called p3 (following α-secretase cleavage), or Aβ (following β-secretase cleavage), and an APP intracellular domain (AICD). The soluble fragment released following α-secretase cleavage is neuroprotective and promotes neurite outgrowth and synaptogenesis (Mattson et al., 1993; Furukawa et al., 1996a; Furukawa et al., 1996b; Mattson, 1997; Gakhar-Koppole et al., 2008; Ma et al., 2009). In fact, *in vivo* studies have found that this fragment promotes learning and memory (Meziane et al., 1998; Taylor et al., 2008). In contrast, the soluble fragment released following APP cleavage by β-secretase is cell toxic. Studies have found that this fragment can be further cleaved to become a ligand for death receptor 6, which activates caspase 6, and causes axonal pruning and neuronal death (Nikolaev et al., 2009).

Both α- and β-secretase cleavage result in a truncated APP that is subsequently subjected to γ-secretase cleavage. This second cleavage releases either p3, which is rapidly degraded and does not have a cellular function, or Aβ, and the AICD (Lu et al., 2000; Passer et al., 2000; Sastre et al., 2001; Yu et al., 2001). Aβ has been extensively

studied for its role in AD and is neurotoxic. AICD is rapidly degraded, and therefore rarely detected *in vivo*. However, *in vitro* studies have found that AICD has a role in transcription following complex formation with Fe65 and Tip60, and may regulate expression of several genes, including p53, glycogen synthase kinase-3β (GSK-3β) and the epidermal growth factor receptor (EGFR) (Baek et al., 2002; Kim et al., 2003; Cao and Sudhof, 2004; Pardossi-Piquard et al., 2005; Alves da Costa et al., 2006; Zhang et al., 2007). Over-expression of AICD is cytotoxic, an effect mediated either by its binding partners or the genes it regulates (Lu et al., 2000; Taru et al., 2002; Kim et al., 2003; Alves da Costa et al., 2006; Xu et al., 2007).

Lastly, APP can also be cleaved by caspase at its carboxy-terminal, releasing a short peptide fragment (Lu et al., 2003). Mutation of the caspase cleavage site prevents seizure susceptibility observed in mutant APP expressing mice, suggesting this fragment is also neurotoxic (Galvan et al., 2006).

Presenilins

PSs are nine transmembrane helix proteins (Laudon et al., 2005; Spasic et al., 2006) that reside in the endoplasmic reticulum (ER) in their immature holoprotein forms. They are interchangeable in function and display a variety of cellular functions, including acting as the catalytic subunit of the γ-secretase complex, regulating $[Ca^{2+}]_i$ signaling (see below), autophagy (Nixon and Yang, 2011), β-catenin turnover (Kang et al., 2002), axonal transport (Morfini et al., 2002; Pigino et al., 2003), modulating signaling pathways (Weihl et al., 1999; Baki et al., 2004; Kang et al., 2005), and trafficking and turnover of membrane proteins (Repetto et al., 2007). Genetic ablation of the gene encoding PS1 results in prenatal death (Shen et al., 1997; Wong et al., 1997), whereas

PS2 null mice exhibit only minor pulmonary fibrosis and hemorrhages with age (Herreman et al., 1999). Forebrain specific conditional double knock-out (DKO) of both PS genes in adult mice causes cortical and hippocampal degeneration, indicating that PSs are needed for proper neuronal physiology (Feng et al., 2004; Saura et al., 2004).

Although PSs have many cellular functions, they are best studied as the catalytic core of the γ-secretase responsible for cleaving ~60 type 1 membrane proteins (Prox et al., 2012), including APP (De Strooper et al., 1998). Following assembly of the γ-secretase complex composed of PS, nicastrin, presenilin enhancer-2, and anterior pharynx-defective-1, PS undergoes endoproteolysis and the complex is exported from the ER (Dries and Yu, 2008). The γ-secretase is then able to function in APP metabolism, generating Aβ, which is the main component of the extracellular plaques observed in AD.

Hypothesized Mechanisms of Alzheimer's Disease Pathogenesis

Possible etiological mechanisms for AD have largely focused on extracellular Aβ plaques, driven by the finding that PSs comprises the catalytic core of γ-secretase, the protease responsible for APP cleavage and Aβ release. These observations have lead to the amyloid-cascade hypothesis of AD, which places Aβ as the key initiator of the disease (Hardy and Selkoe, 2002). The amyloid cascade hypothesis postulates that accumulation of Aβ, resulting from overproduction, altered processing or a failure of clearance, is the initiating molecular event that triggers neurodegeneration in sporadic and familial Alzheimer's disease (Hardy and Selkoe, 2002). However, extensive research during the last two decades has failed to convincingly produce data consistent with the idea that amyloid is the main cause of AD. It has become apparent that Aβ load does not

correlate well with disease severity. Moreover, this hypothesis does not fully explain formation of neurofibrillary tangles.

In addition to cleavage of APP PSs have several cellular functions that are disrupted by FAD mutations, including a role in $[Ca^{2+}]_i$ homeostasis (LaFerla, 2002). An alternative, but not mutually exclusive hypothesis is the Ca^{2+} hypothesis of AD, which states that sustained disturbances in $[Ca^{2+}]_i$ homeostasis are a proximal cause of neurodegeneration in AD (Khachaturian, 1994). In fact, a substantial and growing body of literature (see below) demonstrates that FAD mutations in PS result in $[Ca^{2+}]_i$ dysregulation as a proximal event, and that $[Ca^{2+}]_i$ dysregulation can contribute to AD pathogenesis. These studies have provided support for the Ca^{2+} hypothesis of AD.

Ca^{2+} Homeostasis

$[Ca^{2+}]_i$ signaling is a dynamic process involving the plasma membrane (PM), the ER, acidic organelles and mitochondria. Sub-cellular compartments have strikingly different $[Ca^{2+}]$, and deviations from narrow concentration ranges within these compartments results in incorrect activation of signaling pathways. Therefore $[Ca^{2+}]$ is tightly regulated in time, space, and intensity.

Ca^{2+} is maintained at very low resting levels in the cytosol (50-300 nM) by multiple mechanisms, including plasma membrane Ca^{2+} ATPases (PMCA), which extrude Ca^{2+} from the cell, the secretory pathway Ca^{2+} ATPases (SPCA) that sequester Ca^{2+} into acidic secretory pathway organelles, and sarco/endoplasmic reticulum Ca^{2+} ATPase (SERCA) pumps, which are responsible for Ca^{2+} uptake into the ER. Ca^{2+} signals arise from influx across the PM or release from the ER, the major intracellular Ca^{2+} store with $[Ca^{2+}]$ ~100-700 μM, in response to agonist binding of PM localized G-proteins.

This binding causes activation of phospholipase C, which catalyzes the hydrolysis of phosphatidylinositol 4,5-bisphosphate to generate $InsP_3$, the ligand for the ER localized $InsP_3R$. $InsP_3R$-dependent Ca^{2+} release is amplified by Ca^{2+} release through the ryanodine receptor (RyR) in a Ca^{2+}-induced Ca^{2+} release (CICR) manner. In opposition to the ER filling function of SERCA, a constitutively active, passive ER Ca^{2+} leak exists, which allow for Ca^{2+} to flow down its concentration gradient from the ER to the cytosol. Although controversial, it has been suggested that the PS holoprotein forms channels that mediate the ER Ca^{2+} leak (Tu et al., 2006).

Disruption of Ca^{2+} Homeostasis in Alzheimer's Disease

PSs do not contain any known Ca^{2+} binding motifs, so their effects on $[Ca^{2+}]_i$ signaling must be indirect, mediated through a binding partner, due to a γ-secretase cleavage product, or a currently unknown function of PSs. The effects of FAD PS mutations on $[Ca^{2+}]_i$ signaling are: (1) enhanced magnitudes of Ca^{2+} release from ER stores upon stimulation of the $InsP_3R$ or RyR, (2) increased sensitivity to agonists of Ca^{2+} release and (3) elevated cytosolic $[Ca^{2+}]$ (Ito et al., 1994; Guo et al., 1996; Hirashima et al., 1996; Etcheberrigaray et al., 1998; Leissring et al., 1999a; Leissring et al., 1999b; Chan et al., 2000; Leissring et al., 2000; Smith et al., 2002; Stutzmann et al., 2004; Smith et al., 2005; Lee et al., 2006; Stutzmann et al., 2006; Tu et al., 2006; Nelson et al., 2007; Stutzmann et al., 2007; Cheung et al., 2008; Lopez et al., 2008; Cheung et al., 2010; McCombs et al., 2010; Nelson et al., 2010; Zhang et al., 2010; Muller et al., 2011; Boyle et al., 2012; Honarnejad et al., 2013). These abnormalities are commonly referred to as exaggerated $[Ca^{2+}]_i$ signaling and have been reported in a variety of FAD patients' cell lines, neuronal and non-neuronal cell lines, and mouse models of AD. Additionally, this

phenomenon occurs during the initial phases of AD, before onset of overt symptoms and canonical histopathology, suggesting that disturbances in $[Ca^{2+}]_i$ homeostasis may be a proximal event in AD pathogenesis.

Patient cell lines

Studies on AD patients' skin fibroblasts provided the first indication that $[Ca^{2+}]_i$ homeostasis is disrupted in the disease. These experiments demonstrated exaggerated ER Ca^{2+} signaling – enhanced $[Ca^{2+}]_i$ signals in response to application of $InsP_3$-generating agonists (bradykinin and bombesin) and responses to lower concentrations of agonists – compared to controls (Ito et al., 1994; Hirashima et al., 1996). These abnormalities precede the clinical manifestations of AD; aberrations in $[Ca^{2+}]_i$ signaling were present in a large proportion of FAD patients' fibroblasts prior to clinical onset of AD, but not present in family members that survived symptom-free past the average age of onset for the family (Etcheberrigaray et al., 1998). Recently, these observations were confirmed in human B lymphoblast cells from FAD patients (Cheung et al., 2010). These studies established the existence of exaggerated $[Ca^{2+}]_i$ signaling in FAD patients.

Neuronal and non-neuronal cell lines

Neuronal and non-neuronal cell lines have been used to further study FAD mutant PS-associated exaggerated $[Ca^{2+}]_i$ signaling. Studies on PC12 cells (a neuronal-like cell line derived from a pheochromocytoma of the rat adrenal medulla) stably expressing FAD mutant PS alleles observed exaggerated $[Ca^{2+}]_i$ signaling in response to both carbocol and bradykinin (Guo et al., 1996). To determine if this difference was due to alterations in $InsP_3$ production, subsequent studies employed caged $InsP_3$ injected into

Xenopus oocytes expressing FAD mutant PS1 or PS2. These studies observed larger magnitudes of Ca^{2+} releases following $InsP_3$ uncaging in oocytes expressing FAD mutant PS alleles than in controls, indicating that this phenomenon is not due to differences in $InsP_3$ generation (Leissring et al., 1999a; Leissring et al., 1999b). Investigators observed exaggerated caffeine-induced (a RyR agonist) Ca^{2+} release in hippocampal neurons from PS1M146V-knock-in (M146V) embryos compared to WT (Chan et al., 2000). This study confirmed that FAD mutant PS causes alterations in hippocampal neuron $[Ca^{2+}]_i$ handling. Subsequently, several groups have reproduced these observations in a variety of cell types, including fibroblasts from FAD mutant PS transgenic mice (Leissring et al., 2000), PS DKO mouse embryonic fibroblasts (MEF) that were subsequently transfected to express human PS FAD alleles (Cheung et al., 2010), neurons from FAD PS expressing mice (Smith et al., 2005; Lopez et al., 2008; Cheung et al., 2010), SH-SY5Y human neuroblastoma cells (Smith et al., 2002; Muller et al., 2011; Boyle et al., 2012), DT40 chicken B cells (Cheung et al., 2008), human embryonic kidney cells (HEK) over-expressing FAD mutant PS alleles (Honarnejad et al., 2013) and Sf9 insect ovarian cells (Cheung et al., 2008; Cheung et al., 2010). These *in vitro* studies have repeatedly confirmed the effects of FAD mutant PS expression on $[Ca^{2+}]_i$ signaling.

Alzheimer's disease mouse models

FAD mutant PS-associated exaggerated $[Ca^{2+}]_i$ signaling has also been studied in *ex vivo* experiments conducted on brain slices from mutant PS expressing mice. Using whole-cell patch clamping, investigators loaded cortical neurons in brain slices from M146V, 3xTg (which contain the M146V mutation) and WT mice with a caged $InsP_3$ and a Ca^{2+} indicator. Photolysis of the caged $InsP_3$ revealed faster rates and increased

magnitudes of Ca^{2+} release in AD mice compared to WT (Stutzmann et al., 2004; Stutzmann et al., 2006; Stutzmann et al., 2007; Chakroborty et al., 2009; Goussakov et al., 2010a; Goussakov et al., 2010b). These experiments were conducted on young (5-6-wk-old) animals, and the M146V mouse does not display accumulation of Aβ or hyperphosphorylated tau even at old ages, suggesting that exaggerated $[Ca^{2+}]_i$ signaling is a proximal event in AD, independent of AD pathology.

Contributions of Exaggerated $[Ca^{2+}]_i$ Signaling to Alzheimer's Disease Pathogenesis

The observation that exaggerated $[Ca^{2+}]_i$ signaling precedes other AD phenotypes suggests that it may play a central role in disease development. Ca^{2+} regulates many cellular and neuronal processes, including APP metabolism, tau kinase activity, cell death, neurotransmitter release and synaptic plasticity. Accumulating *in vitro* and *in vivo* evidences suggests that alterations in $[Ca^{2+}]_i$ signaling may contribute to AD pathogenesis by affecting these pathways.

Amyloid precursor protein processing and Aβ generation

Studies demonstrating that changes in $[Ca^{2+}]_i$ handling alter APP metabolism (Buxbaum et al., 1994; Querfurth and Selkoe, 1994; Querfurth et al., 1997; Yoo et al., 2000; LaFerla, 2002; Pierrot et al., 2004; Lesne et al., 2005; Pierrot et al., 2006; Cheung et al., 2008; Green et al., 2008; Hoey et al., 2009; Bordji et al., 2010; Verges et al., 2011) are in agreement with the hypothesis that AD might result from a life-long "calciumopathy." Initial studies addressing the influence of Ca^{2+} on APP metabolism employed HEK cells over-expressing APP. These studies examined the effects of elevated cytosolic $[Ca^{2+}]$ on Aβ generation, and observed that elevated cytosolic $[Ca^{2+}]$,

resulting from either Ca^{2+} entry from extracellular sources or from ER Ca^{2+} store release, enhanced Aβ secretion (Querfurth and Selkoe, 1994; Querfurth et al., 1997). In PCNs, sustained increases in cytosolic [Ca^{2+}] inhibit α-secretase and trigger the accumulation of the β-secretase cleavage products (Pierrot et al., 2004; Pierrot et al., 2006). Mechanistic insights are provided by the observation that prolonged treatment of PCNs with sub-lethal concentrations of N-methyl-D-aspartic acid (NMDA), an agonist for the Ca^{2+}-permeable NMDA receptor, increases the production and secretion of Aβ (Lesne et al., 2005), whereas short NMDA receptor activation with low agonist concentrations stimulates α-secretase processing of APP (Hoey et al., 2009). In sum, these studies suggest Ca^{2+} entry through NMDA receptors can either activate (Lesne et al., 2005) or inhibit (Hoey et al., 2009) Aβ production depending on the duration of the rise in cytosolic [Ca^{2+}]. These conflicting effects may be due to activation of different populations of NMDA receptors – activation of extra-synaptic NDMA receptors, but not synaptic NMDA receptors, was found to increase Aβ production by modulating APP pre-mRNA splicing towards Kunitz protease inhibitor domain-containing APP that favors amyloid production (Bordji et al., 2010).

Other Ca^{2+}-dependent mechanisms appear to influence APP processing in a rapid manner, independent of *de novo* transcription. *In vivo* experiments have found that APP has a role in modulating synapse function (Priller et al., 2006). In fact, interstitial fluid Aβ levels are directly influenced by synaptic activity (Kamenetz et al., 2003; Cirrito et al., 2005) and Aβ inhibits neuronal excitability (Kamenetz et al., 2003; Shankar et al., 2008). Recently, it was observed that interstitial fluid Aβ levels are affected in opposite directions depending on the dose of NMDA administered (Verges et al., 2011). Lower

NMDA doses increased synaptic transmission and led to elevated Aβ production, whereas high doses of NMDA diminished Aβ production (Verges et al., 2011).

Alternatively, research has also suggested that Ca^{2+} can increase Aβ generation by activating the Ca^{2+}-dependent phosphatase calcineurin. Subsequently, calcineurin dephosphorylates and activates the nuclear factor of activated T-cells (NFAT) transcription factor, leading to elevated expression of β-secretase (Cho et al., 2008). Increased levels of active calcineurin and NFAT are observed in the nuclear fraction of cortical tissues obtained from AD patients (Wu et al., 2010) and β-secretase expression and enzymatic activity are enhanced in the brains of AD mice and human subjects (Fukumoto et al., 2002; Apelt et al., 2004). Although the mechanisms are not well understood, previous research clearly indicates that Ca^{2+} influences APP metabolism.

Tau hyperphosphorylation

Tau is a microtubule-associated protein that promotes microtubule assembly and stability. Although no mutations in tau are linked to AD, hyperphosphorylated tau is the major component of NFT. Multiple kinases regulate the function of tau by acting on 84 phosphorylatable residues (Morishima-Kawashima et al., 1995a; Morishima-Kawashima et al., 1995b; Hanger et al., 2007; Hanger et al., 2009). Tau obtained from AD brains is phosphorylated at forty of these sites, compared to only nine in unaffected individuals (Hanger et al., 2007; Hanger et al., 2009).

Ca^{2+} may influence the production of NFT by activating tau kinases, including GSK-3β and cyclin-dependent kinase 5 (CDK5). Studies have found that tau is phosphorylated in response to elevated somal [Ca^{2+}] in a duration-dependent manner

(Hartigan and Johnson, 1999). In cultured neurons, Ca^{2+} influx resulting from a 30 min membrane depolarization is sufficient to induce phosphorylation of tau mediated by both GSK-3β and CDK5 (Pierrot et al., 2006). GSK-3β is a constitutively active kinase whose activity is inhibited by phosphorylation on Ser-9 and enhanced by phosphorylation on Tyr-216. Treatment of SH-SY5Y cells with a low concentration of Ca^{2+} ionophore results in tyrosine phosphorylation of GSK-3β and GSK-3β-dependent tau phosphorylation (Hartigan and Johnson, 1999). GSK-3β is a substrate for proline-rich tyrosine kinase 2 (Pyk2), and $[Ca^{2+}]_i$ signaling, resulting from activation of the endogenous $InsP_3$-generating pathway, causes Pyk2- and GSK-3β-dependent tau phosphorylation (Sayas et al., 2006). GSK-3β transgenic mice display tau hyperphosphorylation and neurodegeneration (Lucas et al., 2001). GSK-3β co-localizes with NFT (Pei et al., 1997), and its expression is upregulated in peripheral lymphocytes in AD patients and patients with mild cognitive impairment (MCI), a condition commonly preceding AD (Hye et al., 2005).

Increased cytosolic $[Ca^{2+}]$ may also activate CDK5-mediated tau phosphorylation. p35, the membrane-bound activator of CDK5, is cleaved in a Ca^{2+}- and calpain-dependent manner into the more stable and soluble p25, which causes prolonged and mislocalized activity of CDK5 (Lee et al., 2000). Ca^{2+} influx in PCN induces the production of p25 (Lee et al., 2000), and p25 accumulates in the brains of AD patients (Patrick et al., 1999). Mice over-expressing p25 show hyperphosphorylation of tau (Ahlijanian et al., 2000) and double transgenic mice over-expressing p25 and tau_{P301L} develop NFT (Noble et al., 2003). These studies clearly demonstrate that changes in $[Ca^{2+}]_i$ homeostasis can affect the phosphorylation state of tau.

Neurodegeneration

Elevated cytosolic [Ca^{2+}] activates the necrotic cell death pathway, which is thought to contribute to the neurodegeneration observed in AD. The necrotic pathway is dependent on the Ca^{2+}-activated calpain protease, which cleaves a variety of cellular proteins. Calpain is aberrantly activated in the brains of AD patients, (Saito et al., 1993) and the level of calpain's endogenous inhibitor, calpastatin, is decreased (Nilsson et al., 1990). Aberrant calpain activation appears to be involved in AD as treatment of APP_{SWE} and PS1M146L transgenic mice with calpain inhibitors restores normal synaptic function in hippocampal slices and improves spatial-working memory and associative fear memory (Trinchese et al., 2008). In agreement, administration of a calpain inhibitor to 3xTg mice lowered Aβ levels and phospho-tau accumulation (Medeiros et al., 2012). Over-expression of the endogenous calpain inhibitor, calpastatin, in AD mice correlated with reduced plaque burden and phospho-tau accumulation (Liang et al., 2010). These studies found that inhibition of calpain was associated with reduced levels of β-secretase expression and CDK5 activation (Liang et al., 2010; Medeiros et al., 2012), indicating that aberrant Ca^{2+}-dependent calpain activation may contribute to AD pathogenesis.

Synaptic deficits

Ca^{2+} release from intracellular stores plays an important role in hippocampal synaptic plasticity (Bashir et al., 1993; Futatsugi et al., 1999; Fujii et al., 2000; Raymond and Redman, 2006; Mellentin et al., 2007) and is known to modulate different forms of long-term potentiation (LTP) (Raymond and Redman, 2006). If fact, enhanced LTP is observed in mice lacking either RyR3 (Futatsugi et al., 1999), or $InsP_3R1$ (Fujii et al.,

2000), indicating that intracellular Ca^{2+} store release plays an opposing role to Ca^{2+} influx via the NMDA receptor in LTP induction.

Genetic ablation of the two PS genes has confirmed their essential role in proper synaptic function and plasticity. PSs are involved in homeostatic synaptic scaling (Pratt et al., 2011), a form of plasticity that functions to maintain action potential firing rates in an optimal range. Additionally, PSs were reported to associate with NMDA receptors, and genetic deletion of both PS homologs resulted in lower synaptic NMDA receptor levels, and synaptic dysfunction (Saura et al., 2004). Studies on hippocampal region CA1 or CA3 conditional PS DKO mice revealed that presynaptic (CA3) PS expression is essential for modulating $[Ca^{2+}]_i$ signaling that, in part, regulates neurotransmitter release (Zhang et al., 2009). These studies confirmed a role for PSs in synaptic transmission and plasticity.

The effects of FAD mutant PS expression on synaptic transmission and plasticity have been investigated in the M146V mouse (Odero et al., 2007; Auffret et al., 2010). These studies reported enhanced hippocampal region CA1 early-LTP (E-LTP) and NMDA receptor-mediated transmission. E-LTP is a form of transient synaptic plasticity resulting from a single tetanus and is normally short-term (~1 hr). Previous studies on FAD mutant PS expressing mice have identified enhancements in the induction (the initial change in synaptic strength following tetanus application) and maintenance (the long-lasting, maintained changes in synaptic strength) phases of E-LTP and found that these phenomena are due to a decease in the threshold for eliciting potentiation without changes in the maximum amount of potentiation achievable (Zaman et al., 2000; Schneider et al., 2001). This decreased threshold is postulated to be due to changes in

$[Ca^{2+}]_i$ handling associated with FAD mutant PS (Parent et al., 1999; Barrow et al., 2000; Schneider et al., 2001; Odero et al., 2007).

Reports on young 3xTg mice also suggest that exaggerated $[Ca^{2+}]_i$ signaling results in changes in hippocampal basal synaptic transmission and synaptic plasticity (Chakroborty et al., 2009). These studies found that enhanced RyR-mediated Ca^{2+} release masks subtle changes in hippocampal synaptic transmission, presynaptic facilitation and LTP, which only became apparent following inhibition of RyR-mediated Ca^{2+} release (Chakroborty et al., 2009).

AD pathology also appears to affect hippocampal plasticity. Initial reports on 3xTg mice observed an age-dependent impairment in hippocampal CA1 region late-LTP (L-LTP) present in mice 6-mths-of-age (Oddo et al., 2003). L-LTP is a form of long-lasting synaptic potentiation that is elicited by multiple increases in cytosolic $[Ca^{2+}]$, which activate *de novo* CREB-dependent gene expression. The age dependence of this impairment lead the author's to postulate that it is due to AD pathology accumulation. In sum, these findings suggest that PSs have a role in synaptic homeostasis and plasticity and that loss of PS expression or FAD mutations in PSs are sufficient to disrupt hippocampal circuits independent of AD pathology.

Targeting exaggerated $[Ca^{2+}]_i$ signaling

The potential contribution of exaggerated $[Ca^{2+}]_i$ signaling to AD pathogenesis is further emphasized by studies showing that pharmacologic or genetic targeting of $[Ca^{2+}]_i$ signaling influences Aβ generation and tau kinase activation. Over-expression of SERCA, which results in overfilling of the ER Ca^{2+} stores and enhanced $[Ca^{2+}]_i$ signaling, causes an increase in Aβ generation. In agreement, knock-down of SERCA

decreases Aβ generation (Green et al., 2008). Similarly, depletion of ER Ca^{2+} stores by inhibition of the SERCA pump results in a depression in Aβ release (Buxbaum et al., 1994). Genetic ablation of all three $InsP_3R$ homologs dramatically reduces the level of Aβ secreted from APP_{SWE} expressing cells and rectifies the PS1M146L enhancement of Aβ secretion (Cheung et al., 2008). GSK-3β-dependent tau phosphorylation is blocked by a RyR antagonist (Resende et al., 2008), and stabilization of neuronal $[Ca^{2+}]_i$ signaling decreases calpain activation, p25 production, and subsequent CDK5 mediated tau phosphorylation (Chen et al., 2008). In conclusion, these data suggest that exaggerated $[Ca^{2+}]_i$ signaling may contribute to AD pathogenesis, and normalizing these signals could impinge upon AD histopathology.

Recent *in vivo* studies investigating the contribution of exaggerated $[Ca^{2+}]_i$ signaling to AD pathogenesis have employed pharmacological approaches targeting RyR but have produced conflicting results. One study identified a worsening of AD-like phenotypes (Zhang et al., 2010) and two reported amelioration (Oules et al., 2012; Peng et al., 2012). Although all three reports employed the same RyR antagonist, they used different routes of administration, dosing parameters, and employed different AD mouse models. These differences make the conflicting results of these studies difficult to interpret and suggest that future experiments should employ a consistent method to rescue exaggerated $[Ca^{2+}]_i$ signaling.

Hypothesized Mechanisms of Familial Alzheimer's Disease Mutant PS Exaggerated $[Ca^{2+}]_i$ Signaling

Although FAD PS mutations have repeatedly been shown to result in exaggerated $[Ca^{2+}]_i$ signaling, the mechanism underling this phenomenon is controversial (Kasri et al.,

2006; Stutzmann et al., 2006; Tu et al., 2006; Cheung et al., 2008; Green et al., 2008; Rybalchenko et al., 2008). Hypothesized mechanisms can be grouped into two categories:

(1) Increased driving force due to elevated ER [Ca^{2+}], termed the ER overfilling hypothesis, which results in enhanced Ca^{2+} release upon Ca^{2+} release channel activation. Hypothesized mechanisms postulate that FAD PS mutations either:

(A) *Result in a gain-of-function enhancement of SERCA ER filling activity* (Green et al., 2008). Support for this hypothesis comes from studies showing that PSs are SERCA binding partners (Green et al., 2008; Jin et al., 2010), that lack of PS expression results in smaller releases of Ca^{2+} from ER stores via the passive ER Ca^{2+} leak, and that over-expression of WT PSs increases clearance rates of cytosolic Ca^{2+}, which are further enhanced by over-expression of FAD mutant PS alleles (Green et al., 2008). In agreement with this proposed mechanism, it was recently found that FAD mutant PS expressing cells have attenuated store-operated Ca^{2+} re-entry, a cellular process to refill depleted ER Ca^{2+} stores, which was rescued by inhibition of SERCA activity (Boyle et al., 2012). However, it has also been reported that WT PS2 and FAD mutant PS2 reduce SERCA activity in SH-SY5Y and MEF cells (Brunello et al., 2009).

(B) *Decrease the conductance of the passive ER Ca^{2+} leak channel* (Tu et al., 2006). Support for this mechanism comes from the observation that ER Ca^{2+} release, following SERCA inhibition, is elevated in cells expressing mutant PS1 (Leissring et al., 2000). Additionally, Tu and colleagues reported that WT PS, but not FAD mutant PS, form low-conductance divalent cation permeable pores in

planar lipid bilayers (Tu et al., 2006; Nelson et al., 2007). However, several groups have not made observations consistent with this mechanism. Kasri et al. found a decrease in ER [Ca^{2+}] as measured by ER-targeted aequorin (Kasri et al., 2006) and Zatti et al. observed that several FAD mutations in PS1 and PS2 cause a decrease in ER [Ca^{2+}], as measured by both fura-2 and aequorin in three different cell lines (Zatti et al., 2006). Other studies have also produced data conflicting with the hypothesis that PSs form the passive ER Ca^{2+} leak channel, a function disrupted by FAD mutations (Stutzmann et al., 2004; Zatti et al., 2004; Giacomello et al., 2005; Smith et al., 2005; Cheung et al., 2008; Brunello et al., 2009; Cheung et al., 2010; Jin et al., 2010; McCombs et al., 2010; Muller et al., 2011; Boyle et al., 2012).

Recently, the first crystal structure of an intramembrane aspartate protease (PS-like) protein was reported (Li et al., 2012). The authors identified a large hole that transverses the entire protein, lined by hydrophobic residues on transmembrane (TM) regions TM2, TM3, TM5, and TM7. The hydrophobicity of the pore lead the authors to postulate that is it likely plugged by lipid molecules and/or PS binding partners (Li et al., 2012). Additionally, previous reports mapping the putative conductance pore of the PS holoprotein suggested that the pore was on the opposite side of TM7, lined by residues on TM7 and TM9 (Nelson et al., 2011).

(2) Increased Ca^{2+} conductance of the ER membrane. The hypothesized mechanisms in this category postulate that FAD PS mutations cause exaggerated Ca^{2+} release by:

(A) *Acting indirectly to upregulate expression of the $InsP_3R$* (Kasri et al., 2006). Kasri et al. reported a 4-fold increase in $InsP_3R1$ expression as the likely mechanism for the reduced ER [Ca^{2+}] they observed in PS DKO MEF cells (Kasri et al., 2006). This report has not been independently verified.

(B) *Acting indirectly to upregulate expression of the RyR* (Chan et al., 2000). Several groups have suggested that upregulation of RyR may underlie FAD mutant PS exaggerated $[Ca^{2+}]_i$ signaling (Chan et al., 2000; Stutzmann et al., 2006; Stutzmann et al., 2007). In fact, two-photon imaging experiments conducted on cortical neurons in *ex vivo* brain slices revealed that M146V-associated exaggerated $[Ca^{2+}]_i$ signaling is largely attenuated by a RyR antagonist (Stutzmann et al., 2006; Stutzmann et al., 2007). However, there are conflicting reports regarding the specific isoform that is upregulated, with groups reporting either RyR2 (Chakroborty et al., 2009) or RyR3 (Chan et al., 2000).

<u>RyR3 upregulation</u> – Initial reports observed that RyR3 is upregulated in FAD mutant PS expressing PC12 cells and in hippocampal neurons from M146V mice (Chan et al., 2000). Subsequently, RyR3 upregulation has been reported in cortical neurons from TgCRND8 mice (Supnet et al., 2006; Supnet et al., 2010).

<u>RyR2 upregulation</u> – Other groups have observed that FAD mutant PS expression results in RyR2 upregulation. RyR2 mRNA is elevated in 3xTg hippocampal tissues compared to WT mice (Chakroborty et al., 2009) and in mid-temporal tissues from mild-cognitive impairment patients (Bruno et al., 2012).

(C) *A direct physical interaction that modulates the gating properties of the RyR* (Rybalchenko et al., 2008). Studies have shown that the N-terminus of PS1 and PS2 can interact with RyR and increase single channel activity (Hayrapetyan et al., 2008; Rybalchenko et al., 2008). An analysis of how FAD PS mutations affect RyR gating has not been reported.

(D) *A direct physical interaction that modulates the gating properties of the $InsP_3R$* (Cheung et al., 2008). PSs physically interacts with the $InsP_3R$, and FAD mutations in PS enhance the modal gating activity of the $InsP_3R$, stabilizing the channel's open-state and increasing its ligand sensitivity (Cheung et al., 2008; Cheung et al., 2010). Although other studies have made observations consistent with this hypothesis (McCombs et al., 2010), independent replication of the effects of FAD mutant PS on $InsP_3R$ gating have not been reported.

Rationale

Developing a better understanding of the mechanisms and contributions of exaggerated $[Ca^{2+}]_i$ signaling to AD pathogenesis may identify new therapeutic targets to treat FAD, and could provide insights into the more common, sporadic form of AD. Therefore, in Chapter 2 we test the hypotheses that PSs acts as the Ca^{2+}-permeable leak channel within the ER membrane, with FAD-linked mutations disrupting this function and resulting in overfilling of the ER Ca^{2+} stores. In Chapter 3 we show that exaggerated $[Ca^{2+}]_i$ signaling is mediated by $InsP_3R1$, a proximal event in AD, and contributes to the onset and progression of the disease. The experiments presented in this dissertation serve

to elucidate the manner in which FAD mutant PS disrupts $[Ca^{2+}]_i$ signaling and determine the role of exaggerated $[Ca^{2+}]_i$ signaling to AD pathogenesis *in vivo*.

Published in the *Journal of Biological Chemistry.* 2012 Mar 30; 287(14):10933-44

Chapter 2: Lack of Evidence for Presenilins as Endoplasmic Reticulum Ca^{2+} Leak Channels

Dustin Shilling[1], Don-On Daniel Mak[1], David E. Kang[3] and J. Kevin Foskett[1,2,¶]

From the Departments of Physiology[1] and Cell and Developmental Biology[2], Perelman School of Medicine, University of Pennsylvania, Philadelphia, Pennsylvania 19104 and the Department of Neuroscience[3], University of California, San Diego, La Jolla, California 92093

[¶]**Address correspondence to**: Dr. J. Kevin Foskett, Department of Physiology, 726 Clinical Research Bldg., 415 Curie Blvd., University of Pennsylvania, Philadelphia, PA 19104-6085, E-mail: foskett@mail.med.upenn.edu, Fax 215-573-6808

Number of Figures/Supplemental Figures: 9/0

Number of Pages: 36

SUMMARY

Familial Alzheimer's disease (FAD) is linked to mutations in the presenilin (PS) homologs. FAD mutant PS expression has several cellular consequences, including exaggerated intracellular Ca^{2+} ($[Ca^{2+}]_i$) signaling due to enhanced agonist sensitivity and increased magnitude of $[Ca^{2+}]_i$ signals. The mechanisms underlying these phenomena remain controversial. It has been proposed that PS are constitutively active, passive ER Ca^{2+} leak channels, and that FAD PS mutations disrupt this function resulting in ER store overfilling that increases the driving force for release upon ER Ca^{2+} release channel opening. To investigate this hypothesis, we employed multiple Ca^{2+} imaging protocols and indicators to directly measure ER Ca^{2+} dynamics in several cell systems. However, we did not observe consistent evidence that PS act as ER Ca^{2+} leak channels. Nevertheless, we confirmed observations made using indirect measurements employed in previous reports that proposed this hypothesis. Specifically, cells lacking PS or expressing a FAD-linked PS mutation displayed increased area under the ionomycin-induced $[Ca^{2+}]_i$ vs time curve (AI) compared with cells expressing WT PS. However, an ER-targeted Ca^{2+} indicator revealed that this did not reflect overloaded ER stores. Monensin pre-treatment selectively attenuated the AI in cells lacking PS or expressing a FAD PS allele. These findings contradict the hypothesis that PS form ER Ca^{2+} leak channels and highlight the need to use ER-targeted Ca^{2+} indicators when studying ER Ca^{2+} dynamics.

INTRODUCTION

Alzheimer's disease (AD)[2] is the most common cause of dementia among individuals over 60 years old, affecting ~2% of people in industrialized countries. Although most AD is idiopathic with late onset (>60 years of age), a small percentage of AD is characterized by early-onset and dominant-negative inheritance. Familial AD (FAD) is linked to mutations in three genes encoding the amyloid precursor protein (APP) and the two presenilin (PS) homologs. Mutations in PS1 cause the majority of FAD cases.

PS are nine transmembrane helix proteins (Laudon et al., 2005; Spasic et al., 2006) that reside in the endoplasmic reticulum (ER) in their immature holoprotein forms. Following assembly of the γ-secretase complex composed of PS, nicastrin, pen-2, and aph-1, PS undergoes endoproteolysis and the complex is exported from the ER (Dries and Yu, 2008). Possible etiological mechanisms for AD pathogenesis have focused on one of its two major histopathological hallmarks, extracellular Aβ plaques, driven by the finding that PS comprises the catalytic core of γ-secretase, the protease responsible for APP cleavage and Aβ release (Herreman et al., 2000). However, a large body of evidence suggests that PS is involved in intracellular Ca^{2+} ($[Ca^{2+}]_i$) homeostasis, and that FAD mutations result in $[Ca^{2+}]_i$ dysregulation (Stutzmann, 2005; Gandy et al., 2006; Thinakaran and Sisodia, 2006; Marx, 2007; Mattson, 2007; Bezprozvanny and Mattson, 2008; Berridge, ; Mattson).

Studies of FAD patients' fibroblasts provided the first evidence that $[Ca^{2+}]_i$ homeostasis is disrupted in the disease. These experiments demonstrated increased sensitivity and enhanced Ca^{2+} release in response to $InsP_3$-generating agonists in FAD

patients' fibroblasts compared with those from unaffected family members (Ito et al., 1994; Hirashima et al., 1996; Etcheberrigaray et al., 1998). These findings have since been extended in numerous *in vitro* and *in vivo* studies (Stutzmann et al., 2004; Smith et al., 2005; Kasri et al., 2006; Stutzmann et al., 2006; Stutzmann et al., 2007; Cheung et al., 2008; Green et al., 2008; Chakroborty et al., 2009; Cheung et al., 2010). Despite intensive investigation, the mechanisms of mutant PS-enhanced Ca^{2+} signaling remain controversial (Smith et al., 2005; Kasri et al., 2006; Tu et al., 2006; Zatti et al., 2006; Nelson et al., 2007; Cheung et al., 2008; Green et al., 2008; Cheung et al., ; McCombs et al., ; Nelson et al., ; Zhang et al., ; Nelson et al.).

$[Ca^{2+}]_i$ signaling is a dynamic process involving the plasma membrane (PM), the ER, acidic organelles and mitochondria. Basal cytoplasmic $[Ca^{2+}]$ is maintained at ~100 nM by multiple mechanisms, including plasma membrane Ca^{2+} ATPases (PMCA), which extrude Ca^{2+} from the cell, the secretory pathway Ca^{2+} ATPases (SPCA) that sequester Ca^{2+} into acidic secretory pathway organelles, and sarco/endoplasmic reticulum Ca^{2+} ATPase (SERCA) pumps, which are responsible for Ca^{2+} uptake into the ER. The ER is the major intracellular Ca^{2+} store, with basal $[Ca^{2+}]_{ER}$ ~100-700 μM. Ca^{2+} is released from the ER through two main ion channels, the inositol 1,4,5-trisphosphate ($InsP_3R$) (by $InsP_3$) and the ryanodine receptor (RyR) (by Ca^{2+}-induced Ca^{2+} release). A constitutively active, passive ER Ca^{2+} leak also exists, although its molecular identity is controversial.

It has been proposed that PS holoproteins are Ca^{2+} channels that comprise the passive ER Ca^{2+} leak, with FAD PS mutations disrupting this function (Tu et al., 2006; Nelson et al., 2007; Nelson et al., ; Zhang et al., ; Nelson et al.). Disruption of this function was suggested to result in Ca^{2+} overloading of the ER store, with consequent

exaggerated Ca^{2+} release in response to agonists. However, overfilling of ER Ca^{2+} stores has not been observed in several studies (Kasri et al., 2006; Zatti et al., 2006; Cheung et al., 2008; Cheung et al., ; McCombs et al.). Furthermore, the putative channel function of PS has been reported by only one laboratory (Tu et al., 2006; Nelson et al., 2007; Nelson et al., ; Zhang et al., ; Nelson et al.). Accordingly, we here investigated the hypothesis that PS form Ca^{2+} permeable leak pathways in the ER. We performed a series of imaging experiments designed to directly measure ER Ca^{2+} filling rates, basal ER Ca^{2+} levels, and ER passive Ca^{2+} leak rates, using multiple cell systems, Ca^{2+} indicators, and imaging protocols. Our results fail to provide consistent evidence in agreement with predictions made by the hypothesis that PS holoproteins function as ER Ca^{2+} leak channels.

EXPERIMENTAL PROCEDURES

Transgenic mice – PS1M146V knock-in (KIN) mice were generated and characterized previously (Guo et al., 1999) and kindly provided by Dr. M. Mattson (NIH). Mice were housed in a pathogen-free, temperature and humidity controlled facility, with a 12 hr light/dark cycle. Mice were fed a standard laboratory chow diet and double distilled water, *ad libitum*. All procedures involving mice were approved by the Institutional Animal Care and Use Committee of the University of Pennsylvania, in accordance with the NIH's *Guidelines for the Care and Use of Experimental Animals*.

Isolation of primary cell lines – Primary cortical neuron (PCN) cultures were established from single E14-16 mouse embryos following described protocols (Miller, 2003). Cultures were maintained in neurobasal (Invitrogen) medium supplemented with B27 (Invitrogen), L-glutamine (Mediatech) and antibiotics and antimycotics (Invitrogen) at 37°C with 5% CO_2. Half of the medium was replaced every other day. Experiments were performed on 7- to 8-day-old cultures. Genotyping of embryos was conduced on non-cortical brain tissue obtained from each embryo, using described protocols (Guo et al., 1999). PS conditional double knock-out (PS cDKO) and WT B cells were kindly provided by Dr. D. Allman (University of Pennsylvania) and used within 10 hr of isolation.

Mouse embryonic fibroblast (MEF) cell line culture – PS double knock-out (PS DKO) MEF cells and retrovirally transfected PS DKO cells were generated previously (Repetto et al., 2007), and cultured in Dulbecco's modified Eagle's/F12 media (Invitrogen) containing 10% fetal bovine serum (Hyclone) and antibiotics and

antimycotics (Invitrogen). Retrovirally transfected MEF cell lines were maintained in 3 μg/ml puromycin (Calbiochem). All cell lines were maintained at 37°C with 5% CO_2.

MEF cell line transfection – MEF cells were transfected with the D1-ER-cameleon plasmid, kindly provided by Dr. R. Tsien (University of California, San Diego) or the D1-Golgi-cameleon plasmid, kindly provided by Dr. T. Pozzan (University of Padua, Italy), using Lipofectamine 2000 (Invitrogen) following the manufacturer's recommended protocol.

Ca^{2+} measurements – All imaging was conducted on a Nikon Eclipse microscope using a Perkin Elmer Ultraview imaging system. *Permeabilized cells:* MEF cells were incubated with 10 μM Mag-Fura 2-AM (Invitrogen) in Hepes Hank's balanced salts solution (HHBSS): HBSS supplemented with (mM): 10 Hepes, 4.2 $NaHCO_3$, 1.8 $CaCl_2$, pH 7.3, with 1% bovine serum albumin (BSA) at room temperature for 30 min. The same protocol was used to load PCN, but at 37°C and 5% CO_2. Cells were washed briefly with cytoplasmic-like media (CLM) (mM): 100 KCl, 20 NaCl, 1 EGTA, 0.375 $CaCl_2$, 20 Pipes, pH 7.3 to remove the loading solution, and then permeabilized under microscopic observation for 45 s with 2 μg/ml digitonin. Prior to recording, cells were perfused at a rate of 1-2 ml/min with CLM for 25 min. Imaging of Mag-Fura 2 was conducted by capturing images at 510 nm every 15 s following excitation at 340 nm and 380 nm. Microsoft® Excel was used to perform background subtraction for each time point, and Igor Pro was used to fit single exponential functions to the intracellular Ca^{2+} store filling and release phases, and to determine the Δ(340/380) for each cell. Using an iterative nonlinear least square fitting algorithm, the single-exponential equation $F(t) = \Delta(340/380)[1-\exp(-t/\tau_{fill}) + F_o$ was fitted to the observed data for the filling phase, where F_o is the

basal 340/380 ratio and $1/\tau_{fill}$ is the filling rate. The steady-state fill level is $F(t\rightarrow\infty)$. Similarly, the release phase was fitted with a single-exponential equation $F(t) = (F_o - F_{min}) \exp(-t/\tau_{release}) + F_{min}$, with $1/\tau_{release}$ being the release rate. Single exponential functions are the simplest model that assumes only time independence of the multiple complex processes involved in ER Ca^{2+} filling and release, and they provide reasonable fits to the observed data. For example, analyses of Figure 1 data revealed fitting errors of 8% and 17% for the fill and release phases, respectively, which reflect the 95% confidence interval. It should be noted that this analysis assumes linearity of the relationship between indicator signal and free $[Ca^{2+}]_{ER}$ and does not considered the possible effects of ER Ca^{2+} buffering on the fluorescence measurements. To confirm indicator saturation does not occur at steady-state Ca^{2+} fill levels, saturation emission ratios were determined. The average R_{max} for Mag-Fura 2 was 0.89, well above the steady-state emission ratios observed in our experiments. In intact cells the basal emission ratio of D1-ER cameleon was 88% of the total ΔR (e.g. the ratio at saturating $[Ca^{2+}]$ less the ratio at 0-Ca^{2+}), and the basal emission ratio of D1-Golgi cameleon was 54% of ΔR. Both of these values are within the linear region of the $\%\Delta R$ vs $[Ca^{2+}]$ curve (Palmer et al., 2004). All cells for each experiment were averaged for presentation and data analyses. Imaging of the cameleon Ca^{2+} indicators was conducted by capturing images at 535 nm (yellow fluorescent protein (YPF)) and 485 nm (cyan fluorescent protein (CFP)) following excitation at 440 nm. Background subtraction and data analysis were conducted as described above. Cyclopiazonic acid (CPA) was purchased from Calbiochem; $InsP_3$ from Invitrogen. *Intact cells:* Cells were loaded with 2 μM Fura 2 for 30 min in HHBSS with 1% BSA at room temperature. Images were captured every 10 s

using the emission/excitation parameters described above for Mag-Fura 2. Background subtracted 340/380 ratios for each time point were analyzed off-line for individual cells, and were averaged for each experiment for presentation. Igor Pro software was used to determine the $[Ca^{2+}]_i$·s under the ionomycin-induced Ca^{2+} release vs time curve using the standard equation (Grynkiewicz et al., 1985). Ionomycin was purchased from Invitrogen. Experiments using the D1-Golgi-cameleon indicator were conducted as described for D1-ER. Unless otherwise stated, all chemicals were purchased from Sigma-Aldrich, and were of the highest purity.

Protein extraction and immunoblotting – Cells were sonicated in lysis buffer (mM): 1% triton X-100, 50 Tris pH 8.0, 250 NaCl and protease inhibitors (Roche). Homogenates were spun at 14,000 rpm for 15 min at 4°C. The supernatant was added to 4x loading buffer (mM): 250 Tris pH 6.8, 275 sodium dodecyl sulfate, 5.7 bromophenol blue, 40% glycerol, 8% β-mercaptoethanol (Bio-Rad), incubated at 95°C for 2 min, and stored at -20°C until used. Lysates were run on SDS-PAGE or Tris Acetate 3-8% gradient gels (RyR) (NuPAGE), transferred onto a nitrocellulose membrane (GE Healthcare), blocked with 5% non-fat dried milk, and probed with primary antibody at 4°C. We used anti-amino-terminal fragment (NTF)-PS1 1:1000 (Millipore), anti-carboxy-terminal fragment (CTF)-PS1 1:500 (Cell Signaling), anti-CTF-PS2 1:2000 (Calbiochem), anti-$InsP_3R1$ 1:1000, kindly provided by Dr. S. Joseph (Thomas Jefferson University), and anti-panRyR 1:2000 (Affinity Bioreagents), and secondary horseradish peroxidase conjugated antibodies: 1:4000 anti-rat (Chemicon), 1:10,000 anti-mouse (Cell Signaling), 1:10,000 anti-rabbit (GE Healthcare). An Alpha Innotech FlourChem® Q imaging system was used to visualize proteins bands. Bands were quantified with respect

to anti-β-tubulin 1:5000 (Invitrogen) or anti-heat shock protein 90 (HSP90) 1:1000 (Cell Signaling) using AlphaView® software version 3.1.1.0.

RNA extraction, reverse transcription and real-time polymerase chain reaction (RT-PCR) – RNA was isolated using Qiagen RNeasy Mini Kit and manufacturer's recommended protocol. 5 μg total RNA was used to synthesize cDNA using Oligo(dT)12-18 primers (Invitrogen), a M-MLV Reverse Transcriptase kit (Invitrogen), and manufacturer's recommended protocols. A volume of cDNA, corresponding to 10 ng of starting RNA, was evaluated using a 7300 Real Time PCR System (Applied Biosystems), SYBR green PCR Master Mix (Applied Biosystems), 3 μM primers, and cycling of: 2 min at 50°C, 10 min at 95°C, followed by 40 cycles at 95°C for 15 s and 60°C for 1 min. Primer specificity was validated by the presence of a single PCR product for each primer set following agarose gel analysis. Additionally, a dissociation phase was used at the end of each RT-PCR assay, which yielded only a single peak for each primer set. Oligonucleotide primers were synthesized by Integrated DNA Technologies: $InsP_3R1$ forward (F): 5'-GTATGCGGAGGGATCTACGA-3' reverse (R): 5'-AACACAACGGTCATCAACCA-3', $InsP_3R2$ (F): 5'-GTCAATGGCTTCATCAGCAC-3' (R): 5'-TGAACTTCTTGGGTGGGTTG-3', $InsP_3R3$ (F): 5'-GACCGTTGTGTGGTGGAAC-3' (R): 5'-GTTCATGGGGCACACTTTG-3', RyR1 (F): 5'-CATCTGCTCTGGCTGTGAAG-3' (R): 5'-CAGAAGGGGAGATGGTCAAA-3', RyR2 (F): 5'-GCGAGGATGAGATCCAGTTC-3' (R): 5'-CTGCTGTTCTTTGTGGATGG-3', RyR3 (F): 5'-ATGTAGGTCTGCGGGAACAT-3' (R): 5'-ACCTTTGTTTGGAAGCAGGA-3', PMCA1 (F): 5'-GTGGGCAGGTCATCCAGATA-3' (R): 5'-CCATCAGCTGGAAGAAGGTC-3',

PMCA2 (F): 5'-ATCTCCCTGGGACTGTCCTT-3' (R): 5'-GCTTCACCTTCATCCTCTGC-3', PMCA3 (F): 5'-GAGGTGGCTGCTATCGTCTC-3' (R): 5'-CACCAGACACATTCCCACAG-3', PMCA4 (F): 5'-GGGAGATATTGCCCAGATCA-3' (R): 5'-CCTGGATTAGAATTCCATCTGC-3'. The geometric mean of three reference genes (Actin) (F): 5'-CCAACCGTGAAAAGATGACC- 3' (R): 5'-ACCAGAGGCATACAGGGACA- 3'), β2 microglobin (B2M) ((F): 5'-CTGACCGGCCTGTATGCTAT- 3' (R): 5'-TATGTTCGGCTTCCCATTCT- 3'), and β-glucuronidase (GUSB) ((F): 5'-GGTTTCGAGCAGCAATGGTA- 3' (R): 5'-TGCTTCTTGGGTGATGTCATT- 3') was used to control for [cDNA]. The comparative cycle threshold ($\Delta\Delta C_t$) method was used to analyze amplification data.

Statistical Analyses – Statistical analysis was performed using STATA software. Unpaired two-tailed Student's t-test or analysis of variance (ANOVA), when more than two independent variables were present, were used. Statistical significance was set at a threshold of $p < 0.05$. All data are reported as mean ± standard error of the mean (S.E.M).

RESULTS

Neuronal ER Ca^{2+} dynamics are not affected by the PS1M146V FAD mutation

To investigate whether PS form constitutively active Ca^{2+} leak channels in the ER, and if FAD-linked mutations disrupt such a function, we directly measured ER Ca^{2+} dynamics in PCN expressing endogenous levels of FAD mutant PS. We employed a PS1M146V-KIN FAD mouse, in which the M146V mutation has been targeted to the PS1 locus, resulting in expression of the FAD-linked PS allele at endogenous levels and under proper regulatory controls (Guo et al., 1999). PCN were isolated from individual embryos generated from PS1M146V$^{+/-}$ crosses to allow for comparisons between littermates (Fig. 1A). In agreement with previous reports (Guo et al., 1999), WT and PS1M146V$^{+/+}$ PCN expressed similar levels of PS1 (Fig. 1B). Also in agreement with previous reports (Thinakaran et al., 1996), we detected high levels of the mature PS1-amino-terminal fragment (NTF), but were unable to detect immature holoprotein (data not shown).

If FAD mutations disrupt the ER Ca^{2+} leak function of PS, we predicted that cells expressing PS1M146V would be able to more quickly fill depleted ER Ca^{2+} stores, have a higher steady-state ER Ca^{2+} fill level and display a decreased rate of passive Ca^{2+} leak from the ER. To test these predictions, neurons were loaded with the low affinity ratiometric Ca^{2+} indicator, Mag-Fura 2. The plasma membrane was then permeabilized with a low concentration of digitonin under visual inspection to allow escape of cytoplasmic dye and pharmacological access to intracellular Ca^{2+} stores, while leaving Mag-Fura 2-loaded intracellular compartments intact. PCN were then perfused with a cytoplasmic-like medium (CLM) lacking MgATP to allow for digitonin washout and ER

Ca^{2+} depletion. Following a baseline recording, the perfusion solution was switched to CLM containing MgATP, which stimulated the SERCA pump to fill the intracellular Ca^{2+} stores (Fig. 1, C and D). WT and PS1M146V$^{+/+}$ PCN had similar store filling rates (WT: 0.022 ± 0.0027 s^{-1}, PS1M146V$^{+/+}$: 0.018 ± 0.00096 s^{-1}; $p > 0.1$) (Fig. 1D). In addition, the steady-state level of ER filling (the asymptote approached by the single exponential fit of the filling rate) was not different (Δ(340/380): WT: 0.19 ± 0.018, PS1M146V$^{+/+}$: 0.22 ± 0.020; $p > 0.2$) (Fig. 1, C and E). Upon filling of the ER Ca^{2+} stores, the cells were perfused with CLM lacking MgATP and containing the SERCA pump inhibitor cyclopiazonic acid (CPA). This allowed for direct measurement of the passive leak of Ca^{2+} from the ER. There were no differences ($p > 0.9$) between the two groups; WT and PS1M146V$^{+/+}$ PCN had leak rates of 0.0019 ± 0.00023 s^{-1} and 0.0018 ± 0.00023 s^{-1}, respectively (Fig. 1, C and F).

Upregulation of RyR Ca^{2+} release channels does not compensate for loss of putative PS leak channels in PS1M146V$^{+/+}$ primary cortical neurons

It has been suggested that enhanced expression of the RyR Ca^{2+} release channel may compensate for loss of PS-mediated ER Ca^{2+} leak in FAD PS-expressing cells (Zhang et al.). To test this possibility, we preformed reverse transcriptase real time polymerase chain reaction assays (RT-PCR) on lysates obtained from PS1M146V$^{+/+}$ and WT PCN. PCN express RyR isoforms 2 and 3 (Fig. 2A), but not isoform 1 (data not shown). PS1M146V$^{+/+}$ PCN had ~50% the levels of RyR2 and RyR3 mRNAs compared with WT PCN (n = 2 embryos of each genotype) (Fig. 2A). Western blot analysis of PS1M146V$^{+/+}$ and WT PCN lysates (n = 4 embryos of each genotype), using an antibody

that detects all three murine RyR isoforms indicated a trend ($p > 0.05$) towards decreased total RyR protein level in PS1M146V$^{+/+}$ PCN compared to WT PCN (Fig. 2, B and C). Thus, the observed lack of differences in ER Ca^{2+} store handling between PCN from WT and PS1M146V$^{+/+}$ cannot be accounted for by upregulation of RyR expression.

ER Ca^{2+}dynamics are not altered in MEF PS DKO cells expressing FAD-linked PS1M146L

Our results do not support the hypothesis that FAD mutations in PS disrupt the passive Ca^{2+} permeability properties of the ER. To extend these studies further, we employed mouse embryonic fibroblasts (MEF) with both PS alleles genetically ablated (MEF PS DKO) (Herreman et al., 2000) that were retrovirally transduced to constitutively express either recombinant WT human PS1 (hPS1) or PS1 harboring the FAD-linked M146L mutation (hPS1M146L) (Repetto et al., 2007). These cells allow for comparisons between the two PS alleles without confounding effects of endogenous PS expression. PS DKO MEF cells lack PS1 expression, but retroviral transduction with hPS1 or hPS1M146L induced expression and rapid endoproteolysis resulting in low levels of PS1 holoprotein, with the mature N- and C-terminal fragments readily detectable (Fig. 3A).

The above described plasma membrane permeabilization protocol was applied to the two cell lines (hPS1 and hPS1M146L), using Mag-Fura 2 as the Ca^{2+} indicator. The rate of loading of Ca^{2+} into the ER (0.019 ± 0.00072 s^{-1} and 0.019 ± 0.00067 s^{-1}; $p > 0.9$), the steady-state level of store loading ($\Delta(340/380)$: 0.16 ± 0.0081 and 0.15 ± 0.0071; $p > 0.9$), and the passive Ca^{2+} leak rate (0.00022 ± 0.000062 s^{-1} and 0.00034 ± 0.000094 s^{-1}; $p > 0.2$) were not different between WT hPS1 and hPS1M146L-expressing MEF cells (Fig.

3, B-E). These findings also fail to support the notion that FAD-linked PS mutations disrupt ER Ca^{2+} leak pathways.

To explore this further, we considered that contributions from non-ER intracellular compartments might have minimized subtle differences between the cell lines. To test this, we employed the genetically-encoded, ER-targeted D1-ER-cameleon Ca^{2+} indicator in the above described permeabilization protocol. This indicator provides sensitive and specific measurements of $[Ca^{2+}]_{ER}$ (Palmer and Tsien, 2006). The hPS1 cells had a faster ER filling rate compared with the hPS1M146L cells (0.020 ± 0.00055 s^{-1} vs 0.016 ± 0.00083 s^{-1}; $p < 0.005$) (Fig. 4, A and B), a lower steady-state ER Ca^{2+} fill level (Δ(YFP/CFP): 0.53 ± 0.016 vs 0.60 ± 0.0088; $p < 0.0005$)) (Fig. 4, A and C), and a slower ER Ca^{2+} leak rate (0.0019 ± 0.00018 s^{-1} vs 0.0027 ± 0.00028 s^{-1}; $p < 0.05$)) (Fig. 4, A and D). While the elevated steady-state ER Ca^{2+} fill level observed in the hPS1M146L cells is consistent with the hypothesis that the PS1M146L allele disrupts an ER Ca^{2+} permeability, the faster rate of filling and the slower leak rate observed in these cells do not support such a model.

PS1 holoprotein level does not affect ER Ca^{2+} dynamics in MEF cells

Our results indicate that PS1M146V and PS1M146L FAD mutations do not disrupt ER Ca^{2+} leak permeability in primary cortical neurons and fibroblasts, respectively. However, it has been suggested that the Ca^{2+} leak channel function of PS resides within the holoprotein (Tu et al., 2006), whereas we observed that the ER-localized PS holoprotein rapidly undergoes endoproteolysis. We therefore performed additional experiments using cells expressing PS1 that accumulates in the ER as a holoprotein. Aspartic acid at position 257 (D257) is required for intramolecular cleavage

of PS1 into mature fragments. Mutation of this residue causes the accumulation of PS holoprotein in the ER (Dries and Yu, 2008; Fassler et al., 2010) (Fig. 3A). Importantly, this mutation was reported to be without effect on the putative Ca^{2+} leak channel function of PS1 (Tu et al., 2006). We therefore performed experiments using MEF PS DKO cells and a MEF PS DKO cell line constitutively expressing hPS1 containing a D257A missense mutation (hPS1D257A). Using the above described permeabilization protocol with Mag-Fura 2 as the Ca^{2+} indictor, we observed a difference in the steady-state Ca^{2+} fill level (Δ(340/380): 0.14 ± 0.0072 PS DKO vs 0.17 ± 0.0074 hPS1D257A; $p < 0.05$) (Fig. 3, B and D), but no differences in the Ca^{2+} filling rate (0.018 ± 0.00078 s^{-1} PS DKO vs 0.018 ± 0.00069 s^{-1} hPS1D257A; $p > 0.9$) (Fig. 3, B and C) or leak rate (0.00033 ± 0.000068 s^{-1} PS DKO vs 0.00033 ± 0.000060 s^{-1} hPS1D257A; $p > 0.9$) (Fig. 3, B and E) between the two cell lines. None of these results are consistent with the notion that PS holoprotein acts as a passive ER Ca^{2+} leak channel.

To verify these findings, we performed similar experiments using D1-ER. By comparison with the PS DKO cells, hPS1D257A-expressing cells had a faster ER Ca^{2+} filling rate (0.024 ± 0.00085 s^{-1} vs 0.020 ± 0.00038 s^{-1}; $p < 0.00005$) (Fig. 4, A and B), and a decreased steady-state ER Ca^{2+} fill level ((ΔYFP/CFP): 0.50 ± 0.011 vs 0.58 ± 0.0094; $p < 0.0005$) (Fig. 4, A and C), both results are inconsistent with PS acting as an ER Ca^{2+} leak channel. Furthermore, the two cell lines did not differ in their ER Ca^{2+} leak rates (0.0015 ± 0.00018 s^{-1} vs 0.0017 ± 0.00018 s^{-1}; $p > 0.8$) (Fig. 4, A and D).

In agreement, comparison of PS DKO and hPS1 ER Ca^{2+} filling rates (Fig. 3, B and C, Fig. 4 A and B), steady-state ER Ca^{2+} fill levels (Fig. 3, B and D, Fig. 4 A and C), and ER Ca^{2+} leak rates (Fig. 3, B and E, Fig. 4 A and D) identified only a decrease in

hPS1 steady-state ER Ca^{2+} fill level ((ΔYFP/CFP): 0.58 ± 0.0094 PS DKO vs 0.53 ± 0.016 hPS1; $p < 0.05$) (Fig. 4 A and C) with use of the D1-ER cameleon as the Ca^{2+} indicator. No other differences in ER Ca^{2+} dynamics were observed between these two cell lines. Thus, no evidence was found in these cell-based assays for a Ca^{2+} leak permeability associated with PS1, even in cells that expressed quite high levels of ER-localized PS1 holoprotein.

We considered that the permeabilization protocol might result in the loss of a critical cytoplasmic co-factor(s) required for PS Ca^{2+} leak channel function. To test this possibility, we employed D1-ER to monitor resting $[Ca^{2+}]_{ER}$ and the passive leak of Ca^{2+} from the ER in intact cells following inhibition of the SERCA pump, in PS DKO, hPS1 and hPS1D257A MEF cells. A period of perfusion in Ca^{2+}-containing Hepes Hank's balanced salts solution (HHBSS) was used to determine the resting (YFP/CFP) ratio of the cameleon indicator in each cell line (Fig. 5A). The basal (YFP/CFP) ratio was not different ($p > 0.10$ for all comparisons) among the three cell lines (YFP/CFP: PS DKO: 1.84 ± 0.017; hPS1: 1.83 ± 0.019; hPS1D257A: 1.87 ± 0.010) (Fig. 5B). Switching the perfusion solution to HHBSS containing CPA resulted in a diminution of $[Ca^{2+}]_{ER}$ due to passive leak of Ca^{2+} from the ER. However, no differences were observed ($p > 0.9$ for all comparisons) in the rates of Ca^{2+} leak from the ER among PS DKO (0.0015 ± 0.00016 s^{-1}), hPS1 (0.0013 ± 0.00020 s^{-1}), and hPS1D257A (0.0015 ± 0.00015 s^{-1}) cells (Fig. 5, A and C). These results in intact cells are in good agreement with those obtained from permeabilized cells, and again indicate that PS is not an ER Ca^{2+} leak channel.

RyR and $InsP_3R$ ER Ca^{2+} release channels do not compensate for loss of the putative PS Ca^{2+} leak channel in MEF PS DKO cells

As mentioned above, it has been suggested that upregulation of RyR may compensate for loss of the putative PS-mediated ER Ca^{2+} leak in cells expressing FAD PS alleles (Zhang et al.). However, we did not detect RyR1-3 protein (Western blot) or mRNA (RT-PCR) in the MEF cells (data not shown). To verify these molecular data, we conducted imaging experiments on permeabilized cells using the Mag-Fura 2 Ca^{2+} indicator. Following Ca^{2+} store loading, cells were perfused with 2 mM caffeine, a RyR agonist. However, no Ca^{2+} release was observed (Fig. 6A). These data suggest that upregulation of RyR is not responsible for any putative Ca^{2+} leak compensation in PS DKO cells.

Upregulation of the expression of $InsP_3R1$ has been reported in MEF PS DKO cells (Kasri et al., 2006). In agreement, RT-PCR experiments revealed a ~3-fold increase in $InsP_3R1$ mRNA in PS DKO cells compared with hPS1-expressing cells (Fig. 6B). $InsP_3R2$ and $InsP_3R3$ mRNA levels were both slightly diminished (PS DKO/hPS1 ~ 0.65) (Fig. 6B). Western blot analysis confirmed that $InsP_3R1$ protein level was elevated ($p < 0.05$) in the PS DKO cells by ~1.6-fold compared with the hPS1 cell line (Fig. 6, C and D). To evaluate the contribution of enhanced $InsP_3R1$ expression in PS DKO cells to the passive ER Ca^{2+} leak, we repeated the permeabilization experiments in the presence of 100 μg/ml heparin, an inhibitor of $InsP_3$-induced Ca^{2+} release. Consistent with a previous report (Kasri et al., 2006), there was no difference ($p > 0.8$) in the ER Ca^{2+} leak rate between the PS DKO (0.000082 ± 0.000035 s^{-1}) and hPS1 (0.000065 ± 0.000036 s^{-1}) cells in the presence of 100 μg/ml heparin (Fig. 6E). This result suggests that the

observed upregulation of $InsP_3R1$ expression in the PS DKO cells does not compensate for a putative loss of PS-mediated ER Ca^{2+} leak.

PS does not influence ER Ca^{2+} dynamics in primary B cells from PS cDKO mice

To rule out the possibility that use of stable cell lines occluded the observation of a role for the PS holoprotein as an ER Ca^{2+} leak channel, we repeated experiments using primary B cells obtained from mice in which peripheral B cells lack expression of both PS isoforms (PS cDKO) (Fig. 7). The PS2 locus in these mice was disrupted by deletion of exon 5. Exon 4 of PS1 is flanked by loxP elements, which was deleted in mature B cells using CD19+/Cre mice (Rickert et al., 1995). The Cre-mediated deletion of the floxed alleles is initiated in bone marrow pre-B cells and is completed as B cells first enter peripheral lymphoid tissues. As shown in Figure 7A, the PS cDKO B cells have no PS2 nor PS1 holoprotein expression, whereas B cells obtained from WT littermates express both PS homologs.

With Mag-Fura 2 as the ER Ca^{2+} indicator, WT B cells had a faster ($p < 0.05$) rate of ER Ca^{2+} filling compared with PS cDKO B cells ($0.025 \pm 0.0011\ s^{-1}$ vs $0.029 \pm 00015\ s^{-1}$) (Fig. 7, B and C). However, no differences in the steady-state fill level ($\Delta(340/380)$: 0.11 ± 0.0075 vs 0.10 ± 0.0080; $p > 0.5$) (Fig. 7, B and D) or the passive Ca^{2+} release rate ($0.0019 \pm 0.00049\ s^{-1}$ vs $0.0022 \pm 0.00033\ s^{-1}$; $p > 0.5$) (Fig. 7, B and E) were observed. Again, these data fail to provide support for a role for the PS holoprotein as an ER Ca^{2+} leak channel.

PS influence total cellular, but not ER, ionomycin-induced Ca^{2+} release in fibroblasts

Our results, obtained in several cell systems with two ER Ca^{2+} indicators, failed to observe a putative Ca^{2+} leak function associated with expression of PS. How can we account for the different conclusions reached by the other lab (Tu et al., 2006; Nelson et al., 2007; Nelson et al., ; Zhang et al., ; Nelson et al.)? The previous reports ascribing a Ca^{2+} channel function to PS largely utilized the increase in $[Ca^{2+}]_i$ upon application of the Ca^{2+} ionophore ionomycin as an indirect measurement of $[Ca^{2+}]_{ER}$. We therefore employed this indirect approach, using Fura 2 to measure $[Ca^{2+}]_i$. Using the four MEF cell lines described above, resting $[Ca^{2+}]_i$ in HHBSS was recorded before cells were perfused with 5 μM ionomycin in 0-Ca^{2+} HHBSS. Ionomycin caused a rapid elevation in $[Ca^{2+}]_i$ due to release from intracellular stores that subsequently declined to baseline levels. Of note, the elevation of $[Ca^{2+}]_i$ was more prolonged in the MEF PS DKO cells, and to a lesser extent in the hPS1M146L cells, compared with the hPS1 and hPS1D257A cells (Fig. 8A). The areas under the ionomycin-induced $[Ca^{2+}]_i$ vs time curves (AI; the metric used in the previous studies) in PS DKO (111 ± 4.25 μM·s) and PS1M146L (63 ± 2.21 μM·s) were larger ($p < 0.0001$) than those observed in hPS1 (45.4 ± 1.03 μM·s) and hPS1D257A (42.5 ± 1.34 μM·s) cells (Fig. 8B open bars). There was no difference in the AI between hPS1 and hPS1D257A cells ($p > 0.09$). These results recapitulate and are consistent with previous observations that lead to the hypothesis that PS function as ER Ca^{2+} leak channels, disrupted by FAD-linked mutations (Tu et al., 2006; Nelson et al., 2007; Nelson et al., ; Zhang et al., ; Nelson et al., 2011).

How can we reconcile the failure to obtain results consistent with PS as Ca^{2+} leak channels in the multiple experiments described above with the results obtained using

ionomycin? To rule out the possibility that the different AI were a result of different rates of Ca^{2+}clearance across the plasma membrane, we performed RT-PCR for plasma membrane Ca^{2+}-ATPase isoforms 1-4. However, no differences in expression of these genes were observed (data not shown). If PS holoproteins are ER Ca^{2+} leak channels, the prolongation of the ionomycin-induced Ca^{2+} signal in the PS DKO cells compared with the hPS1 cells should be specific to the ER. To test this, we repeated the ionomycin experiments using D1-ER (Fig. 8C). Contrary to findings using Fura 2, we observed a larger fall of $[Ca^{2+}]_{ER}$ in hPS1 cells compared with PS DKO cells (Δ(YFP/CFP): 0.57 ± 0.0089 vs 0.52 ± 0.0067; $p < 0.0001$) (Fig. 8D). Using this direct measure of ER Ca^{2+}, these results again do not support the proposition that PS function as ER Ca^{2+} leak channels. In contrast, these results suggest that PS may influence Ca^{2+} homeostasis within non-ER intracellular stores.

Several subcellular compartments act as Ca^{2+} stores, including the Golgi apparatus. To determine if PS influences resting $[Ca^{2+}]_{Golgi}$ or ionomycin-induced Ca^{2+} release from the Golgi, we employed D1-Golgi-cameleon (Lissandron et al.). Basal Golgi apparatus YFP/CFP ratios were not different ($p > 0.1$) between the PS DKO (2.45 ± 0.07) and hPS1 (2.61 ± 0.07) cells (Fig. 9, A and B). Switching the perfusion solution to HHBSS with 0-Ca^{2+} and ionomycin also revealed no difference ($p > 0.7$) in the Δ(YFP/CFP) between the PS DKO (0.57 ± 0.04) and hPS1 (0.59 ± 0.03) cells. This suggests that the influence of PS1 on intracellular Ca^{2+} homeostasis is not a result of changes in $[Ca^{2+}]_{Golgi}$.

PS alleles influence the kinetics of ionomycin-induced Ca^{2+} release in fibroblasts

Ionomycin is a H^+/Ca^{2+} exchanger with a 1:1 Ca^{2+} stoichiometry (Liu and Hermann, 1978). Consequently, it is expected that its rate of Ca^{2+} release will depend upon the membrane potential and pH (Fasolato et al., 1991). We reasoned that the larger AI seen here and previously (Tu et al., 2006; Nelson et al., 2007; Nelson et al., 2010; Zhang et al., 2010; Nelson et al., 2011) might reflect the influence of PS in the maintenance of intracellular ionic composition. To test this hypothesis, we repeated the ionomycin experiments in the four MEF cell lines following pre-treatment with 2.5 μg/ml monensin, a Na^+/H^+ exchanger, for 2 min to dissipate pH gradients. Monensin pre-treatment reduced the AI specifically in PS DKO (68.3 ± 1.55 μM·s; $p < 0.0005$) and hPS1M146L (54.6 ± 1.42 μM·s; $p < 0.005$) cells, whereas it was without effect on the AI for hPS1 (44.4 ± 1.75 μM·s; $p > 0.6$) and hPS1D257A (42.7 ± 1.13 μM·s; $p > 0.8$) cells (Fig. 8B filled bars). Notably, this decrease in area was due to a faster return of the (340/380) ratio to baseline. This finding suggests that the AI is influenced by factors other than the $[Ca^{2+}]_{ER}$ and is therefore not a reliable indicator of the amount of Ca^{2+} in the ER lumen.

DISCUSSION

Many studies have reported aberrant $[Ca^{2+}]_i$ homeostasis associated with expression of FAD-linked PS alleles (Stutzmann, 2005; Gandy et al., 2006; Thinakaran and Sisodia, 2006; Marx, 2007; Mattson, 2007; Bezprozvanny and Mattson, 2008; Berridge, ; Mattson). Several mechanisms have been proposed to account for these phenomena (Kasri et al., 2006; Stutzmann et al., 2006; Tu et al., 2006; Stutzmann et al., 2007; Cheung et al., 2008; Green et al., 2008; Cheung et al., 2010), including the hypothesis that FAD mutations in PSs disrupt their normal function as an ER Ca^{2+} leak channel (Tu et al., 2006; Nelson et al., 2007; Nelson et al., 2010; Zhang et al., 2010; Nelson et al., 2011). However, our observations here, as well as those from other labs (Kasri et al., 2006; Zatti et al., 2006; McCombs et al.), do not support predictions made by this hypothesis. Another mechanism proposed to explain aberrant $[Ca^{2+}]_i$ homeostasis observed in FAD PS expressing cells postulates that these mutations result in a gain-of-function interaction with the SERCA pump, and thereby result in enhanced filling of ER Ca^{2+} stores (Green et al., 2008). Although we did not analyze this hypothesis explicitly in the present study, our results do not provide consistent evidence to support it.

Our experiments employed direct monitoring of ER Ca^{2+} dynamics in three cell systems, including mouse primary cortical neurons, fibroblasts and primary PS cDKO B cells. We found that cells expressing FAD-linked mutant PS1 and cells devoid of PS expression do not have diminished ER $[Ca^{2+}]$ leak rates or consistent differences in ER loading rates or steady-state $[Ca^{2+}]_{ER}$ compared with cells expressing WT PS1. Additionally, no compensatory upregulation of RyRs (Zhang et al.) was observed that could account for failure to observe phenotypes consistent with the notion that PS

function as ER Ca^{2+} channels. Although we did observe some differences in ER Ca^{2+} dynamics between cell lines expressing WT hPS1 and those expressing FAD-linked hPS1 alleles, these differences were not consistently observed using different cell lines or experimental paradigms, calling into question their biological significance. We conclude, therefore, that PS do not function as ER Ca^{2+} leak channels.

Although we have not specifically investigated the role of PS2 in ER Ca^{2+} homeostasis in our current study, other studies (Zatti et al., 2004; Giacomello et al., 2005; Zatti et al., 2006; Brunello et al., 2009) have shown that expression of FAD mutant PS2 alleles do not result in overfilling of ER Ca^{2+} stores, consistent with our results here with PS1.

Previous reports suggesting that PS holoproteins form ER Ca^{2+} leak channels used several experimental protocols but nevertheless relied heavily on the ionomycin-induced Ca^{2+} release protocol. Initial studies employed planar lipid bilayer experiments, in which increases in conductance were observed upon incorporation of WT PS1 and PS2, but not upon incorporation of PS harboring FAD mutations (Tu et al., 2006; Nelson et al., 2007). However, single channel conductance could not be resolved, requiring noise analysis to estimate unitary currents. Studies to more firmly establish a Ca^{2+} channel basis for the conductance have not been forthcoming. Another approach used by the authors was to gauge the level of ER filling by monitoring increases in $[Ca^{2+}]_i$ following SERCA pump inhibition in intact MEF PS DKO and WT MEF (Tu et al., 2006). However, this indirect measurement is compromised by strong influences of Ca^{2+} clearance and buffering. Mag-Fura 2 was measured in permeabilized PS DKO and WT MEF cells (Tu et al., 2006) and in PS DKO transiently and stably expressing FAD mutants (Nelson et al., ; Nelson et al.)

to quantify $[Ca^{2+}]_{ER}$. However, Mag-Fura 2 may compartmentalize into many distinct intracellular compartments. As shown here, differential results can be obtained depending upon whether Mag-Fura 2 or D1-ER, as a direct indicator of $[Ca^{2+}]_{ER}$ is used. Subsequent reports employed D1-ER measurements in transfected primary hippocampal neurons from triple transgenic mice (harboring the PS1M146V-KIN mutation), but only a qualitative description was provided without quantitative analyses of leak rates (Zhang et al., 2010). The use of the AI as an indirect estimate of $[Ca^{2+}]_{ER}$ to infer conclusions regarding the role of PS in ER Ca^{2+} permeability has been the basis of the primary quantitative analysis in the previous studies (Tu et al., 2006; Nelson et al., 2007; Nelson et al., 2010; Zhang et al., 2010). When we measured the AI, we observed the phenomenon reported in these studies - PS DKO and hPS1M146L expressing fibroblasts had an enhanced area under their whole cell ionomycin-induced Ca^{2+} release vs time curve compared to WT hPS1 and hPS1D257A expressing cells. Notably, the increase in AI was mainly due to a slower decay of $[Ca^{2+}]_i$ back to basal levels. Importantly, our results obtained using the ER-targeted cameleon Ca^{2+} indicator found that this increase in AI in PS DKO cells is not due to enhanced filling of the ER.

A question is why the different protocols do not produce the same experimental answer. We observed that pre-treatment with the Na^+/H^+ exchanger monensin before ionomycin application resulted in a specific decrease in the area under the ionomycin-induced Ca^{2+} release vs time curve in PS DKO and hPS1M146L cells, whereas it was without effect on hPS1 and hPS1D257A cells. The mechanism underlying the attenuation by monensin is not clear. However, it does reveal the pitfall of utilizing the kinetics of

ionomycin-induced $[Ca^{2+}]_i$ transients to infer the Ca^{2+} content of specific organelles such as the ER.

In summary, we have shown that PS holoproteins do not form ER Ca^{2+} leak channels, in contrast to what has been previously proposed (Tu et al., 2006; Nelson et al., 2007; Nelson et al., ; Zhang et al., ; Nelson et al.). This conclusion is based on quantitative analyses of ER Ca^{2+} filling rates, steady-state ER Ca^{2+} fill levels and ER Ca^{2+} leak rates, from three different cell systems, and using different Ca^{2+} indicators. Upregulation of intracellular Ca^{2+} release channels as compensatory mechanisms cannot account for the failure to provide evidence in support of a function of PS as ER Ca^{2+} leak channels. We have identified an experimental detail that may account for the discrepancies between these conclusions and those of previous reports. Thus, use of the indirect approach to estimate $[Ca^{2+}]_{ER}$, integrating the area under the whole cell ionomycin-induced Ca^{2+} release vs time curve, is influenced by factors other than $[Ca^{2+}]_{ER}$. Our findings highlight the need to use ER-targeted Ca^{2+} indicators when using ionomycin to study ER Ca^{2+} levels. When we performed such an experiment, we found that PS does not confer an ER Ca^{2+} permeability.

ACKNOWLEDGEMENTS

We thank Dr. M. Mattson for providing PS1M146V-KIN mice, Dr. D. Allman for providing WT and PS cDKO B cells, Dr. R. Tsien for providing the ER-targeted cameleon Ca^{2+} indicator, Dr. T. Pozzan for providing the Golgi apparatus-targeted cameleon Ca^{2+} indicator, and Dr. S. Joseph for providing the anti-$InsP_3R1$ antibody. We also thank M. Muller, Dr. K. Cheung and A. Siebert for technical assistance and stimulating discussions.

CONTRIBTUIONS

D.S. and J.K.F conceived of this research and contributed to experimental design. D.E.K. developed the MEF cell lines. D.S. carried out the experiments. D.S. and D.M. contributed to data analysis. D.S., J.K.F. and D.M. contributed to the writing of the paper and all authors contributed to final edits.

FIGURES AND LEGENDS

Figure 2.1

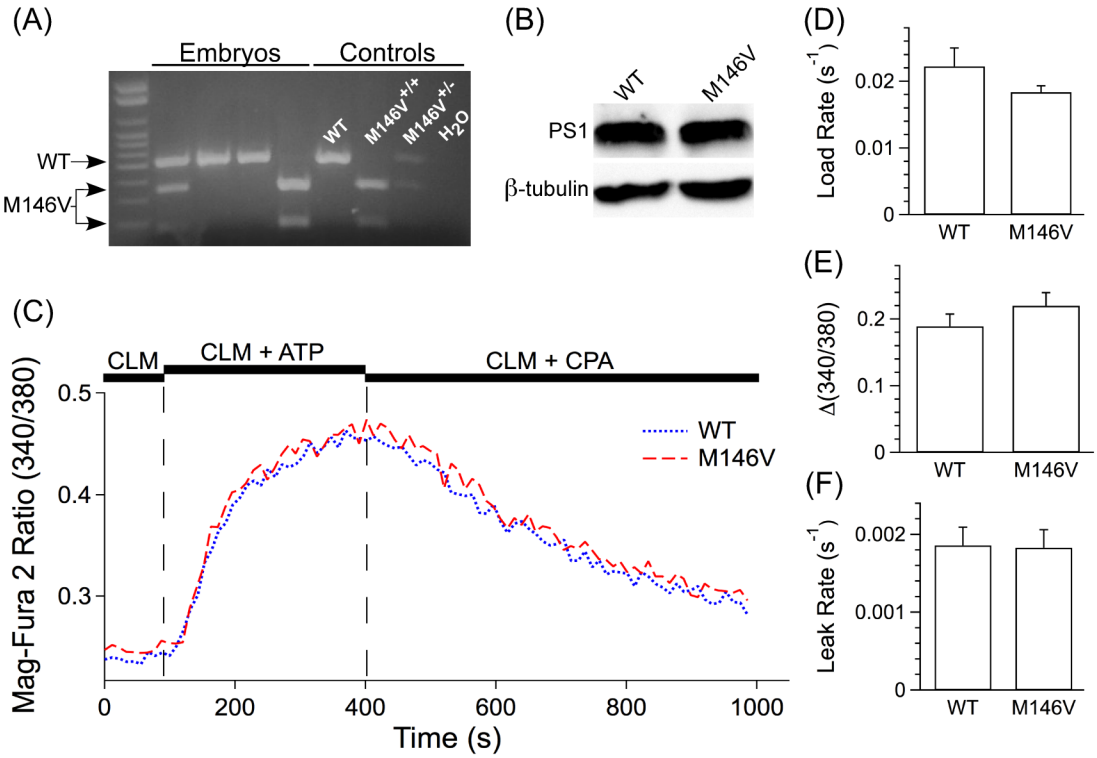

Figure 2.1 Single cell ER Ca^{2+} dynamics in wild-type (WT) and PS1M146V$^{+/+}$ (M146V) primary cortical neurons.

A, Genotyping of PCN obtained from individual embryos. *B,* Western blot analysis of PCN lysates, using an antibody specific to the PS1 amino-terminus. An antibody against β-tubulin was used as loading control. *C,* Representative single cell Mag-Fura 2 signals in permeabilized WT (blue) and M146V (red) PCN during exposure to a cytoplasmic-like medium (CLM). Addition of 1.5 mM MgATP enhanced ER luminal [Ca^{2+}] whereas removal of MgATP and addition of cyclopiazonic acid (CPA), to inhibit SERCA, revealed the passive Ca^{2+} leak. *D-F,* Summaries of single cell intracellular Ca^{2+} store loading rates following SERCA pump activation (*D*), steady-state Ca^{2+} loading (*E*), and passive Ca^{2+} leak rates following SERCA pump inhibition (*F*). *D-F,* Data presented as mean ± S.E.M. N = 3 embryos of each genotype. n ≥ 25 cells of each genotype. No differences were observed ($p > 0.05$) by Student's t-test.

Figure 2.2

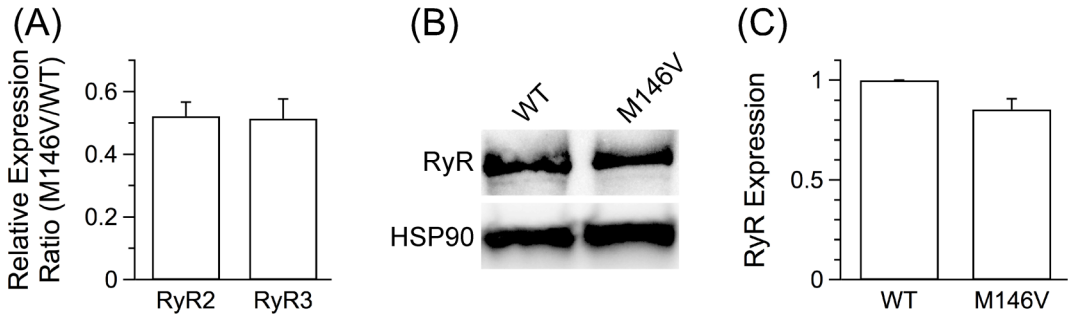

Figure 2.2 Ryanodine receptor (RyR) expression in wild-type (WT) and PS1M146V$^{+/+}$ (M146V) primary cortical neurons.

A, RT-PCR analysis of PCN RNA for RyR2 and RyR3 expression, using primer sets specific to each. The RyR1 isoform was not detected. The relative expression ratio (M146V/WT) is presented. N = 2 embryos of each genotype. *B,* RyR Western blot analysis of lysates obtained from M146V and WT PCN using an antibody that detects all three murine RyR isoforms. HSP90 used as loading control. *C,* Quantification of total RyR protein expression in WT and M146V PCN. N = 4 embryos of each genotype. *A* and *C,* Data presented as mean ± S.E.M. No differences were observed ($p > 0.05$) by Student's t-test.

Figure 2.3

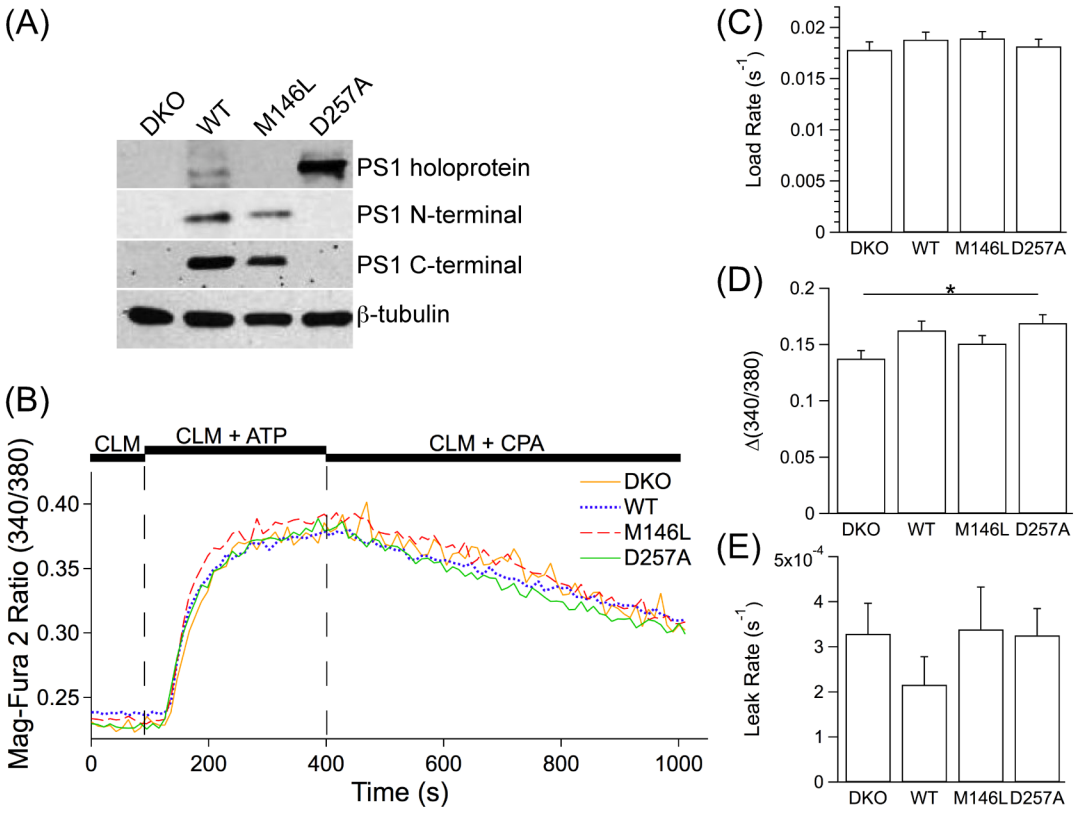

Figure 2.3 Single cell ER Ca^{2+} dynamics in permeabilized MEF PS DKO (DKO) cells and MEF PS DKO cells retrovirally transfected to express hPS1 (WT), hPS1M146L (M146L), or hPS1D257A (D257A).

A, Western blot analysis of cell lysates using antibodies specific to PS1 N- and C-termini. The N-terminus antibody also detected the PS1 holoprotein. β-tubulin used as a loading control. *B,* Representative single cell Mag-Fura 2 signals in permeabilized MEF DKO (yellow), WT (blue), M146L (red), and D257A (green) cells in response to protocols as described in Figure 1. *C-E,* Summaries of single cell intracellular Ca^{2+} store loading rates following SERCA pump activation (*C*), steady-state Ca^{2+} loading (*D*), and passive Ca^{2+} leak rates following SERCA pump inhibition (*E*). *C-E,* Data presented as mean ± S.E.M. $N \geq 3$ experiments per cell line. $n \geq 52$ cells per cell line. *$p \leq 0.05$ by ANOVA.

Figure 2.4

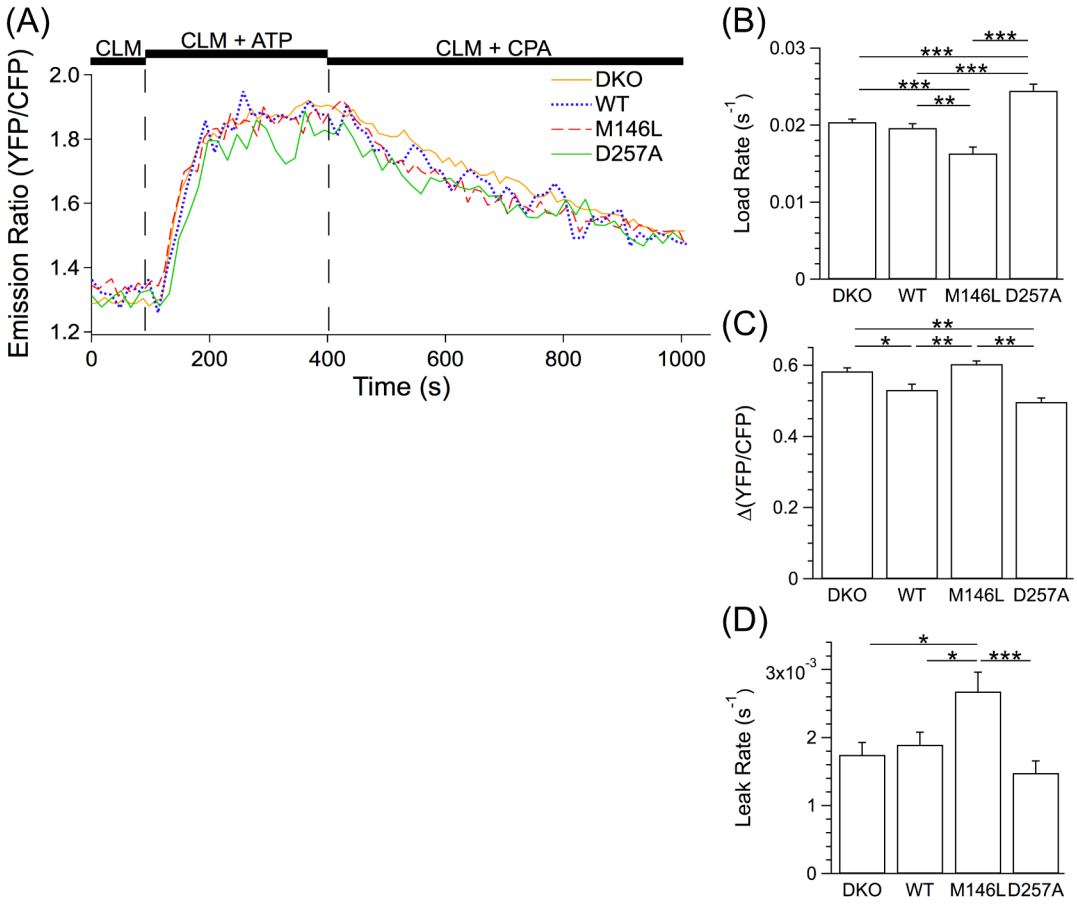

Figure 2.4 Single MEF cell ER Ca^{2+} dynamics in permeabilized cells measured with D1-ER-cameleon.

$[Ca^{2+}]_{ER}$ was imaged in D1-ER-cameleon-expressing permeabilized MEF PS DKO (DKO) cells and MEF PS DKO cells retrovirally transfected to express hPS1 (WT), hPS1M146L (M146L), or hPS1D257A (D257A). *A,* Representative single cell traces for DKO (yellow), WT (blue), M146L (red), and D257A (green) cells in response to protocols described in Figure 1. *B-D,* Summaries of single cell ER Ca^{2+} loading rates following SERCA pump activation (*B*), steady-state Ca^{2+} loading (*C*), and passive Ca^{2+} leak rates following SERCA pump inhibition (*D*). *B-D,* Data presented as mean ± S.E.M. $N \geq 3$ experiments per cell line. $n \geq 78$ cells per cell line. *** $p \leq 0.0005$; ** $p \leq 0.005$; * $p \leq 0.05$ by ANOVA.

Figure 2.5

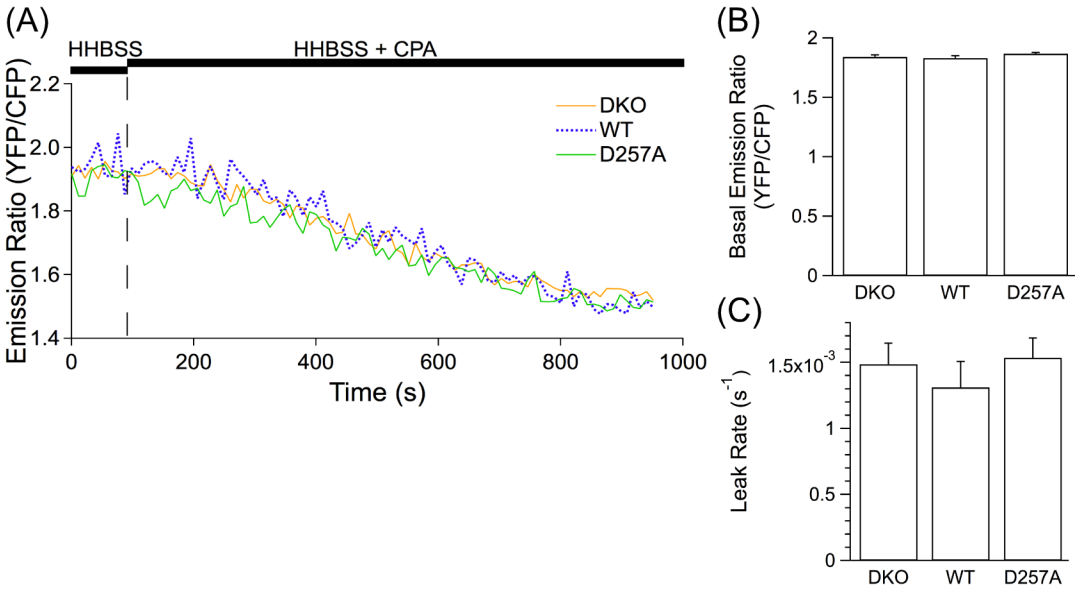

Figure 2.5 Single MEF cell ER Ca^{2+} dynamics in intact cells measured with D1-ER-cameleon.

$[Ca^{2+}]_{ER}$ was imaged in D1-ER-cameleon-expressing intact MEF PS DKO (DKO) cells and MEF PS DKO cells retrovirally transfected to express hPS1 (WT) or hPS1D257A (D257A). *A,* Representative single cell traces for DKO (yellow), WT (blue), and D257A (green) cells perfused with HHBSS and then with HHBSS containing cyclopiazonic acid (CPA) to inhibit the SERCA pump. *B-C,* Summaries of single cell $[Ca^{2+}]_{ER}$ measured as the resting YFP/CFP emission ratio (*B*), and passive Ca^{2+} leak rates following SERCA pump inhibition *(C)*. *B* and *C,* Data presented as mean ± S.E.M. N = 3 experiments for each cell line. n ≥ 38 cells for each cell line. No differences were observed ($p > 0.05$) by ANOVA.

Figure 2.6

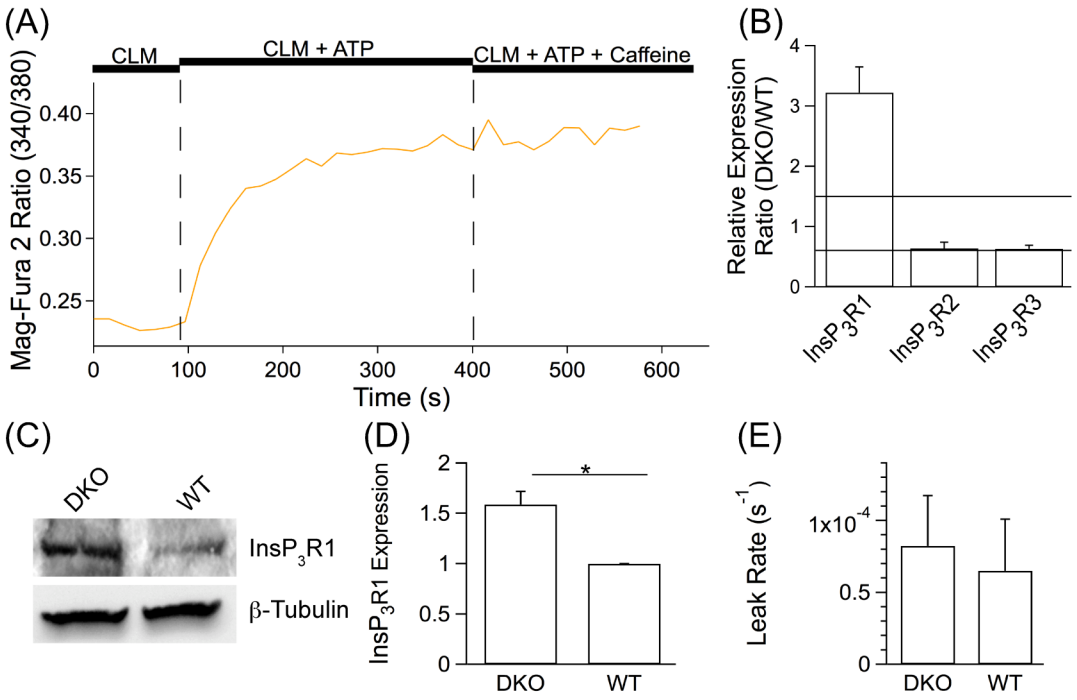

Figure 2.6 RyR and $InsP_3R$ do not compensate for loss of putative Ca^{2+} channel function of PS1.

A, Representative single cell Mag-Fura 2 signal in permeabilized MEF PS DKO cells in response to activation of the SERCA pump by addition of 1.5 mM MgATP, and subsequent responses to addition of 2 mM caffeine. *B,* Relative mRNA expression ratio of the three $InsP_3R$ isoforms (DKO/WT MEF cells) determined by RT-PCR. Area between horizontal lines indicates a less than a 1.5-fold change in expression level. *C,* Western blot analysis of DKO and WT MEF cell lysates using an $InsP_3R1$-specific antibody, and β-tubulin as loading control. *D,* Quantification of $InsP_3R1$ protein expression in DKO and WT MEF cells. *E,* Quantification of ER Ca^{2+} leak rates in the presence of 100 µg/ml heparin. *B, D and E,* Data presented as mean ± S.E.M. $N \geq 3$ experiments for each cell line. $n \geq 22$ cells for each cell line. *$p \leq 0.05$ by Student's t-test.

Figure 2.7

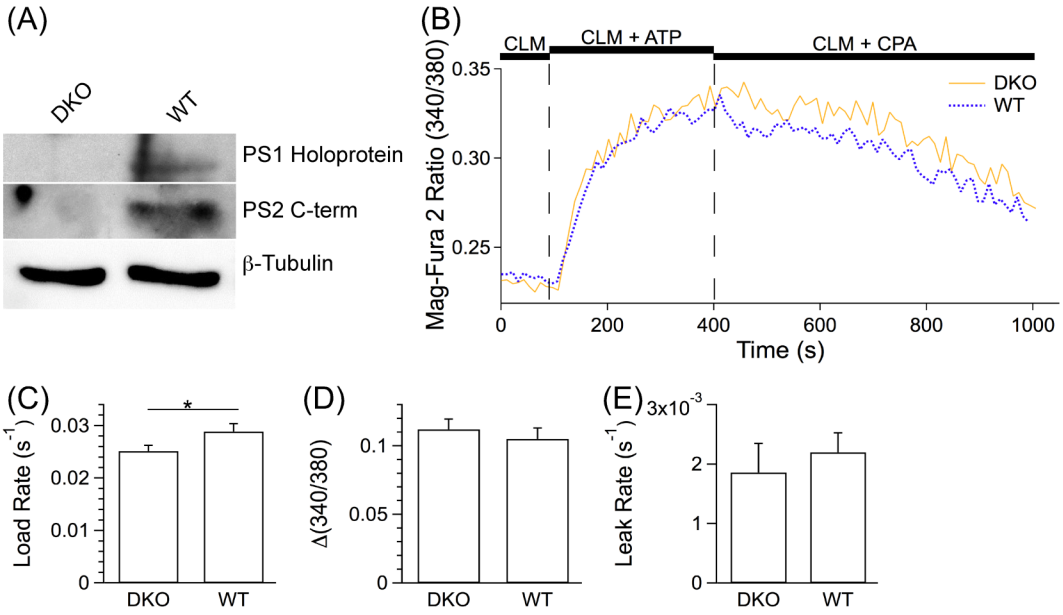

Figure 2.7 Single cell ER Ca^{2+} dynamics in permeabilized primary B cells isolated from PS cDKO (DKO) and wild-type (WT) mice.

A, Expression of PS1 holoprotein and PS2 C-terminal fragment in WT and DKO B cells. Antibodies specific to PS1 or PS2 were used to detect expression; β-tubulin as loading control. *B,* Representative single permeabilized cell Mag-Fura 2 signals for DKO (yellow) and WT (blue) cells in response to protocols described in Figure 1. *C-E,* Summaries of single cell ER Ca^{2+} loading rates following SERCA pump activation (*C*), steady-state Ca^{2+} loading (*D*) and passive Ca^{2+} leak rates following SERCA pump inhibition (*E*). *C-E,* Data presented as mean ± S.E.M. N = 4 experiments for each genotype. n ≥ 82 cells for each genotype. *p ≤ 0.05 by Student's t-test.

Figure 2.8

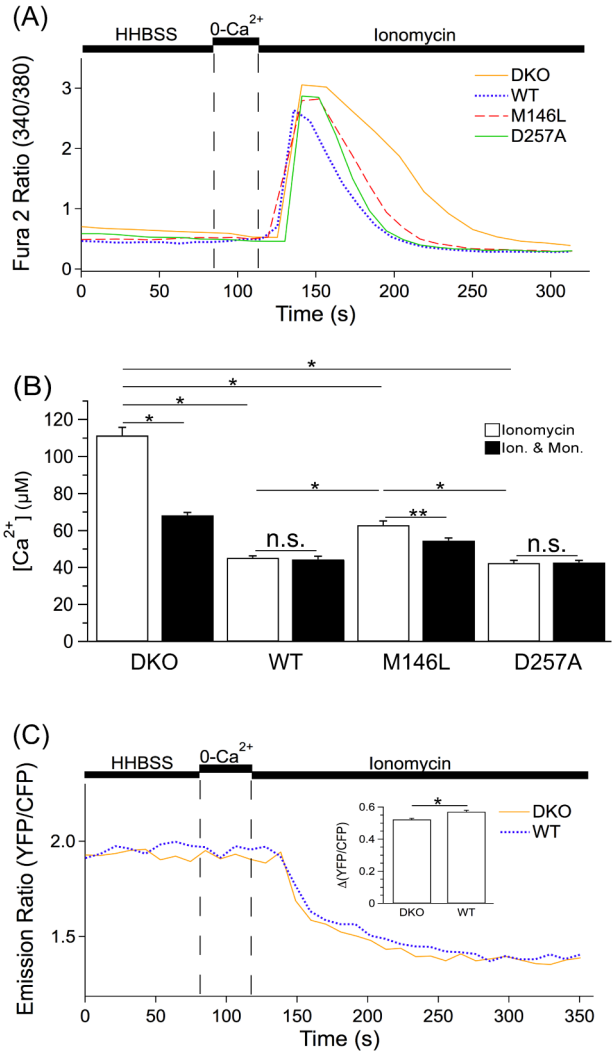

Figure 2.8 Ionomycin-induced Ca^{2+} release in MEF PS DKO (DKO) cells and MEF PS DKO cells retrovirally transfected to express hPS1 (WT), hPS1M146L (M146L), or hPS1D257A (D257A).

A, Representative single cell $[Ca^{2+}]_i$ responses in Fura 2 loaded DKO (yellow), WT (blue), M146L (red), and D257A (green) MEF cells in response to 5 μM ionomycin in the absence of extracellular Ca^{2+}. *B,* Quantification of the area under the ionomycin-induced $[Ca^{2+}]_i$ vs time curve without (open bars), or with (filled bars) pre-treatment with 2.5 μg/ml monensin for 2 min (n.s.; not significant). *C,* Representative single cell $[Ca^{2+}]_{ER}$ recordings from D1-ER-cameleon expressing DKO (yellow) and WT (blue) MEF cells in response to 5 μM ionomycin in the absence of extracellular Ca^{2+}. Insert shows quantification of the Δ(YFP/CFP) emission ratio. *B and C,* Data presented as mean ± S.E.M. N ≥ 3 experiments for each cell line. n ≥ 76 cells for each cell line. *p < 0.0001; **p < 0.005 by ANOVA *B,* or Student's t-test *C.*

Figure 2.9

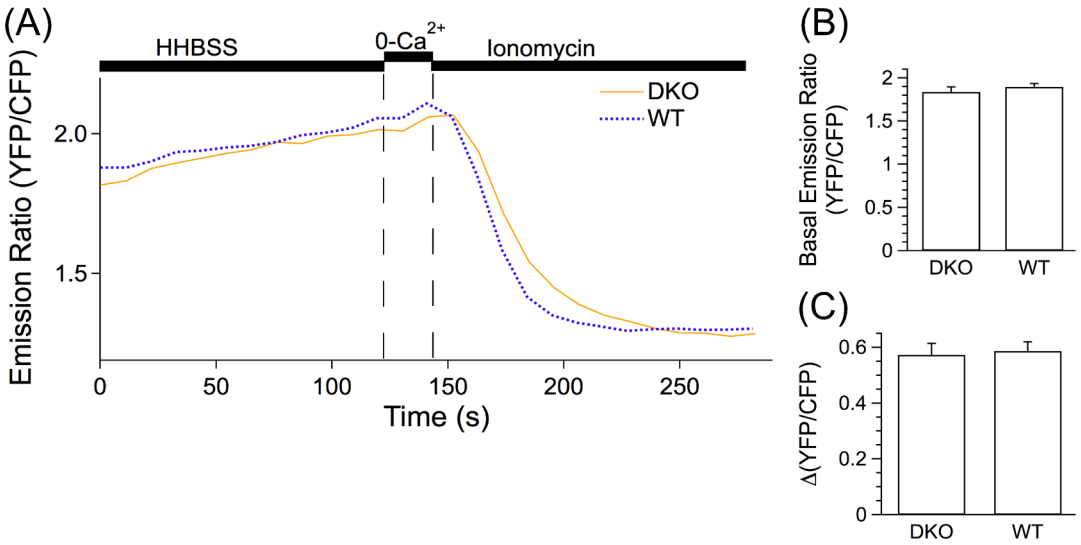

Figure 2.9 Trans-Golgi [Ca^{2+}] in MEF PS DKO (DKO) cells and MEF PS DKO cells retrovirally transfected to express hPS1 (WT).

A, Representative single cell recordings of D1-Golgi-cameleon in response to 5 μM ionomycin in absence of extracellular Ca^{2+} in DKO (yellow) and WT (blue) MEF cells. *B-C,* Summaries of the resting D1-Golgi-cameleon (YFP/CFP) ratio in each cell line (*B*), and the ionomycin-induced Δ(YFP/CFP) emission ratio of each cell line following ionomycin perfusion (*C*). N ≥ 3 experiments for each cell line. n ≥ 25 cells for each cell line. Data presented as mean ± S.E.M.

Portions to be submitted for peer-review publication

Chapter 3: Exaggerated Intracellular Calcium Signaling and Phenotypes of Two AD-mouse Models are Attenuated by Decreasing Inositol 1,4,5-trisphosphate Receptor Type 1 Protein Level

Dustin Shilling[1], Marioly Muller[1], Hajime Takano[4], Don-On Daniel Mak[1], Ted Abel[3], Doug Coulter[4] and J. Kevin Foskett[1,2,¶]

From the Departments of Physiology[1] and Cell and Developmental Biology[2], Perelman School of Medicine, University of Pennsylvania, Department of Biology[3], University of Pennsylvania, Philadelphia Pennsylvania, Division of Neurology and the Pediatric Regional Epilepsy Program[4], the Children's Hospital of Philadelphia, Philadelphia, PA 19104, USA

[¶]**Address correspondence to**: Dr. J. Kevin Foskett, Department of Physiology, 726 Clinical Research Bldg., 415 Curie Blvd., University of Pennsylvania, Philadelphia, PA 19104-6085, E-mail: foskett@mail.med.upenn.edu, Fax 215-573-6808

Number of Figures/Supplemental Figures: 6/7

Number of Pages: 64

SUMMARY

The majority of familial Alzheimer's disease (FAD) is linked to mutations in the presenilin (PS) homologs. FAD mutations have several cellular consequences, including exaggerated intracellular Ca^{2+} ($[Ca^{2+}]_i$) signaling – increased magnitudes and rates of intracellular Ca^{2+} store release and enhanced sensitivity to agonists of ER Ca^{2+} release. Single channel recordings suggest that exaggerated $[Ca^{2+}]_i$ signaling is due to an interaction between FAD mutant PS and the inositol 1,4,5-trisphosphate receptor ($InsP_3R$) that modulates its gating. However, the *in vivo* significance of the PS-$InsP_3R$ interaction to exaggerated $[Ca^{2+}]_i$ signaling and the contribution of exaggerated $[Ca^{2+}]_i$ signaling to the development of AD are unknown. If exaggerated $[Ca^{2+}]_i$ signaling is $InsP_3R$-dependent, we hypothesize that decreasing $InsP_3R$ protein expression will normalize $[Ca^{2+}]_i$ signaling. Therefore, we crossed the *Opisthotonos* (Opt) mouse, deficient in $InsP_3R1$ protein, to the PS1M146V knock-in (M146V) and triple transgenic (3xTg) AD-mouse models. We observed that the Opt allele rescues exaggerated $[Ca^{2+}]_i$ signaling *in vitro* and *ex vivo* in both AD models. Additionally, we observed that the Opt allele rescues mild cognitive impairment-(MCI) and AD-like phenotypes in these mice. In M146V mice, the Opt allele rescued enhanced hippocampal ryanodine receptor protein level, enhanced hippocampal synaptic potentiation, and constitutive activation of the CaMKIV-CREB transcriptional pathway. In 3xTg mice, the Opt allele attenuated Aβ and phospho-tau accumulation and hippocampal electrophysiology and memory impairments. These findings indicate that FAD mutant PS-associated exaggerated $[Ca^{2+}]_i$ signaling is $InsP_3R1$-mediated, occurs early in AD, and contributes to the progression of AD *in vivo*.

INTRODUCTION

Alzheimer's disease (AD) is the most common form of dementia, estimated to affect 5.4 million people in the United States with an estimated cost of 200 billion dollars in 2012 (Alzheimer's Association, 2012). It is characterized by memory impairment and its end-stage pathology, including extracellular plaques composed of Aβ and intracellular tangles composed of hyperphosphorylated tau. Most patients develop AD sporadically, but mutations in the genes encoding the presenilin (PS) homologs or the amyloid precursor protein (APP) are linked to early onset, familial AD (FAD). Although FAD presents earlier in life than sporadic AD, it shares the hallmark features of the disease suggesting overlapping pathogenic mechanisms. The observation that PSs form the catalytic core of the γ-secretase enzyme responsible for APP cleavage and Aβ release gave rise to the amyloid cascade hypothesis, which places Aβ as the key initiator of the disease (Hardy and Selkoe, 2002). However, the repeated failure of clinical trials targeting Aβ calls into question the significance of this peptide to the development of AD and highlights the need to understand how other aberrant physiology observed may contribute to AD pathogenesis.

PSs have several cellular consequences that are disrupted by FAD mutations, including a role in intracellular calcium ($[Ca^{2+}]_i$) release (LaFerla, 2002). FAD mutations in PS result in enhanced magnitudes and release rate of Ca^{2+} from the endoplasmic reticulum (ER) stores, the major Ca^{2+} store within the cell, and an increase in sensitivity to agonists of Ca^{2+} release (Stutzmann et al., 2004; Smith et al., 2005; Stutzmann et al., 2006; Stutzmann et al., 2007; Cheung et al., 2008; Cheung et al., 2010).

Accumulating evidence suggests that alterations in $[Ca^{2+}]_i$ signaling are a proximal event and may contribute to AD pathogenesis. Exaggerated $[Ca^{2+}]_i$ signaling is observed in fibroblasts obtained from FAD patients (Ito et al., 1994; Hirashima et al., 1996) and at early ages in AD mouse models (Stutzmann et al., 2004; Stutzmann et al., 2006). Ca^{2+} regulates many cellular and neuronal processes, including kinase activity, gene expression, apoptosis and necrosis, neurotransmitter release, and synaptic plasticity (Berridge, 1998; Berridge et al., 2000; Woods and Padmanabhan, 2012). In fact, multiple groups have observed that alterations in $[Ca^{2+}]_i$ signaling can affect Aβ production, tau phosphorylation and synaptic plasticity (Bashir et al., 1993; Buxbaum et al., 1994; Querfurth et al., 1997; Futatsugi et al., 1999; Hartigan and Johnson, 1999; Fujii et al., 2000; Pierrot et al., 2004; Lesne et al., 2005; Pierrot et al., 2006; Cheung et al., 2008; Green et al., 2008; Hoey et al., 2009). These reports have provided evidence in support of the calcium hypothesis of AD, which postulates that sustained changes in $[Ca^{2+}]_i$ homeostasis could provide a final common pathway for the neuropathological changes associated with AD (Khachaturian, 1994).

Although the phenomenon has been widely reported, the mechanism by which FAD PS mutations disrupt $[Ca^{2+}]_i$ signaling is controversial (Stutzmann et al., 2004; Stutzmann et al., 2006; Tu et al., 2006; Nelson et al., 2007; Stutzmann et al., 2007; Cheung et al., 2008; Green et al., 2008; Hayrapetyan et al., 2008; Rybalchenko et al., 2008; Cheung et al., 2010; Nelson et al., 2010; Zhang et al., 2010; Nelson et al., 2011; Shilling et al., 2012). Recently, it was reported that FAD mutations in PS result in a gain-of-function enhancement of the ER localized inositol-1,4,5-trisphosphate receptor's ($InsP_3R$) gating properties and enhance its ligand sensitivity (Cheung et al., 2008; Cheung

et al., 2010). Here we test this hypothesis *in vivo* using a genetic approach. We reasoned that if FAD mutant PS results in exaggerated $[Ca^{2+}]_i$ signaling through an enhancement of $InsP_3R$-mediated Ca^{2+} release, decreasing the amount of $InsP_3R$ present may restore normal $[Ca^{2+}]_i$ signaling.

$InsP_3R1$ is the predominant $InsP_3R$ in the central nervous system (Furuichi et al., 1993), and it is strongly expressed in hippocampal neurons (Hertle and Yeckel, 2007). Therefore, we crossed the *Opisthotonos* (Opt) mouse (Street et al., 1997), deficient in $InsP_3R1$ protein, to two AD mouse models, the PS1M146V knock-in (M146V) (Guo et al., 1999) and the triple transgenic (3xTg), which harbors the PS1M146V-KIN mutation and the human APP_{SWE} and tau_{P301L} transgenes (Oddo et al., 2003). The Opt allele is a spontaneous occurring in-frame deletion of exons 2 and 3 of the ITPR1 gene that encodes the $InsP_3R1$ receptor. This deletion removes two exons from the mRNA, but does not interrupt the translational reading frame (Street et al., 1997). Studies on mice with targeted deletion of the $InsP_3R1$ identified an analogous phenotype to the Opt mouse – severe ataxia, convulsions, and early death (Matsumoto et al., 1996). However, heterozygote $InsP_3R1$ knock-out mice do not demonstrate obvious impairments, showing only minor deficits in the rotating rod test without differences in spontaneous motor activity, muscle strength or walking patterns (Ogura et al., 2001).

Here we study the effects of the Opt allele on M146V-associated exaggerated $[Ca^{2+}]_i$ signaling and the contribution of exaggerated $[Ca^{2+}]_i$ signaling to the development of AD *in vivo*. We observe that a single Opt allele rescues M146V-associated exaggerated $[Ca^{2+}]_i$ signaling *in vitro* and *ex vivo* in both AD-mouse models. Further, we report that a single Opt allele rescues several phenotypes observed in these AD-mice,

including increased hippocampal ryanodine receptor (RyR) type 2 protein levels and enhanced hippocampal synaptic potentiation in the M146V mouse and AD-like pathology and hippocampal late long-term potentiation (L-LTP) and memory deficits in the 3xTg mouse. These observations suggest that exaggerated $[Ca^{2+}]_i$ signaling is a proximal event in AD and contributes to the development AD-like phenotypes in these mouse models.

EXPERIMENTAL PROCEDURES

Transgenic mice – M146V knock-in (Guo et al., 1999), 3xTg (Oddo et al., 2003) and $InsP_3R1^{Opt+/-}$ (Opt) (Street et al., 1997) mice were generated and characterized previously and kindly provided by Dr. M. Mattson (National Institutes of Health), Dr. H. Wei (University of Pennsylvania) and Dr. J. Chen (University of San Diego), respectively. Mice were housed in a pathogen-free, temperature and humidity controlled facility, with a 12 hr light/dark cycle. Mice were fed a standard laboratory chow diet and double distilled water, *ad libitum*. All procedures involving mice were approved by the Institutional Animal Care and Use Committee of the University of Pennsylvania, in accordance with the NIH's *Guidelines for the Care and Use of Experimental Animals*.

To generate $PS1M146V^{+/+}$;$InsP_3R1^{Opt+/-}$ (M146V;Opt) and control mouse lines, $M146V^{+/+}$ mice were crossed to Opt mice (both on the C57BL/6 background). First generation $M146V^{+/-}$;Opt were crossed to $M146V^{+/-}$; $InsP_3R1^{Opt-/-}$ littermates to generate the M146V;Opt line and to isolate the Opt allele on the wild-type (WT) background. Two sets of crosses were used to produce the four genotypes employed in our experiments; $M146V^{+/+}$ mice were mated to M146V;Opt mice and Opt mice were mated to WT mice. Genotyping was conducted as previously described (Street et al., 1997; Guo et al., 1999).

To generate the 3xTg;$InsP_3R1^{Opt+/-}$ (3xTg;Opt) and its respective control mouse lines, a C57BL/6 mouse carrying the Opt allele was crossed to C57BL/6/129S6 3xTg mice. First generation $3xTg^{+/-}$;Opt were either backcrossed to parental 3xTg mice to restore M146V to homozygosity and the APP_{SWE} and tau_{P301L} transgenes' copy number, or crossed to $InsP_3R1^{Opt-/-}$ littermates to generate Opt and WT control lines. Real-time polymerase chain reaction (RT-PCR) experiments were conducted on genomic DNA to

verify restoration of the APP_{SWE} and tau_{P301L} transgenes' copy number in the 3xTg;Opt line using a 7300 Real Time PCR System (Applied Biosystems), SYBR green PCR Master Mix (Applied Biosystems), 3 μM primers, and cycling of: 2 min at 50°C, 10 min at 95°C, followed by 40 cycles at 95°C for 15 s and 60°C for 1 min. Primer specificity was validated by the presence of a single PCR product for each primer set following agarose gel analysis. Additionally, a dissociation phase was used at the end of each RT-PCR assay, which yielded only a single peak for each primer set. Two sets of primers for each transgene were used. Oligonucleotide primers were synthesized by Integrated DNA Technologies: APP set 1 forward (F): 5'-GGACCAAAACCTGCATTGAT-3', reverse (R): 5'-CTGGTTGGTTGGCTTCTACC-3'; APP set 2 (F): 5'-CACCAGGAGAGGATGGATGT-3', (R): 5'-CTACCCCTCGGAACTTGTCA-3'; tau set 1 (F): 5'-GGGGGACAGGAAAGATCAG-3', (R): 5'-GTGACCAGCAGCTTCGTCTT-3'; tau set 2 (F): 5'-AAGACGAAGCTGCTGGTCAC-3', (R): 5'- GGCGATCTTCGTTTTACCAT-3'. Two sets of primers for β-actin (set 1 (F): 5'-ACTGGGACGACATGGAGAAG-3', (R): 5'-CTTTTCACGGTTGGCCTTAG-3'; set 2 (F): 5'-TACAGCTTCACCACCACAGC-3', reverse (R): 5'-TCTCCAGGGAGGAAGAGGAT-3') were used to control for [DNA]. The comparative cycle threshold ($\Delta\Delta C_t$) method was used to analyze amplification data. Six back-crosses to parental 3xTg were required to restore transgene copy number, after which two sets of crosses were used to produce the four genotypes employed in our experiments; 3xTg mice were mated to 3xTg;Opt mice and Opt mice were mated to WT mice.

Reverse transcriptase RT-PCR (RT-RTPCR) – Immediately after euthanization brains were quickly removed and washed in ice-cold phosphate buffered saline (PBS).

Hippocampal and cortical tissues were isolated and stored in RNAlater (Qiagen) following manufacturer's protocol. Samples were stored at -80° C until processing for RNA isolation. RNA was isolated using an RNeasy Mini Kit (Qiagen) and manufacturer's recommended protocol. To synthesize cDNA, a M-MLV Reverse Transcriptase kit (Invitrogen), Oligo(dT)12-18 primers (Invitrogen) and manufacturer's recommended protocols, or a high capacity reverse transcription kit (Applied Biosystems) using random primers and manufacturer's recommended protocols were used. A volume of cDNA, corresponding to 10 ng of starting RNA, was evaluated using a 7300 Real Time PCR System as described above. RyR2 (Chakroborty et al., 2009) (F): 5'-TCAAACCACGAACACATTGAGG-3', (R): 5'-AGGCGGTAAAACATGTCAG-3', PS1 (F): 5'-GTCTGAGGACAGCCACTCCA-3', (R): 5'-TGGCTCAGGGTTGTCAAGTC-3', human tau (htau) primer sets described above. The relative mRNA expression was calculated using the (ΔC_t) method, with $2^{(Ct(ref) - Ct(exp))}$ as the reported value.

Isolation of primary cell lines – Primary cortical neuron (PCN) cultures were established from single E14-16 mouse embryos following described protocols (Miller, 2003). Cultures were maintained in neurobasal (Invitrogen) medium supplemented with B27 (Invitrogen), L-glutamine (Mediatech) and antibiotics and antimycotics (Invitrogen) at 37°C with 5% CO_2. Half of the medium was replaced every third day. 1 μM cytosine β-D-arabinofuranoside was added to the culture medium 3 days after plating. Experiments were performed on 9-day-old cultures. Genotyping of embryos was conducted on non-cortical brain tissue obtained from each embryo.

Ca^{2+} measurements – All imaging was conducted on an Eclipse FN1 (Nikon) microscope with a mounted Live Scan Swept Field Confocal head equipped with an Innova 70C Ar/Kr ion laser (Coherent) and operated from NIS-Elements software (Nikon). A Cascade 512B EM-CCD camera (Photometrics) was used with continuous exposure through slit mode. ImageJ (National Institutes of Health) was used for image analysis and Microsoft® excel was used to perform background subtraction at each time point. Igor Pro was used to determine the magnitudes and rates of the Ca^{2+} indicator's fluorescence change. The magnitude of the change in Ca^{2+} indicator fluorescence is expressed as the ratio ($\Delta F/F_0$) of the change in fluorescence ($F-F_0$) relative to the resting fluorescence (F_0). To determine rates, curves were filtered using the minimum amount of Gaussian smoothing required to obtain a dominant peak in the graph of the derivative of $\Delta F/F_0$ vs time. This value is reported as $\partial(\Delta F/F_0)/\partial t$. ***PCN imaging*:** PCNs were plated onto poly-D-lysine coated glass coverslips at a density of 50,000/ml. Prior to loading, PCNs were washed once in the buffer used for loading and imaging (mM): 120 NaCl, 4 KCl, 20 HEPES, 2 $CaCl_2$, 1 $MgSO_4$, 15 glucose, then incubated for 60 min at 37°C and 5% CO_2 with 1 μM Oregon Green 488 BAPTA-1 AM (Oregon Green) (Invitrogen) and 5 μM caged $InsP_3$-AM (c-$InsP_3$) (Sirius Fine Chemicals). Since Ca^{2+} stores are depleted in PCNs of this age (Smith et al., 2005), a 90 s depolarization pulse was provided by replacing Na^+ with K^+ to a $[K^+]$ of 50 mM, followed by a 60 s recovery period prior to each photolysis experiment. Photolysis of c-$InsP_3$ was achieved by whole field illumination (350-400 nm; ~40 mW/mm^2) derived from a X-Cite 120 PC (Lumen Dynamics) coupled to a shutter (Uniblitz) and controlled by a Master-8 pulse generator (A.M.P.I.). Images were captured at 25 Hz using a 16x water immersion lens (N.A.= 0.8).

Stimulus strength was regulated by pulse duration and use of neutral density (ND) filters. Only one ultra-violet (UV) pulse was applied to each coverslip. ***Ex vivo slice imaging:*** Brains were quickly removed from 10-12 day-old pups and transferred to ice-cold sucrose artificial cerebral spinal fluid (aCSF) (mM): 87 NaCl, 75 sucrose, 2.5 KCl, 26 $NaHCO_3$, 1.25 NaH_2PO_4, 1 $CaCl_2$, 2 $MgSO_4$, 10 glucose bubbled with 95%O_2/5%CO_2. Following removal of the cerebellum, the tissue was mounted to the stage of a vibratome and 300 μm coronal sections containing hippocampal tissue were obtained. Non-hippocampal tissue was trimmed from sections prior to loading with 4 mM Oregon Green in sucrose aCSF bubbled with 95%O_2/5%CO_2 at 39°C for 60 min. Slices were then transferred to a holding chamber containing sucrose aCSF until used.

For imaging, slices were transferred to a recording chamber and perfused at a rate of 1-2 ml/min with aCSF (mM): 125 NaCl, 2.5 KCl, 26 $NaHCO_3$, 1.25 NaH_2PO_4, 2 $CaCl_2$, 1 $MgSO_4$, 10 glucose bubbled with 95%O_2/5%CO_2 for 10 min prior to the start of each experiment. Images were captured at 10 Hz using a 40x water immersion lens (N.A.= 0.8). Following a baseline recording, the solution was switched to aCSF containing 10 μM dihydroxyphenylglycine (DHPG) for the remainder of the recording period. When more than one Ca^{2+} release event was observed, only the first was analyzed.

Protein extraction and immunoblotting – PCNs or brain tissue was sonicated in lysis buffer (mM): 1% triton X-100, 5 EGTA, 50 Tris pH 7.4, 100 NaCl, protease inhibitors (Roche), phosphatase inhibitor (Roche). Homogenates were spun at 14,000 rpm for 20 min at 4°C. The supernatant was added to 4x loading buffer (mM): 250 Tris pH 6.8, 275 sodium dodecyl sulfate, 5.7 bromophenol blue, 40% glycerol, 8% β-

mercaptoethanol (Bio-Rad), incubated at 95°C for 2 min, and stored at -80°C until used. Lysates were run on SDS-PAGE or Tris Acetate 3-8% gradient gels (RyR) (NuPAGE), transferred onto a nitrocellulose membrane (GE Healthcare), blocked with 5% non-fat dried milk, and probed with primary antibody at 4°C overnight. We used anti-$InsP_3R1$ 1:1000, kindly provided by Dr. R. Neumar (University of Pennsylvania), anti-CaMKIV 1:2000 (Cell Signaling), anti-phospho-CaMKIV (Thr-196) 1:1000 (Santa Cruz Biotechnology), anti-CREB 1:2000 (Cell Signaling), anti-phospho-CREB (Ser-133) 1:1000 (Millipore), anti-c-fos 1:1000 (Cell Signaling), anti-nNOS 1:1000 (Cell Signaling), anti-BDNF 1:1000 (Millipore), anti-GAPDH 1:1000 (Millipore), anti-acetyl-histone 3 (H3) 1:1000 (Millipore) anti-panRyR 1:2000 (MA3-925, Affinity Bioreagents), anti-RyR2 1:1000 (MA3-916, Affinity Bioreagents), anti-RyR3 1:1000 (AB9082, Millipore), anti-β-amyloid 1:500 (clone 6E10, Covance), anti-htau 1:500 (clone HT7, Thermo Scientific), anti-phospho-tau 1:500 (AT8, Thermo Scientific; AT180, Thermo Scientific) and secondary horseradish peroxidase conjugated antibodies: 1:5000 anti-mouse (GE Healthcare), 1:5000 anti-rabbit (GE Healthcare). An Alpha Innotech FlourChem® Q imaging system was used to visualize proteins bands. Bands were quantified with respect to anti-β-tubulin 1:5000 (Invitrogen) or anti-heat-shock protein 90 (HSP90) 1:1000 (Cell Signaling) using AlphaView® software version 3.1.1.0.

Immunofluorescence – ***Fresh frozen tissue***: Brains were quickly removed and immediately washed in ice-cold PBS followed by embedding in OCT. Tissue was stored at -80°C until processed. 8 μm sections were obtained using a cryostat and stored at -80°C. For staining, slides were transferred to -20°C for 20 min, then immersed for 10 min in ice-cold PBS to remove OCT. Sections were fixed for 10 min in 4%

paraformaldehyde in PBS, washed 3 times for 10 min each in cold PBS, then permeabilized for 30 min at room temperature (RT) in PBS containing 5% bovine serum albumin (BSA), pH 7.4 (BSA/PBS) and 0.05% Triton X-100. Sections were blocked in PBS/BSA for an hr at RT followed by overnight incubation at 4°C in a moist chamber with anti-RyR2 1:100 (Millipore) in BSA/PBS. On the following day slides were washed 3 times for 10 min each in PBS/BSA, incubated for 90 min in 1:500 anti-rabbit 488 alexa fluor (Invitrogen) in BSA/PBS, and washed 3 times for 10 min each in PBS/BSA. Slides were mounted using anti-fade medium with DAPI (hardest, vectashield) and kept in the dark at 4°C until analysis using a Zeiss confocal microscope (LSM 710). ***Paraffin embedded tissue*** - Half of the brain was paraformaldehyde-fixed (4% in PBS) overnight at 4°C and then processed for paraffin embedding by the University of Pennsylvania Cancer Histology Core. 5 μm sections were mounted onto silane-coated slides and dried overnight at 37°C. Slices were de-paraffinized by: 2 washes in 100% xylene (Fisher Scientific) for 20 min at 37 °C, 2 washes in 100% ethanol for 10 min, one wash in 90% ethanol for 10 min, one wash in 70% ethanol for 10 min and 2 washes in H_2O for 10 min. Antigen retrieval was accomplished by placing slices in 96°C Target Retrieval Solution (Dako) for 30 minutes followed by a 20 min cool-down incubation at RT. Slides were then washed twice for 10 min in H_2O, permeabilized for 30 min in BSA/PBS containing 0.025% triton X-100, and blocked for 1 hr in BSA/PBS at RT. Following blocking, kimwipes were used to wipe around each section and primary antibodies - anti-phospho-CaMKIV (Thr-196) 1:100 (Santa Cruz), anti-phospho-CREB (Ser-133) 1:100 (Cell Signaling), and anti-$InsP_3R1$ (1:100) (kindly provided by Dr. R. Neumar) - diluted in BSA/PBS, were added to each slice. Slices were incubated in primary antibody overnight

at 4°C in a moist chamber. The next day, slices were washed 3 times for 10 min each in BSA/PBS at RT. Slices were incubated with secondary Alexa fluor antibodies (1:500) in BSA/PBS for an hr at RT, then washed 3 times for 10 min in BSA/PBS at RT, mounted using Vectashield with Dapi (Vector Laboratories) and sealed with nail polish. Slides were stored in the dark at 4°C for up to 10 wk. A Zeiss confocal scanning microscope (LSM 710) was used to visualize the sections.

Immunohistochemistry (IHC) – Half of the brain was fixed and processed as described for immunofluorescence with the following modifications: 10 μm sections were obtained and antigen retrieval was accomplished by placing slides into 96°C PT Module Buffer 1 (Thermo Scientific) (antibodies AT180 and AT8) for 30 minutes followed by a 30 min cool-down incubation at RT, or 70% formic acid for 30 min (antibodies 6E10 and 12F4). Following overnight incubation with primary antibody (AT8 1:100; AT180 1:250; 6E10 1:1000; 12F4 1:1000), a DAB detection system (Covance) was used to visualize antigen localization using manufacturer's recommended protocol. Slices were counter stained using Hematoxylin Gill 3x (Fisher) for 20 s, rinsed in tap water, and cleared by: 95% ethanol for 5 min, 2 washes in 100% ethanol for 10 min, 2 washes in xylene for 10 min. Slides were mounted using Permount (Fisher).

Enzyme-linked immunosorbent assay (ELISA) – Invitrogen ELISA kits were used to determine Aβ content in cortical and hippocampal lysates following the manufacturer's recommended protocol. Briefly, homogenates were prepared from dissected cortical or hippocampal tissue by adding eight v/w 5 M guanidine buffered with 50 mM Tris HCl pH 8.0 in 90 μl aliquots and grinding thoroughly with a hand-held pestle after each addition. Homogenates were then rocked at RT for 3-4 hrs. All lysates were

stored at -80°C till used. All samples of each age were run on a single ELISA plate following manufacturer's recommended protocol. Plates were read on a Spectr max 340 pc (Molecular Devices). Plate results were normalized to total [protein] in each homogenate as determined by protein assay (Bio-Rad) using an Evolution 60 spectrophotometer (Thermo Scientific).

Hippocampal electrophysiology – Mice were sacrificed by cervical dislocation, and hippocampi quickly collected in ice-cold oxygenated sucrose aCSF bubbled with 95% O_2/5% CO_2. Transverse, 400 μm hippocampal slices were obtained using a Mcllwain tissue chopper, transferred to an interface recording chamber, and perfused (1-2 ml/min) with oxygenated aCSF containing (mM): 124 NaCl, 4.4 KCl, 1.3 $MgSO_4$, 1 NaH_2PO_4, 26.2 $NaHCO_3$, 2.5 $CaCl_2$ and 10 D-glucose at 28°C for at least 2 hr prior to recording. A bipolar 0.5 mm nichrome stimulating electrode (AM Systems) was positioned in the Shaffer collateral pathway and a glass micropipette (2-5 mΩ) (AM Systems) filled with oxygenated aCSF was placed adjacent to the stimulating electrode in the CA1 hippocampal region. Data were acquired using Clampex 9.2 and a Digidata 1322 A/D converter (Axon Instruments) at 20 KHz and low pass filtered at 2 KHz. Slices were used only if they provided a maximum amplitude response ≥ 5 mV. Synaptic strength was measured by the initial slope of the field excitatory post-synaptic potential (fEPSP) and the pre-synaptic fiber volley (PFV) amplitude resulting from application of voltages to the stimulation electrode starting at 30 V and decreasing stepwise until the PFV was not longer detected. Long-term potentiation (LTP) experiments were conducted by applying a stimulus strength that elicited 40% of the maximum evoked fEPSP amplitude.

The first 20 min baseline values were averaged and used to normalize the initial fEPSP slopes. Tetani were applied at 100 Hz for 1s.

Behavioral experiments – All behavioral experiments were conducted in the Behavioral Core at the University of Pennsylvania. Mice were singly-housed for one week followed by five days of handling prior to testing. Handling was done in the experimental room for 90 s per day for each mouse. Spatial object recognition experiments were conducted as previously described (Wimmer et al., 2011). Briefly, mice were placed into the training arena four times, each for 10 min. Between trials, mice were returned to their home cage. The first session was a context habituation period without objects in the arena, whereas for the next 3 sessions mice were placed into the arena with 2 distinct objects. The objects used were a glass bottle, a metal rectangular tower, and a plastic cylinder tower. Objects and the training arena were cleaned with 70% ethanol prior to each session. 24 hr after training, mice were placed back into the arena for a 10 min trial with one of the objects displaced to a new location while the other object was not moved. All sessions were recorded using a digital camera and subsequently scored for time spent exploring each object, blinded to the mouse genotype. Object exploration was defined as the amount of time a mouse was oriented toward the object with its nose within 0.5 cm of the object. Object preference was calculated as the time spent exploring the displaced object relative to the total time spent exploring both objects.

Open-field testing was conducted to assess locomotion. Mice were brought to the testing room and allowed to acclimate for 30 min prior to testing. Mice were placed into a Plexiglas arena (14 in^2) with a white floor and clear walls. Activity data was collected as

beam breaks during a 10 min trial for each mouse using a Photobeam Activity System (San Diego Instruments).

Fear conditioning tests were conducted by placing mice into a conditioning chamber (Med Associates) for 2 min prior to the onset of a 2800 Hz, 85 dB tone for 30 s. During the last 2 s of the tone a 0.7 mA continuous foot shock was applied. The mouse remained in the chamber for 30 s following foot shock application, then was returned to its home cage. 24 hr later the mouse was tested for time spent frozen (motionless except for respiratory movements) in the chamber during a 3 min period. Mice were also placed into a novel chamber with unique context. Following a 2 min habituation period mice were tested for time spent frozen in response application of a 2800 Hz, 85 dB tone during a 3 min period. Scoring of time spent frozen was automated using FreezeScan software.

Materials – The photoactivatable membrane-permeant $InsP_3$ was dissolved in dimethyl sulfoxide (DMSO) with 10% Pluronic F-127 to a stock concentration of 2.5 mM, aliquoted and stored at -80°C until needed. Each aliquot was thawed only once. Oregon Green was dissolved in DMSO with 10% Pluronic F-127 to a stock concentration of 4 mM and used fresh daily. Unless otherwise stated, all chemicals were purchased from Sigma-Aldrich, and were of the highest purity.

Statistical Analyses – Statistical analysis was accomplished by performing hypothesis-driven unpaired two-tailed Student's t-tests using STATA software. To determine if the AD mouse models were abnormal, the null hypothesis that AD mice = WT was tested. If rejected, two additional Student's t-tests were perform to determine if the Opt allele attenuated or rescued the abnormality; AD-mice;Opt = WT and AD-mice;Opt = AD-mice. Multiple testing adjustments were not necessary since all Student's

t-tests performed were hypothesis driven. For LTP data, STATISTICA software was used to conduct repeated ANOVA tests. Statistical significance was set at a threshold of $p \leq 0.05$. All data are reported as mean ± standard error (SE).

RESULTS

M146V-associated exaggerated $[Ca^{2+}]_i$ signaling is $InsP_3R1$-dependent

If FAD mutant PS-associated exaggerated $[Ca^{2+}]_i$ signaling is due to an enhancement of $InsP_3R$ gating (Cheung et al., 2008; Cheung et al., 2010), we predict that decreasing $InsP_3R$ protein levels will normalize the phenotype. To test this hypothesis, we employed the Opt mouse. This spontaneous mutation acts as a null-like allele, resulting in approximately half of the level of $InsP_3R1$ hippocampal protein compared to WT littermates (Supp. Figs. 1E, 2A, 3A & 5, B and F), without compensatory upregulation of $InsP_3R2$ or $InsP_3R3$ expression (data not shown). We crossed the Opt mouse to the M146V AD-mouse model that contains a targeted FAD mutation in the endogenous PS1 locus (Guo et al., 1999) (Supp. Fig. 1, A and B). In agreement with previous reports (Guo et al., 1999), we found that PS is expressed at similar levels in M146V and WT mice, and we did not observe an effect of the Opt allele on PS expression (Supp. Fig. 5G).

The Opt allele rescues M146V-associated exaggerated $[Ca^{2+}]_i$ signaling in vitro

To determine if the Opt allele is capable of normalizing FAD mutant PS-associated exaggerated $[Ca^{2+}]_i$ signaling, PCN cultures were established from single embryonic day 14-16 embryos. Following 9 days *in vitro* (DIV), PCNs obtained from M146V;Opt embryos have 0.48 ± 0.05 ($n = 4$; $p < 0.005$) of the amount of $InsP_3R1$ protein as WT PCNs, whereas M146V PCNs have a similar amount (1.02 ± 0.08, $n = 4$) compared to WT (Supp. Fig. 2A). Additionally, at 9-DIV M146V PCNs do not express different amounts of RyR protein compared to WT (M146V 2.35 ± 0.61, $n = 4$; $p = 0.11$) (Supp. Fig. 2A).

For imaging, PCNs were loaded with the Oregon Green Ca^{2+} indicator and a membrane permeable, caged $InsP_3$. Because PCNs of this age have depleted Ca^{2+} stores (Smith et al., 2005), we included a 90 s perfusion with 50 mM K^+ to the imaging protocol (data not shown). This perfusion step depolarizes the PCN, causing voltage-gated Ca^{2+} channels to open, thereby allowing Ca^{2+} to enter the cell. Some of this Ca^{2+} is then taken up into $InsP_3$ sensitive Ca^{2+} stores. After repolarization, a 10 s baseline recording was obtained, followed by application of a whole-field UV light pulse of varying duration (~1-500 ms), providing fine control of [$InsP_3$] (Fig. 1, A and B).

To determine if the Opt allele normalizes M146V-associated exaggerated $[Ca^{2+}]_i$ signaling, we analyzed both the magnitudes ($\Delta F/F_0$) and rates ($\partial(\Delta F/F_0)/\partial t$) of Oregon Green fluorescence change following UV illumination. When the magnitudes of the increase in somal [Ca^{2+}] were analyzed, we observed that PCNs obtained from M146V embryos have larger magnitudes of $[Ca^{2+}]_i$ signals compared to PCNs obtained from WT embryos in response to UV pulse durations of 50 ms ($\Delta F/F_0$: M146V 0.25 ± 0.02 vs WT 0.16 ± 0.02; $p < 0.005$), 100 ms ($\Delta F/F_0$: M146V 0.24 ± 0.03 vs WT 0.17 ± 0.01; $p < 0.05$), and 500 ms ($\Delta F/F_0$: M146V 0.23 ± 0.02 vs WT 0.18 ± 0.02; $p < 0.05$) (Fig. 1, B and D). No differences in magnitudes of $[Ca^{2+}]_i$ signals were observed in response to UV flash durations of 25 ms, 10 ms, or 20 ms with a 4xND filter in place (~5 ms exposure). Only M146V PCNs responded to a 16 ms UV illumination with a 16xND filter in place (~1 ms exposure) (Fig. 1, B and D). When the magnitudes of $[Ca^{2+}]_i$ signals were analyzed for PCNs obtained from M146V;Opt embryos, we did not observe differences in response to UV pulse durations of 50 ms, 100 ms or 500 ms compared to WT PCNs ($\Delta F/F_0$: 50 ms 0.16 ± 0.02, 100 ms 0.17 ± 0.02, 500 ms 0.15 ± 0.02) (Fig. 1, B and D).

These findings suggest that the Opt allele rescues the exaggerated magnitudes of $[Ca^{2+}]_i$ signals observed in M146V PCNs.

We then analyzed the rates of Ca^{2+} release from intracellular stores. We observed that PCNs obtained from M146V embryos have faster Ca^{2+} stores release rates, compared to PCNs obtained from WT embryos in response to UV pulse durations of 25 ms ($\partial(\Delta F/F_0)/\partial t$): M146V 0.19 ± 0.04 s^{-1} vs WT 0.08 ± 0.01 s^{-1}; $p < 0.05$), 50 ms ($\partial(\Delta F/F_0)/\partial t$): M146V 0.37 ± 0.05 s^{-1} vs WT 0.12 ± 0.04 s^{-1}; $p < 0.005$), 100 ms ($\partial(\Delta F/F_0)/\partial t$): M146V 0.41 ± 0.09 s^{-1} vs WT 0.13 ± 0.02 s^{-1}; $p < 0.005$), and 500 ms ($\partial(\Delta F/F_0)/\partial t$): M146V 0.33 ± 0.04 s^{-1} vs WT 0.14 ± 0.02 s^{-1}; $p < 0.005$) (Fig. 1, B and E). No differences in Ca^{2+} release rates were observed in response to UV flash durations of 10 ms or 20 ms with a 4xND filter in place. Interestingly, M146V;Opt PCN Ca^{2+} release rates in response to 50 ms, 100 ms or 500 ms UV illuminations were not different than WT PCN Ca^{2+} release rates ($\partial(\Delta F/F_0)/\partial t$): 50 ms 0.13 ± 0.03 s^{-1}, 100 ms 0.14 ± 0.03 s^{-1}, and 500 ms 0.15 ± 0.03 s^{-1}) (Fig. 1, B and E). However, in response to 25 ms UV exposures, M146V;Opt PCNs had slower Ca^{2+} release rates ($\partial(\Delta F/F_0)/\partial t$): 0.05 ± 0.01; $p < 0.05$) compared to PCNs obtained from WT embryos (Fig. 1, B and E). These results indicate that the Opt allele rescues the exaggerated release rates of Ca^{2+} from intracellular stores observed in M146V PCNs.

The Opt allele rescues M146V-associated exaggerated $[Ca^{2+}]_i$ signaling ex vivo

The experiments described above suggest that the Opt allele is capable of rescuing FAD mutant PS-associated exaggerated $[Ca^{2+}]_i$ signaling. The *in vitro* experimental system used has the benefit of providing fine control of $[InsP_3]$, but it may not accurately

reflect the *in vivo* scenario. To better understand the effects of the Opt allele on exaggerated $[Ca^{2+}]_i$ signaling *in vivo,* we employed an experimental paradigm using acute hippocampal slices obtained from post-natal day 10-12 (P10-12) mice. At this age hippocampi obtained from M146V;Opt mice have 0.57 ± 0.06 (n = 6; $p < 0.005$) of the amount of $InsP_3R1$ protein as those obtained from WT mice, whereas hippocampi obtained from M146V mice have a similar amount of $InsP_3R1$ protein (1.32 ± 0.15, n = 6) compared to WT (Supp. Fig. 3A). We did not observe differences in hippocampal RyR protein levels between M146V (1.11 ± 0.12, n = 6; p = 0.40) and WT P10-12 mice using a pan-RyR antibody that detects all three murine RyR isoforms, or when using RyR2 (M146V 1.12 ± 0.18, n = 6; p = 0.45) or RyR3 (M146V 1.28 ± 0.23, n = 6; p = 0.27) isoform specific antibodies (Supp. Fig. 3A).

To determine the effect of the Opt allele on $[Ca^{2+}]_i$ signaling, hippocampal slices were loaded with the Oregon Green Ca^{2+} indicator and granular cell layer neurons in the dentate gyrus were imaged. Following a baseline recording, 10 μM DHPG, a group I metabotropic glutamate receptor agonist, was used to induce $InsP_3R$-mediated Ca^{2+} release (Fig. 2, A and B; Supp. Fig. 3C). This release is independent of neuronal depolarization (Supp. Fig. 3, C and D). We observed that neurons in slices obtained from M146V animals displayed enhanced magnitudes and faster rates of Ca^{2+} release compared to WT ($\Delta F/F_0$: M146V 0.34 ± 0.02 vs WT 0.23 ± 0.02; $p < 0.005$, $\partial(\Delta F/F_0)/\partial t$: M146V 0.23 ± 0.02 s^{-1} vs WT 0.11 ± 0.01 s^{-1}; $p < 0.005$) (Fig. 2, B, C and D). In agreement with the findings from the *in vitro* system, hippocampal neurons in slices obtained from M146V;Opt mice did not display enhanced magnitudes or release rates compared to WT (M146V;Opt $\Delta F/F_0$ 0.25 ± 0.02; $\partial(\Delta F/F_0)/\partial t$) 0.14 ± 0.01) (Fig. 2, B, C

and D). These results indicate that the Opt allele rescues agonist-induced exaggerated $[Ca^{2+}]_i$ signaling observed in acute hippocampal slices from M146V P10-12 animals.

Exaggerated $[Ca^{2+}]_i$ signaling underlies MCI-like phenotypes of the M146V AD-mouse model

Having demonstrated that the Opt allele rescues FAD mutant PS-associated exaggerated $[Ca^{2+}]_i$ signaling, we wanted to determine the contribution of exaggerated $[Ca^{2+}]_i$ signaling to the development of AD. The M146V mouse does not develop the canonical histopathology associated with AD, but it does recapitulate several abnormalities reported in pre-symptomatic FAD mutant PS carriers and patients suffering from mild cognitive impairment (MCI), a condition commonly preceding AD. These include enhanced RyR2 expression (Stutzmann et al., 2006; Bruno et al., 2012) and hippocampal hyperactivity (Dickerson et al., 2005; Odero et al., 2007; Auffret et al., 2010; Quiroz et al., 2010; Reiman et al., 2012). The M146V;Opt mouse provides the opportunity to determine if exaggerated $[Ca^{2+}]_i$ signaling contributes to these phenotypes.

The Opt allele rescues enhanced RyR protein level in M146V mice

To determine the contribution of exaggerated $[Ca^{2+}]_i$ signaling to hippocampal RyR2 upregulation, we conducted Western blot analysis on hippocampal lysates obtained from 5-wk-old animals. At this age, hippocampi from M146V;Opt mice have 0.57 ± 0.03 ($n = 7$; $p < 0.005$) of the amount of $InsP_3R1$ protein compared to WT, whereas hippocampi obtained from M146V mice have 0.95 ± 0.09 ($n = 7$) of the amount of $InsP_3R1$ protein as WT (Supp. Fig. 5B). Western blot analysis using a pan-RyR antibody revealed increased RyR protein in hippocampal lysates obtained from 5-wk-old M146V

animals (1.77 ± 0.33, n = 6; $p < 0.05$) compared to WT (Fig. 3A). Isoform specific antibodies identified that this increase in M146V hippocampal RyR protein is predominantly due to increased RyR2 protein (1.27 ± 0.08, n = 4; $p < 0.05$) without changes in RyR3 protein level (1.01 ± 0.11, n = 5) compared to WT (Fig. 3A). Interestingly, we did not observe enhanced RyR protein levels in hippocampi obtained from M146V;Opt mice using either a pan-RyR antibody (1.11 ± 0.15, n = 6), or a RyR2 specific antibody (0.60 ± 0.11, n = 4). In fact, we observed a decrease in RyR2 protein in M146V;Opt hippocampal lysates ($p < 0.05$) compared to WT (Fig. 3A). To confirm these biochemical data we performed immunofluorescence experiments on brain slices obtained from 5-wk-old animals using the RyR2 specific antibody. In agreement with the Western blot findings, we observed an overall enhancement in hippocampal RyR2 staining in slices obtained from M146V mice compared to WT, which was most prominent in hippocampal region CA1 (Fig. 3B; Supp. Fig. 4B). The enhanced RyR2 staining was not observed in slices obtained from M146V;Opt mice (Fig. 3B; Supp. Fig. 4B). This suggests that the Opt allele rescues enhanced RyR2 protein levels in M146V mice.

To verify that the observed RyR2 upregulation in 5-wk-old M146V animals is not due to developmental differences in RyR expression (Mori et al., 2000), we repeated our experiments in adult (3-mth-old) mice. Hippocampi from adult M146V;Opt mice have 0.48 ± 0.06 (n = 6; $p < 0.005$) of the amount of $InsP_3R1$ protein compared to WT, whereas hippocampi obtained from M146V mice have 1.20 ± 0.17 (n = 6) of the amount of $InsP_3R1$ protein as WT (Supp. Fig. 5F). Again, we observed that M146V mice have increased levels (1.42 ± 0.15, n = 7; $p < 0.05$) of hippocampal RyR2 protein compared to

WT. In contrast, RyR2 protein levels in M146V;Opt hippocampal lysates (0.91 ± 0.19, n = 7) were not different than WT (Supp. Fig. 4C). Therefore, developmental differences do not account for the observed elevation in hippocampal RyR2 protein level in M146V mice.

In contrast to previous reports (Chakroborty et al., 2009), we did not observe that the increase in RyR2 hippocampal protein is due to increased transcription; RT-RTPCR failed to reveal differences in hippocampal RyR2 mRNA levels between M146V and WT mice at 5-wks and 3-mths-of-age (Supp. Fig. 4, A and D).

The Opt allele rescues enhanced hippocampal potentiation in young and adult M146V mice by attenuating aberrant transcriptional pathway activation

Early biomarkers for AD have remained elusive. However, increases in hippocampal activation during the performance of associative memory tasks are observed in pre-symptomatic FAD mutant PS carriers and MCI patients (Dickerson et al., 2005; Quiroz et al., 2010; Reiman et al., 2012) and represent a deleterious process rather than a beneficial compensatory function (Bakker et al., 2012; Sanchez et al., 2012). Although the cause of this hyperactivity is not known, studies on M146V mice provide a similar observation - enhanced synaptic potentiation in hippocampal region CA1 early LTP (E-LTP) studies. This enhancement is postulated to be a result of exaggerated $[Ca^{2+}]_i$ signaling (Odero et al., 2007; Auffret et al., 2010) and is manifested as larger post-tetanus potentiation and maintained increases in synaptic strength in response to a single increase in post-synaptic $[Ca^{2+}]$. Normally multiple increases in post-synaptic $[Ca^{2+}]$ are normally required to activate the *de novo,* CREB-dependent gene expression required for long-lasting L-LTP.

To determine if normalizing exaggerated $[Ca^{2+}]_i$ signaling attenuates enhanced synaptic potentiation in M146V mice, we conducted single tetanus-induced hippocampal E-LTP studies on 5-wk-old animals. To accomplish this, we analyzed fEPSP in hippocampal area CA1 following stimulation of the Schaeffer collateral pathway. We did not observe any difference in basal synaptic transmission between M146V;Opt, M146V, and WT mice when we analyzed the slopes of the input (PFV)-output (fEPSP slope) curves (M146V;Opt 1.78 ± 0.31 ms^{-1} vs M146V 1.91 ± 0.19 ms^{-1} vs WT 1.91 ± 0.24 ms^{-1}), the ratio of the fEPSP slope to the PFV amplitude at each applied voltage (M146V;Opt 2.89 ± 0.49 ms^{-1} vs M146V 4.18 ± 0.75 ms^{-1} vs WT 3.21 ± 0.31 ms^{-1}), or the maximum evoked fEPSP slope (M146V;Opt 7.5 ± 1.0 mV/ms vs M146V 9.5 ± 1.9 mV/ms vs WT 8.7 ± 1.1 mV/ms) (Fig. 4A; Supp. Fig. 5A).

Following a 20 min baseline recording we applied a single 100 Hz, 1 s stimulus to the Schaeffer collateral pathway and monitored the ensuing changes in synaptic strength for 2 hr. Consistent with previous reports, we observed larger potentiation during the first 10 min post-tetanus in slices obtained from M146V mice (245 ± 13% of baseline, n = 5; $p < 0.005$) compared to those obtained from WT animals (176 ± 9% of baseline, n = 6) (Fig. 4B). We also observed maintained increases in synaptic strength in slices obtained from M146V mice. During the last 20 min of the recordings, slices from M146V mice demonstrated fEPSP slopes of 182 ± 7% of baseline (n = 5; $p < 0.005$), whereas slices obtained from WT mice demonstrated fEPSP slopes of 121 ± 7% of baseline (n = 6) (Fig. 4B). Slices obtained from M146V;Opt mice did not exhibit differences in post-tetanus potentiation (168 ± 10% of baseline, n = 5), or in synaptic strength during the last 20 min of recording (115 ± 7% of baseline, n = 5) compared to WT mice. These

observations suggest that the Opt allele rescues the enhanced hippocampal potentiation observed in M146V mice.

Recently, it was reported that M146V mice display constitutive activation of the Ca^{2+}-dependent CaM kinase IV (CaMKIV) cAMP response element binding protein (CREB) transcriptional pathway (Muller et al., 2011). This constitutive activation results in increased expression of CREB-dependent genes known to be important for the conversion of E-LTP to L-LTP (Lu et al., 2008; Steinert et al., 2010; Muller et al., 2011). To provide mechanistic insight into the Opt allele's rescue of enhanced hippocampal potentiation in the M146V mouse, we investigated the activation of this transcriptional pathway. To accomplish this, we performed Western blot analysis on hippocampal lysates obtained from 5-wk-old mice. In agreement with previous reports (Muller et al., 2011), we observed that M146V mice have an increased proportion (2.05 ± 0.40, $n = 5$; $p < 0.05$) of their total CaMKIV phosphorylated at Thr-196, a Ca^{2+}-dependent autophosphorylation that activates its kinase activity (Selbert et al., 1995), compared to WT (Fig. 4C). Immunofluorescence analysis confirmed this biochemical finding, demonstrating strong somal staining for phospho-CaMKIV in hippocampal neurons of M146V mice compared to WT (Fig. 4D; Supp. Fig. 5C). Remarkably, we did not observe a difference in the proportion of CaMKIV phosphorylated at Thr-196 in hippocampal lysates obtained from M146V;Opt mice (1.02 ± 0.19, $n = 5$) compared to WT animals, or differences in immunofluorescence staining patterns between M146V;Opt and WT slices (Fig. 4D; Supp. Fig. 5D). These findings suggest that the Opt allele rescues the constitutive activation of CaMKIV in M146V mice.

Having determined that the Opt allele rescues constitutive CaMKIV activation in M146V mice, we then wanted to investigate the consequence on the downstream CREB transcriptional pathway. Therefore, we preformed Western blot analysis using an antibody specific to CREB phosphorylated on Ser-133, a phosphorylation that activates its transcriptional activity (Gonzalez and Montminy, 1989). We found that M146V mice have an increased proportion of total CREB in a phosphorylated state (1.93 ± 0.06, n = 5; $p < 0.005$) compared to WT. Interestingly, we did not observe a difference in the proportion of CREB phosphorylated at Ser-133 in hippocampal lysates obtained from M146V;Opt mice (1.00 ± 0.09, n = 5) compared to WT (Fig. 4C). Immunofluorescence analysis, using the phospho-CREB specific antibody, produced strong nuclear staining in M146V hippocampal neurons that was not observed in hippocampal neurons in WT or M146V;Opt slices (Fig. 4E; Supp. Fig. 5D).

To confirm that rescue of constitutive CREB transcriptional activity underlies the Opt allele's rescue of enhanced neuronal potentiation in M146V mice, we performed Western blot analysis on hippocampal lysates for several CREB-dependent genes (neuronal nitric oxide synthase (nNOS), c-fos and brain-derived neurotrophic factor (BDNF)). In M146V hippocampal lysates we observed increased protein levels of nNOS (1.84 ± 0.25, n = 5; $p < 0.05$), BDNF (1.65 ± 0.26, n = 5; $p < 0.05$) and c-fos (1.87 ± 0.20, n = 5; $p < 0.005$) compared to WT (Fig. 4C). Strikingly, we did not observe a difference in the protein levels of these CREB-dependent genes in hippocampal lysates obtained from M146V;Opt mice (nNOS 0.67 ± 0.17, BDNF 0.95 ± 0.13, c-fos 1.20 ± 0.13, n = 5) compared to WT (Fig. 4C). These findings confirm that the Opt allele rescues the constitutive transcriptional activity of the CaMKIV-CREB pathway in M146V mice.

To verify the specificity of CREB-pathway activation in M146V mice we investigated a CREB-independent gene, glyceraldehyde 3-phosphate dehydrogenase (GAPDH), which was not elevated in M146V hippocampal lysates (0.97 ± 0.09, n = 5) compared to WT (Supp. Fig. 5B). Additionally, we did not observe any difference in genomic accessibility, as measured by histone-3 acetylation (Turner, 1998), in M146V hippocampal lysates (0.93 ± 0.16, n = 5) compared to WT (Supp. Fig. 5B). These findings suggest that increases in CREB-target gene protein level is due to specific activation of the pathway, not a genome-wide increase in expression.

We confirmed that enhanced hippocampal potentiation and constitutive CREB pathway activation are not due to developmental differences between WT and M146V mice. We did not observe any differences in basal synaptic transmission between 3-mth-old M146V;Opt, M146V and WT mice when we analyzed the input-output slope (M146V;Opt 2.49 ± 0.27 ms^{-1} vs M146V 2.81 ± 0.44 ms^{-1} vs WT 2.45 ± 0.65 ms^{-1}), the ratio of the fEPSP slope to the PFV amplitude at each applied voltage (M146V;Opt 4.06 ± 0.25 ms^{-1} vs M146V 4.69 ± 0.84 ms^{-1} vs WT 2.99 ± 0.32 ms^{-1}) or the maximum evoked fEPSP slope (M146V;Opt 10.6 ± 1.0 mV/ms vs M146V 11.5 ± 1.9 mV/ms vs WT 7.5 ± 0.4 mV/ms) (Fig. 4F; Supp. Fig. 5E). Consistent with the findings in 5-wk-old animals, we observed larger potentiation during the first 10 min post-tetanus in slices obtained from M146V mice (303 ± 30% of baseline, n = 5; $p < 0.05$) compared to those obtained from WT animals (214 ± 13% of baseline, n = 5), and larger maintained increases in synaptic strength during the last 20 min of the recordings in slices from M146V mice (202 ± 10% of baseline, n = 5; $p < 0.005$) compared to WT (129 ± 6% of baseline, n = 5) (Fig. 4G). In slices obtained from 3-mth-old M146V;Opt mice we did not observe

differences in potentiation during the first 10 min post-tetanus (192 ± 6% of baseline, n = 5), or in synaptic strength during the last 20 min of recording (133 ± 9% of baseline, n = 5) compared to WT (Fig. 4G).

Biochemical analysis of hippocampal lysates obtain from adult M146V mice revealed an increased proportion of total CaMKIV (1.61 ± 0.20, n = 6; $p < 0.05$) and CREB (1.65 ± 0.14, n = 6; $p < 0.05$) in a phosphorylated state, and increased protein levels of CREB-dependent genes compared to WT (nNOS 1.84 ± 0.32; $p < 0.05$, BDNF 1.37 ± 0.13; $p < 0.05$, c-fos 1.82 ± 0.24, n = 6; $p < 0.05$) (Fig. 4H). No differences in hippocampal GAPDH protein levels were observed in M146V mice (1.03 ± 0.10, n = 7) compared to WT (Supp. Fig. 5F). Western blot analysis of M146V;Opt hippocampal lysates revealed no differences in the proportion of total CaMKIV (1.22 ± 0.20, n = 6) or CREB (0.96 ± 0.13, n = 6) in a phosphorylated state, or differences in protein levels of CREB-dependent genes: nNOS (1.54 ± 0.22, n = 6), BDNF (1.12 ± 0.09, n = 6) and c-fos (1.46 ± 0.24, n = 6) compared to WT (Fig. 4H). These findings suggest that developmental differences do not underlie enhanced synaptic potentiation and constitutive activation of the CaMKIV-CREB transcriptional pathway in M146V mice.

Exaggerated $[Ca^{2+}]_i$ signaling contributes to AD-like phenotypes of the 3xTg AD-mouse model

To determine the contribution of exaggerated $[Ca^{2+}]_i$ signaling to the development of canonical AD phenotypes – pathology accumulation and hippocampal impairments – we transferred the Opt allele onto the 3xTg's genome, which contains the PS1M146V-KIN mutation and human APP_{SWE} and tau_{P301L} transgenes (Supp. Fig. 1, C and D).

The Opt allele rescues exaggerated $[Ca^{2+}]_i$ signaling in the 3xTg mouse

First, we verified that the Opt allele rescues exaggerated $[Ca^{2+}]_i$ signaling observed in 3xTg mice using the *in vitro* and *ex vivo* experimental paradigms described above. Following 9-DIV, PCNs obtained from 3xTg;Opt have 0.49 ± 0.03 (n = 5; $p < 0.005$) of the amount of $InsP_3R1$ protein compared to WT PCNs, whereas 3xTg PCNs have a similar amount (0.91 ± 0.08, n = 5) of $InsP_3R1$ protein compared to WT PCNs (Supp. Fig. 2B). Additionally, 3xTg PCNs do not express differing amounts of RyR protein compared to WT PCNs (3xTg 1.72 ± 0.62, n = 6; p = 0.29) (Supp. Fig. 2B). Following a 10 s baseline recording, PCNs were subjected to a whole-field UV light pulse of varying duration (Fig. 1C). When the subsequent increases in somal $[Ca^{2+}]$ were analyzed, we observed that PCNs obtained from 3xTg embryos have exaggerated magnitudes of $[Ca^{2+}]_i$ signals, compared to WT, in response to UV pulse durations of 10 ms ($\Delta F/F_0$: 3xTg 0.23 ± 0.02 vs WT 0.15 ± 0.02; $p < 0.05$), 50 ms ($\Delta F/F_0$: 3xTg 0.25 ± 0.02 vs WT 0.18 ± 0.02; $p < 0.05$), 100 ms ($\Delta F/F_0$: 3xTg 0.30 ± 0.02 vs WT 0.19 ± 0.02; $p < 0.005$) and 500 ms ($\Delta F/F_0$: 3xTg 0.36 ± 0.05 vs WT 0.21 ± 0.02; $p < 0.05$) (Fig. 1F). No differences in magnitudes of $[Ca^{2+}]_i$ signals were observed in response to UV flash durations of 25 ms or 20 ms with a 4xND filter in place. Only 3xTg PCNs responded to a 16 ms UV illumination with a 16xND filter in place (Fig. 1, C and F). When we examined PCNs obtained from 3xTg;Opt embryos, we did not observe differences in their magnitudes of $[Ca^{2+}]_i$ signals in response to UV pulse durations of 10 ms, 50 ms, 100 ms or 500 ms compared to WT ($\Delta F/F_0$: 10 ms 0.14 ± 0.02, 50 ms 0.15 ± 0.02, 100 ms 0.19 ± 0.02, 500 ms 0.20 ± 0.02) (Fig. 1F). These findings suggest that the Opt allele rescues exaggerated magnitudes of $[Ca^{2+}]_i$ signals in 3xTg PCNs.

Analysis of the rates of Ca^{2+} release revealed that PCNs obtained from 3xTg embryos have faster release rates, compared to PCNs obtained from WT embryos, in response to all UV pulse durations for which both genotypes responded – 20 ms with 4xND filter ($\partial(\Delta F/F_0)/\partial t$): 3xTg 0.09 ± 0.02 s^{-1} vs WT 0.05 ± 0.01 s^{-1}; $p < 0.05$), 10 ms ($\partial(\Delta F/F_0)/\partial t$): 3xTg 0.22 ± 0.03 s^{-1} vs WT 0.13 ± 0.03 s^{-1}; $p < 0.05$), 25 ms ($\partial(\Delta F/F_0)/\partial t$): 3xTg 0.41 ± 0.08 s^{-1} vs WT 0.23 ± 0.04 s^{-1}; $p < 0.05$), 50 ms ($\partial(\Delta F/F_0)/\partial t$): 3xTg 0.34 ± 0.05 s^{-1} vs WT 0.16 ± 0.03 s^{-1}; $p < 0.005$), 100 ms ($\partial(\Delta F/F_0)/\partial t$): 3xTg 0.37 ± 0.05 s^{-1} vs WT 0.21 ± 0.04 s^{-1}; $p < 0.05$) and 500 ms ($\partial(\Delta F/F_0)/\partial t$): 3xTg 0.62 ± 0.14 s^{-1} vs WT 0.32 ± 0.06 s^{-1}; $p < 0.05$) (Fig. 1G). Interestingly, in response to 10 ms, 50 ms or 100 ms UV illumination 3xTg;Opt PCN Ca^{2+} release rates were not different than WT Ca^{2+} release rates ($\partial(\Delta F/F_0)/\partial t$): 10 ms 0.09 ± 0.02 s^{-1}, 50 ms 0.12 ± 0.03 s^{-1}, 100 ms 0.13 ± 0.02 s^{-1}) (Fig. 1G). However, in response to a 20 ms UV pulse with a 4xND filter in place ($\partial(\Delta F/F_0)/\partial t$): 0.03 ± 0.01 s^{-1}; $p < 0.05$), a 25 ms ($\partial(\Delta F/F_0)/\partial t$): 0.09 ± 0.01 s^{-1}; $p < 0.005$) and a 500 ms ($\partial(\Delta F/F_0)/\partial t$): 0.16 ± 0.02 s^{-1}; $p < 0.05$) UV illumination, 3xTg;Opt PCNs had slower Ca^{2+} release rates compared to WT (Fig. 1F). These results indicate that the Opt allele rescues exaggerated rates of Ca^{2+} release in 3xTg PCNs.

We confirmed these *in vitro* findings in our *ex vivo* experimental paradigm. Hippocampi isolated from P10-12 3xTg;Opt mice have 0.69 ± 0.09 ($n = 7$; $p < 0.05$) of the amount of $InsP_3R1$ protein as WT, whereas hippocampi obtained from 3xTg mice have a similar level of $InsP_3R1$ protein (1.03 ± 0.06, $n = 7$) compared to WT (Supp. Fig. 3B). No differences in total RyR, RyR2, or RyR3 hippocampal protein levels were observed between 3xTg and WT mice ($n \geq 6$ for each genotype) (Supp. Fig. 3B). Slices were loaded with the Oregon Green Ca^{2+} indicator and dentate gyrus granular cell layer

neurons were imaged. Following a baseline recording, slices were perfused with 10 μM DHPG (Fig. 2E). We observed that neurons in 3xTg hippocampal slices displayed exaggerated magnitudes of $[Ca^{2+}]_i$ signals ($\Delta F/F_0$: 3xTg 0.62 ± 0.03 vs WT 0.30 ± 0.02; $p < 0.005$) and faster rates of Ca^{2+} release ($\partial(\Delta F/F_0)/\partial t$): 3xTg 0.29 ± 0.02 s^{-1} vs WT 0.12 ± 0.02 s^{-1}; $p < 0.005$) compared to WT (Fig. 2, E, F and G). Also in agreement with previous findings, we observed that the magnitudes ($\Delta F/F_0$: 0.29 ± 0.02) and release rates ($\partial(\Delta F/F_0)/\partial t$): 0.13 ± 0.01 s^{-1}) of DHPG-induced Ca^{2+} release in 3xTg;Opt neurons were not significantly different from WT (Fig. 2, E, F and G). These results indicate that the Opt allele rescues the agonist-induced exaggerated $[Ca^{2+}]_i$ signaling observed in 3xTg hippocampal neurons.

The Opt allele attenuates hippocampal AD-like pathology in the 3xTg AD-mouse model

Having demonstrated the Opt allele's rescue of 3xTg exaggerated $[Ca^{2+}]_i$ signaling, we then investigated its impact on the age-dependent development of AD-like pathology in this mouse. Initial reports on the 3xTg detected hippocampal Aβ accumulation in mice 6-mths-of-age, whereas pathological phosphorylation of tau was first observed in the hippocampus of 12-mth-old 3xTg mice (Oddo et al., 2003). Therefore, we conducted time course studies employing $Aβ_{40}$ and $Aβ_{42}$ specific ELISA and Western blot analysis on hippocampal tissues isolated from mice ranging from 3- to 18-mths-of-age. Over this age range we observe that hippocampi from 3xTg;Opt mice have ~50% ($n = 3$-5; $p < 0.05$) of the amount of $InsP_3R1$ protein compared to WT,

whereas hippocampi obtained from 3xTg mice (n = 5) have a similar amount of $InsP_3R1$ protein compared to WT (Supp. Fig. 6A).

Prior to conducting ELISA studies, we verified equivalent hippocampal human APP (hAPP) protein levels in 3xTg and 3xTg;Opt mice by Western blot analysis (Fig. 5A). In the ELISA studies, Aβ levels in hippocampal homogenates obtained from Opt and WT mice (n = 3 of each genotype per time-point) were always below the assay's detection threshold. In contrast, we were able to detect Aβ accumulation in 3xTg;Opt and 3xTg mice at 6-mths-of-age (Fig. 5B). At this age we observed that hippocampal homogenates obtained from 3xTg;Opt mice have lower levels of $A\beta_{40}$ (0.01 ± 0.003 pmol/mg protein, n = 6) compared to 3xTg (0.03 ± 0.01 pmol/mg protein, n = 6; $p < 0.05$). However, we did not observe differences in $A\beta_{42}$ levels (3xTg;Opt 0.01 ± 0.001 pmol/mg protein, n = 6 vs 3xTg 0.03 ± 0.01 pmol/mg protein, n = 6). In hippocampal homogenates obtained from 9-mth-old 3xTg;Opt mice we observed attenuated levels of $A\beta_{40}$ (3xTg;Opt 0.03 ± 0.004 pmol/mg protein, n = 6 vs 3xTg 0.04 ± 0.002 pmol/mg protein, n = 6; $p < 0.05$) and $A\beta_{42}$ (3xTg;Opt 0.04 ± 0.01 pmol/mg protein, n = 6 vs 3xTg 0.08 ± 0.01 pmol/mg protein, n = 6; $p < 0.005$) compared to 3xTg littermates. In mice 12-mth of age we again detected an attenuation in 3xTg;Opt hippocampal Aβ content compared to 3xTg littermates ($A\beta_{40}$: 3xTg;Opt 0.13 ± 0.03 pmol/mg protein, n = 6 vs 3xTg 0.37 ± 0.07 pmol/mg protein, n = 6; $p < 0.05$; $A\beta_{42}$: 3xTg;Opt 0.42 ± 0.11 pmol/mg protein, n = 5 vs 3xTg 1.37 ± 0.19 pmol/mg protein, n = 6; $p < 0.005$). At 15-mths-of-age we observed that the Opt allele is not associated with a decrease in hippocampal $A\beta_{40}$ accumulation (3xTg;Opt 0.84 ± 0.27 pmol $A\beta_{40}$/mg protein, n = 6 vs 3xTg 6.0 ± 2.5

pmol/mg protein, n = 5; p = 0.10), but does attenuate levels of $A\beta_{42}$ (3xTg;Opt 4.5 ± 1.4 pmol $A\beta_{42}$/mg protein, n = 6 vs 3xTg 11.9 ± 3.0 pmol/mg protein, n = 5; $p < 0.05$). At the oldest age investigated, 18-mths, we observed that hippocampal homogenates obtained from 3xTg;Opt mice have dramatically attenuated levels of $A\beta_{40}$ (3xTg;Opt 5.0 ± 2.1 pmol/mg protein, n = 5 vs 3xTg 26.5 ± 5.4 pmol/mg protein, n = 7; $p < 0.05$) and $A\beta_{42}$ (3xTg;Opt 14.5 ± 5.1 pmol/mg protein, n = 5 vs 3xTg 41.3 ± 3.8 pmol/mg protein, n = 7; $p < 0.05$) compared to 3xTg.

To visualize these ELISA findings we performed IHC analysis on hippocampal slices obtained from 18-mth-old mice using antibodies 6E10 (recognized both Aβ species and full length APP) and 12F4 (specific to $A\beta_{42}$) (Fig. 5C). IHC analysis of 3xTg hippocampal slices using antibody 6E10 produced strong extracellular and intracellular staining, the latter of which is most likely full length APP (Winton et al., 2011). In contrast, 3xTg;Opt hippocampal slices have less extracellular immunoreactivity without obvious differences in intracellular staining. Analysis with antibody 12F4 provided a similar extracellular staining pattern without detectable intracellular signal. In 3xTg hippocampal slices we observed strong immunoreactivity that was largely attenuated in littermates containing an Opt allele. These findings suggest that the Opt allele attenuates accumulation of $A\beta_{40}$ and $A\beta_{42}$ in the hippocampus of 3xTg mice.

To determine the Opt allele's effect on hippocampal tau pathology we used specific antibodies to htau to monitor transgene protein levels and the accumulation of phospho-htau. We did not observe differences in htau protein levels in hippocampal lysates obtained from 3- (1.03 ± 0.14, n = 5) or 6-mth-old 3xTg;Opt mice (0.85 ± 0.15, n = 5) compared to 3xTg littermates. However, we did observe deceased htau protein levels

in 3xTg;Opt mice at 9-mths-of-age and older compared to 3xTg littermates (9-mth: 0.79 ± 0.04 n = 5; $p < 0.05$; 12-mth: 0.67 ± 0.11 n = 5; $p < 0.05$; 15-mth: 0.75 ± 0.07 n = 5; $p < 0.05$; 18-mth: 0.59 ± 0.05, n = 3; $p < 0.05$) (Fig. 5A). These differences in total htau protein levels are not due to differences in transgene transcription (see below). Rather, this observation is in agreement with previous studies that have found Aβ inhibits proteasomal degradation of tau (Tseng et al., 2008; Martinez-Coria et al., 2010). We first observed pathologic phosphorylation of htau at 12-mths-of-age using antibodies specific to htau phosphorylated at Ser-202 (AT8) and Thr-231 (AT180). As normalized to 3xTg littermates, we observed that 12-mth-old 3xTg;Opt animals have 0.69 ± 0.01 (n = 3; $p < 0.005$) of the amount of htau phosphorylated at Ser-202, and 0.59 ± 0.13 (n = 4; $p < 0.05$) of the amount of htau phosphorylated at Thr-231. Analysis of hippocampal lysates obtained from 15-mth-old mice revealed that 3xTg;Opt mice have 0.67 ± 0.08 (n = 5; $p < 0.05$) of the amount of htau phosphorylated at Ser-202, and 0.59 ± 0.09 (n = 5; $p < 0.05$) of the amount of htau phosphorylated at Thr-231 as 3xTg mice. In lysates obtained from 18-mth-old mice we observed that the Opt allele dramatically attenuates pathologic tau phosphorylation. At this age, 3xTg;Opt mice have 0.25 ± 0.17 (n = 3; $p < 0.05$) of the amount of htau phosphorylated at Ser-202, and 0.32 ± 0.10 (n = 3; $p < 0.05$) of the amount of htau phosphorylated at Thr-231, as 3xTg mice.

IHC analysis on hippocampal slices obtained from 18-mth-old mice confirmed these biochemical data. We observed strong somatic and neuritic staining using antibodies AT8 and AT180 in hippocampal region CA1 in slices obtained from 3xTg mice (Fig. 5C). In contrast, we observed less staining by both antibodies in slices

obtained from 3xTg;Opt mice. These results suggest that the Opt allele attenuates accumulation of pathologically phosphorylated htau in the hippocampus of 3xTg mice.

The Opt allele attenuates cortical AD-like pathology in the 3xTg AD-mouse model

Having observed that the Opt allele attenuates hippocampal AD-like pathology, we then wanted to determine its effects on 3xTg cortical AD-like pathology. Initial reports on 3xTg mice detected cortical Aβ at 3-mths-of-age, whereas pathological phosphorylation of tau was first observed at 15-mths-of-age (Oddo et al., 2003). Therefore we collected cortical tissue from mice ranging in age from 3- to 18-mths for Western blot and ELISA analysis. Over this age range we observe that cortical tissue from 3xTg;Opt mice has ~50% ($n = 3\text{-}5$, $p < 0.05$) of the amount of $InsP_3R1$ protein compared to cortical tissue isolated from WT mice, whereas tissue obtained from 3xTg mice ($n = 5$) has a similar level of $InsP_3R1$ protein compared to WT (Supp. Fig. 6B).

Western blot analysis confirmed equivalent cortical hAPP protein levels in 3xTg and 3xTg;Opt mice over the range of ages investigated (Supp. Fig. 6B). ELISA analysis failed to detect Aβ in WT or Opt cortical homogenates ($n = 3$ of each genotype per time-point). However, analysis of 3xTg and 3xTg;Opt cortical homogenates revealed that the Opt allele decreases the accumulation of $A\beta_{40}$ and $A\beta_{42}$ (Supp. Fig. 6C). At 6-mths-of-age we observed that cortical homogenates obtained from 3xTg;Opt mice have attenuated levels of $A\beta_{40}$ (3xTg;Opt 4.0 ± 0.5 fmol/mg protein, $n = 6$ vs 3xTg 9.3 ± 1.0 fmol/mg protein, $n = 6$; $p < 0.005$) and $A\beta_{42}$ (3xTg;Opt 4.0 ± 0.2 fmol/mg protein, $n = 6$ vs 3xTg 7.5 ± 0.4 fmol/mg protein, $n = 6$; $p < 0.005$) compared to 3xTg. In cortical homogenates obtained from 9-mth-old mice, we again observed that 3xTg;Opt mice have diminished

levels of $A\beta_{40}$ (3xTg;Opt 14 ± 1 fmol/mg protein, n = 6 vs 3xTg 18 ± 1 fmol/mg protein, n = 6; $p < 0.05$) and $A\beta_{42}$ (3xTg;Opt 15 ± 1 fmol/mg protein, n = 6 vs 3xTg 18 ± 1 fmol/mg protein, n = 6; $p < 0.05$) compared to 3xTg littermates. In mice 12-mth-of-age we observed a decrease in Aβ content in cortical homogenates obtained from 3xTg;Opt mice compared to 3xTg ($A\beta_{40}$: 3xTg;Opt 14 ± 1 fmol/mg protein, n = 6 vs 3xTg 43 ± 8 fmol/mg protein, n = 6; $p < 0.05$; $A\beta_{42}$: 3xTg;Opt 8 ± 1 fmol/mg protein, n = 6 vs 3xTg 32 ± 8 fmol/mg protein, n = 6; $p < 0.05$). At 15-mths-of-age the Opt allele is associated with attenuated hippocampal $A\beta_{40}$ (3xTg;Opt 8 ± 1 fmol/mg protein, n = 5 vs 3xTg 51 ± 15 fmol/mg protein, n = 5; $p < 0.05$) and $A\beta_{42}$ accumulation (3xTg;Opt 12 ± 3 fmol/mg protein, n = 4 vs 3xTg 82 ± 21 fmol/mg protein, n = 5; $p < 0.05$). At the oldest time-point investigated, 18-mths, we observed that cortical homogenates obtained from 3xTg;Opt mice have dramatically reduced levels of $A\beta_{40}$ (3xTg;Opt 44 ± 4 fmol/mg protein, n = 5 vs 3xTg 185 ± 57 fmol/mg protein, n = 7; $p < 0.05$) and $A\beta_{42}$ accumulation (3xTg;Opt 132 ± 52 fmol/mg protein, n = 5 vs 3xTg 1440 ± 435 fmol/mg protein, n = 7; $p < 0.05$) compared to 3xTg. These findings demonstrate that the Opt allele attenuates accumulation of $A\beta_{40}$ and $A\beta_{42}$ in the cortex of 3xTg mice.

We attempted to determine the Opt allele's effect on cortical htau pathology. However, we were not able to detect phospho-htau by Western blot analysis using antibodies AT8 or AT180 in cortical lysates obtained from 12-, 15-, or 18-mth-old animals. Interestingly, we did observe attenuated cortical htau protein levels in 3xTg;Opt mice, as normalized to 3xTg littermates, at 6-mths-of-age and older (6-mth: 0.51 ± 0.02, n = 5; $p > 0.005$; 9-mth: 0.52 ± 0.09, n = 5; $p < 0.005$; 12-mth: 0.52 ± 0.06, n = 5; $p <$

0.005; 15-mth: 0.46 ± 0.08, n = 5; $p < 0.005$; 18-mth: 0.39 ± 0.01, n = 3; $p < 0.005$). This difference in htau transgene protein level was not observed in 3-mth-old mice (3xTg;Opt 0.92 ± 0.24, n = 5) (Supp. Fig. 6B), and is not due to a disparity in transgene expression as RT-RTPCR did not identify differences in cortical htau mRNA levels between 6-mth-old 3xTg;Opt and 3xTg mice (Supp. Fig. 6D).

The Opt allele delays the onset and attenuates the severity of hippocampal L-LTP impairments in 3xTg mice

The attenuation of 3xTg AD-like hippocampal pathology by the Opt allele raises the question of whether it can also rescues 3xTg hippocampal functional deficits. Initial reports on 3xTg mice detected impaired hippocampal region CA1 L-LTP in slices obtained from 6-mth-old animals that was not present in 3xTg mice at 1-mth-of-age (Oddo et al., 2003). This impairment was manifested as both a decrease in potentiation following tetani application and failure to maintain long lasting increases in synaptic strength.

Hippocampal electrophysiological experiments were conducted by monitoring fEPSP in hippocampal area CA1 following stimulation of the Schaeffer collateral pathway. We did not observe any differences in basal synaptic transmission between 6-mth-old 3xTg;Opt, 3xTg and WT mice when we analyzed the input-output slope (3xTg;Opt 2.12 ± 0.50 ms^{-1}, n = 9 vs 3xTg 2.81 ± 0.44 ms^{-1}, n = 7 vs WT 2.42 ± 0.50 ms^{-1}, n = 10), the ratio of the fEPSP slope to the PFV amplitude at each applied voltage (3xTg;Opt 3.15 ± 0.47 ms^{-1} vs 3xTg 4.86 ± 0.82 ms^{-1} vs WT 4.03 ± 0.70 ms^{-1}) or the

maximum evoked fEPSP slope (3xTg;Opt 9.99 ± 1.02 mV/ms vs 3xTg 8.79 ± 1.81 mV/ms vs WT 10.34 ± 1.13 mV/ms) (Fig. 6A; Supp. Fig. 7A).

Following a 20 min baseline recording period, we applied four 100 Hz, 1 s stimuli with a 5 min inter-stimulus interval to the Schaeffer collateral pathway and monitored the ensuing changes in synaptic strength for 160 min. In slices obtained from 3xTg mice we observed decreased potentiation during the first 20 min post-tetani (224 ± 11% of baseline, $n = 5$; $p < 0.005$) compared to WT (336 ± 23% of baseline, $n = 5$). Additionally, we observed impaired long-term maintenance of increases in synaptic strength during the last 20 min of recording in slices obtained from 3xTg mice (fEPSP slope 135 ± 11% of baseline, $n = 5$; $p < 0.05$) compared to WT (fEPSP slope 176 ± 9% of baseline, $n = 5$) (Fig. 6B). In hippocampal slices obtained from 3xTg;Opt mice we did not observe differences in post-tetani potentiation (315 ± 24% of baseline, $n = 6$), or in long lasting increases in synaptic strength (191 ± 17% of baseline) compared to WT mice. These observations suggest that the Opt allele is able to rescue impaired hippocampal function in 3xTg animals.

To track the duration of hippocampal L-LTP rescue by the Opt allele we extended these studies to 9- and 12-mth-old animals. At 9-mths-of-age we did not observe any difference in the input-output slope in slices obtained from 3xTg;Opt and 3xTg animals compared to WT (3xTg;Opt 2.09 ± 0.38 ms^{-1}, $n = 6$ vs 3xTg 1.47 ± 0.42 ms^{-1}, $n = 8$ vs WT 1.95 ± 0.23 ms^{-1}, $n = 6$) (Fig. 6B; Supp. Fig. 7B). However, we did observe a decrease in the ratio of the fEPSP slope to the PFV amplitude at each applied voltage in 3xTg slices (3xTg 2.30 ± 0.21 ms^{-1}; $p < 0.05$) compared to WT (3.87 ± 0.60 ms^{-1}) and a decrease in the maximum evoked fEPSP slope (3xTg 4.54 ± 0.44 mV/ms; $p < 0.05$)

compared WT (7.33 ± 0.98 mV/ms). In contrast, we did not observed differences in basal synaptic transmission in slices obtained from 3xTg;Opt mice (fEPSP/PFV 2.40 ± 0.25 ms^{-1}, maximum evoked fEPSP slope 6.57 ± 0.72 mV/ms) compared to WT (Supp. Fig. 7B). Following tetani application, we observed impaired potentiation in slices obtained from 9-mth-old 3xTg mice (200 ± 9% of baseline, n = 5; $p < 0.005$) compared to WT (360 ± 24% of baseline, n = 5) and impaired long-term maintenance of increases in synaptic strength during the last 20 min of the recording (134 ± 9% of baseline; $p < 0.005$) compared WT (193 ± 8% of baseline) (Fig. 6D). In slices obtained from 3xTg;Opt mice we did not observe differences in post-tetani potentiation (284 ± 28% of baseline, n = 5) or long-term maintenance of increases in synaptic strength (174 ± 8% of baseline) compared to WT.

At 12-mths-of-age we did not observe any differences in basal synaptic transmission in slices obtained from 3xTg, 3xTg;Opt and WT animals (input-output curve slope: 3xTg;Opt 2.19 ± 0.75 ms^{-1} vs 3xTg 1.81 ± 0.24 ms^{-1} vs WT 2.23 ± 0.51 ms^{-1}; fEPSP/PFV: 3xTg;Opt 2.76 ± 0.30 ms^{-1} vs 3xTg 2.96 ± 0.41 ms^{-1} vs WT 2.64 ± 0.45 ms^{-1}; max fEPSP: 3xTg;Opt 6.54 ± 0.88 mV/ms vs 3xTg 5.84 ± 1.07 mV/ms vs WT 4.70 ± 1.02 mV/ms, n = 5 for all genotypes) (Fig. 6E; Supp. Fig. 7C). Following tetani application to the Schaeffer collateral pathway, we observed impaired potentiation in slices obtained from 3xTg mice (199 ± 5% of baseline, n = 5; $p < 0.005$) compared to WT (309 ± 14% of baseline, n = 5) and impaired long-term maintenance of increases in synaptic strength (3xTg: 130 ± 3% of baseline; $p < 0.005$) compared to WT (187 ± 5% of baseline) (Fig. 6F). In slices obtained from 12-mth-old 3xTg;Opt mice, we observed

impaired post-tetani potentiation (245 ± 7% of baseline; $p < 0.005$) and impaired long-term maintenance of increases in synaptic strength (155 ± 2% of baseline; $p < 0.005$) compared to WT. However, impairments in 3xTg;Opt slices were significantly less ($p < 0.005$) than those observed in 3xTg slices. These findings indicate that the Opt allele delays the onset and attenuates the severity of hippocampal impairments observed in 3xTg mice.

The Opt allele rescues 3xTg hippocampal-dependent memory impairments

Changes in synaptic strength are thought to be the molecular basis of memory formation. Therefore, we wanted to determine if the Opt allele's rescue of 3xTg hippocampal L-LTP impairments extended to hippocampal-dependent memory. To do this, we conducted three hippocampal-dependent memory tests on mice 12 to 13 mth-of-age, an age at which 3xTg mice display hippocampal-dependent memory deficits (Clinton et al., 2007). The first test we conducted was the spatial object recognition (SOR) test, which assays for hippocampal-dependent spatial memory. As compared to other tests of spatial navigation, SOR does not employ aversive stimuli, such as the threat of drowning, to motivate the animal's performance. Rather, SOR takes advantage of the animal's innate curiosity to explore its environment (Wimmer et al., 2011).

SOR training consisted of three 10 min exposures to an arena that contained two distinct objects. 24 hr after the last training trial mice were returned to the arena, but one object was displaced (DO) to a new location. The preference for the DO was calculated as the percent of exploration time dedicated to it. When we analyzed the preference of mice for the DO, we observed that WT animals spent 61 ± 2% ($n = 16$) of their exploratory time investigating the DO (Fig. 6G). In comparison, 3xTg mice spent a

smaller proportion of their exploratory time investigating the DO (49 ± 3%, n = 15; $p < 0.005$), indicating that 3xTg mice have impaired spatial memory. This decrease in preference was not observed in 3xTg littermates containing an Opt allele (60 ± 4%; n = 14) (Fig. 6G), and is not due to differences in mobility between the genotypes, as determined by open-field testing (3xTg 741 ± 93 beam breaks, n = 16 vs WT: 941 ± 58 beam breaks, n = 17; $p = 0.08$) (Supp. Fig. 7D).

To confirm this deficit in 3xTg hippocampal-dependent memory, we performed contextual fear conditioning tests. For these tests, mice were placed into a conditioning chamber. Following a 2 min habituation period, mice were subjected to a 30 s tone, the last 2 s of which was paired with a foot shock. 24 hrs after training mice were tested for their freezing response during a 3 min period in the context of the conditioning chamber. We observed 3xTg mice spent less time frozen (55 ± 3%; n = 13) compared to WT (67 ± 3%, n = 16; $p < 0.05$), whereas 3xTg;Opt mice did not (73 ± 4%; n = 19) (Fig. 6H).

Previous reports have identified significant AD-like pathology accumulation in the amygdala of 3xTg mice (Oddo et al., 2003). Therefore, we extended these fear conditioning studies to test amygdala-dependent associative memory. To do this, mice were placed into a novel chamber, with a unique context, and following a 2 min habituation period they were tested for their freezing response during a 3 min application of the conditioning tone. We observed 3xTg mice (44 ± 6%; n = 16) spent less time frozen compared to WT (69 ± 3%, n = 17; $p < 0.005$), whereas 3xTg;Opt mice did not (61 ± 5%; n = 15) (Fig. 6I). Together, these behavioral experiments demonstrate that 3xTg mice have hippocampal and amygdala-dependent memory impairments that are rescued by the Opt allele.

DISCUSSION

The identification of proximal cellular events predicting the development of AD has remained elusive. However, compelling evidence suggests that FAD PS mutations result in proximal changes in $[Ca^{2+}]_i$ signaling, which may contribute to AD pathogenesis (Buxbaum et al., 1994; Ito et al., 1994; Hirashima et al., 1996; Querfurth et al., 1997; Hartigan and Johnson, 1999; LaFerla, 2002; Pierrot et al., 2004; Stutzmann et al., 2004; Smith et al., 2005; Pierrot et al., 2006; Stutzmann et al., 2006; Cheung et al., 2008; Green et al., 2008; Hoey et al., 2009; Cheung et al., 2010). Changes in $[Ca^{2+}]_i$ handling can alter cellular transcriptional pathways (Hardingham and Bading, 1999; Muller et al., 2011), synaptic plasticity (Bashir et al., 1993; Futatsugi et al., 1999; Fujii et al., 2000; Raymond and Redman, 2006), APP metabolism (Buxbaum et al., 1994; Querfurth et al., 1997; LaFerla, 2002; Pierrot et al., 2004; Lesne et al., 2005; Pierrot et al., 2006; Cheung et al., 2008; Green et al., 2008; Hoey et al., 2009), and activate kinases responsible for tau phosphorylation (Hartigan and Johnson, 1999; Pierrot et al., 2006; Sayas et al., 2006). Here we examined the *in vivo* mechanism and contribution of exaggerated $[Ca^{2+}]_i$ signaling to the development of AD. Our results indicate that FAD mutant PS-associated exaggerated $[Ca^{2+}]_i$ signaling is $InsP_3R1$-dependent and a proximal event occurring in PCNs and hippocampal neurons from P10-12 mice. We also demonstrate that rescue of exaggerated $[Ca^{2+}]_i$ signaling attenuates AD pathogenesis in two AD mouse models. Our results indicate $InsP_3R1$ as a potential new drug target for treatment of FAD.

FAD-mutant PS-associated exaggerated $[Ca^{2+}]_i$ signaling is $InsP_3R1$-dependent

FAD mutations in PS are hypothesized to modulate the gating of the $InsP_3R1$ receptor (Cheung et al., 2008; Cheung et al., 2010). In agreement with these reports, we

observed that decreasing $InsP_3R1$ protein level in M146V and 3xTg mice (which harbor the PS1M146V-KIN mutation) normalizes M146V-associated enhancement in the magnitudes and release rates of Ca^{2+} stores. These observation were made in both an *in vitro* experimental system, which provided fine control over intracellular [$InsP_3$], and in an *ex vivo* experimental system that allowed us to study neurons in hippocampal tissues. Additionally, we found that M146V and 3xTg PCNs responded to lower [$InsP_3$] than WT, M146V;Opt, and 3xTg;Opt PCNs. In sum, these *in vitro* and *ex vivo* observations are in agreement with the hypothesis that exaggerated $[Ca^{2+}]_i$ signaling is $InsP_3R1$-dependent and due to an interaction that stabilizes the $InsP_3R$ open state and increases the receptor's sensitivity to $InsP_3$ (Cheung et al., 2008; Cheung et al., 2010).

The Opt allele rescues M146V MCI-like phenotypes

The M146V mouse demonstrates phenotypes reminiscent of pre-symptomatic FAD mutant PS carriers and MCI patients, including enhanced RyR2 expression (Stutzmann et al., 2006; Bruno et al., 2012) and neuronal hyperactivity (Dickerson et al., 2005; Odero et al., 2007; Auffret et al., 2010; Quiroz et al., 2010; Reiman et al., 2012). Our results demonstrated that the Opt allele rescues enhanced RyR2 protein levels observed in M146V animals, indicating that this abnormality is downstream of exaggerated $[Ca^{2+}]_i$ signaling. Previous reports on 3xTg found that increased RyR2 hippocampal protein levels are due to increased transcription (Chakroborty et al., 2009). We did not confirm such a mechanism, although differences in genetic background between the M146V and 3xTg mouse lines may account for this discrepancy.

Ca^{2+}release from intracellular stores plays an important role in hippocampal plasticity (Bashir et al., 1993; Futatsugi et al., 1999; Fujii et al., 2000; Raymond and

Redman, 2006; Mellentin et al., 2007). Previous studies on the M146V mouse (Odero et al., 2007; Auffret et al., 2010) and transgenic mice expressing several different FAD mutant alleles (Parent et al., 1999; Barrow et al., 2000; Zaman et al., 2000; Schneider et al., 2001; Auffret et al., 2009) have observed enhanced hippocampal synaptic potentiation. Such studies have found that this enhancement is due to a decease in the threshold for potentiation without changes in the maximum amount of potentiation achievable (Zaman et al., 2000; Schneider et al., 2001), and postulate that this phenomenon is due to changes in $[Ca^{2+}]_i$ handling associated with FAD mutant PS (Parent et al., 1999; Barrow et al., 2000; Schneider et al., 2001; Odero et al., 2007). This indiscriminant long-term enhancement in synaptic potentiation may occlude the selective synaptic enhancement required for normal learning. In fact, several groups have observed that FAD mutant PS expressing mice have selective improvements and deficits in spatial memory tests (Huang et al., 2003; Sun et al., 2005; Odero et al., 2007).

Our hippocampal electrophysiology experiments demonstrated that the Opt allele rescues M146V-associated long-lasting increases in synaptic potentiation resulting from a single increase in $[Ca^{2+}]_i$, supporting the hypothesis that enhanced synaptic potentiation is due to exaggerated $[Ca^{2+}]_i$ signaling. However, this effect may be indirect, mediated by constitutive activation of the CaMKIV-CREB transcriptional pathway. In agreement with previous reports, we observed that FAD mutant PS causes constitutive activation of the CaMKIV-CREB transcriptional pathway in an $InsP_3R$-dependent manner (Muller et al., 2011). CaMKIV overexpressing mice demonstrate enhanced hippocampal synaptic potentiation (Fukushima et al., 2008), whereas CaMKIV-deficient mice, or mice expressing dominant negative CaMKIV, exhibit impaired neuronal CREB

phosphorylation, CREB-dependent gene expression, and L-LTP (Ho et al., 2000; Kang et al., 2001). CREB is a known target of CaMKIV (Matthews et al., 1994; Sun et al., 1994) and CREB is important for the conversion of transient to long-lasting changes in synaptic strength (Yin and Tully, 1996). Mice harboring constitutively active CREB demonstrate a lowered threshold for eliciting long-lasting increases in synaptic strength independent of *de novo* transcription without changes in the maximum amount of potentiation achievable with repeated tetanus application (Barco et al., 2002). It is postulated that constitutive CREB transcriptional activity provides cell-wide synaptic priming for synapse specific long-lasting potentiation by a single stimulus (Barco et al., 2002).

We observed that the Opt allele rescued elevated protein levels of CREB-dependent genes, including BDNF and nNOS, which are specifically upregulated in M146V mice. Both BDNF (Lu et al., 2008) and nNOS (Steinert et al., 2010) have significant roles in regulating synaptic plasticity. In fact, BDNF application can induce transformation of E-LTP to L-LTP in the presence of protein synthesis inhibitors (Pang and Lu, 2004) and was identified as an important component for synaptic capture of L-LTP (Barco et al., 2005). These findings suggest that enhanced hippocampal potentiation in M146V mice results from constitutive activation of the CREB-CaMKIV transcriptional pathway, which in turn is driven by exaggerated $[Ca^{2+}]_i$ signaling.

MCI patients demonstrate enhanced hippocampal activation during performance of memory task (Dickerson et al., 2005). Recently, this observation was also made in pre-symptomatic FAD mutant carriers (Quiroz et al., 2010; Reiman et al., 2012). Administration of levetiracetam, an anticonvulsant that inhibits intracellular Ca^{2+} release (Angehagen et al., 2003), reduces hippocampal activation in AD mice (Sanchez et al.,

2012) and MCI patients (Bakker et al., 2012) and improves memory performance, suggesting that hippocampal hyperactivation is deleterious and does not serve a beneficial compensatory function. Our findings identify a potential molecular mechanism that may underlie enhanced hippocampal activation in MCI patient and pre-symptomatic FAD patients - constitutive activation of the CaMKIV-CREB pathway resulting from exaggerated $[Ca^{2+}]_i$ signaling.

The Opt allele rescues 3xTg AD-like phenotypes

Previous *in vitro* studies have suggested aberrant $[Ca^{2+}]_i$ handling may contribute to AD pathogenesis (Buxbaum et al., 1994; Querfurth et al., 1997; Hartigan and Johnson, 1999; Pierrot et al., 2004; Lesne et al., 2005; Pierrot et al., 2006; Cheung et al., 2008; Green et al., 2008). Recent *in vivo* studies investigating the role of exaggerated $[Ca^{2+}]_i$ signaling to AD pathogenesis have employed pharmacological approaches targeting RyR, but have produced conflicting results. One study identified a worsening of AD-like phenotypes (Zhang et al., 2010) and two studies reported amelioration (Oules et al., 2012; Peng et al., 2012). Although all three reports employed the same RyR antagonist, they used different routes of administration, dosing parameters, and employed different AD mouse models. These differences make the confounding results from these studies difficult to interpret. Our novel 3xTg;Opt mouse lines allowed us to circumvent such confounding issues and it is the first investigation of the contribution of $InsP_3R$-dependent $[Ca^{2+}]_i$ signaling to the development of AD-like pathology *in vivo*.

Strikingly, we observed that the Opt allele was able to attenuate pathology accumulation in the 3xTg mouse. Time course analysis on mice 6- to 18-mths-of-age revealed that 3xTg;Opt mice had a slower accumulation of both Aβ species in the

hippocampus and cortex indicating that exaggerated $[Ca^{2+}]_i$ signaling may influence APP metabolism *in vivo*. This observation is consistent with previous *in vitro* studies that found genetic ablation of $InsP_3R$ dramatically attenuated Aβ production (Cheung et al., 2008). Previous groups have observed that Ca^{2+} can either activate (Lesne et al., 2005) or inhibit (Hoey et al., 2009) Aβ production depending on the duration of the increase in $[Ca^{2+}]$ with longer rises in cytosolic $[Ca^{2+}]$ promoting Aβ production. It follows that environmental insults or genetic susceptibilities may result in proximal changes in $[Ca^{2+}]_i$ signaling and result in enhanced Aβ production and accumulation by promoting β-secretase-mediated APP processing. Additionally, it has been suggested that APP functions in synapse formation and function (Priller et al., 2006). In fact, Aβ levels are directly influenced by synaptic activity (Kamenetz et al., 2003; Cirrito et al., 2005; Bero et al., 2011) and Aβ inhibits neuronal excitability and plasticity (Kamenetz et al., 2003; Shankar et al., 2008). Therefore, early increases in neuronal excitability, resulting from exaggerated $[Ca^{2+}]_i$ signaling, may lead to increased Aβ generation. This may explain the observation that prodromal AD patients with the highest level of hippocampal hyperactivity demonstrate the greatest clinical decline (O'Brien et al., 2010).

Additionally, we found that 3xTg mice carrying the Opt allele have less hippocampal phospho-tau accumulation than 3xTg littermates without the Opt allele. Again, the mechanism underlying this observation requires further investigation. However, this effect on tau phosphorylation may be due to decreased activity of several tau kinases, including GSK-3β and CDK5, which are activated in a Ca^{2+}-dependent manner (Pierrot et al., 2006). Studies have found that tau is phosphorylated in response to elevated somal $[Ca^{2+}]$ in a duration-dependent manner (Hartigan and Johnson, 1999),

suggesting that changes in $[Ca^{2+}]_i$ homeostasis may result in enhanced phospho-tau accumulation. Recent evidence suggests that selective silencing of GSK-3 isoforms attenuates AD-like pathology *in vivo* (Hurtado et al., 2012). Alternatively, attenuated phospho-tau levels in 3xTg;Opt mice may be mediated by a decrease in proteasomal inhibition by Aβ (Tseng et al., 2008). Our observation of decreased total htau levels in 3xTg;Opt mice support such a mechanism.

We found that the Opt allele's attenuation of AD-like pathology in the 3xTg was correlated with an attenuation of hippocampal L-LTP impairments at 6-, 9- and 12-mths-of-age, and hippocampal-dependent memory impairments at 12-mths-of-age. In agreement with previous reports, we observed a deficit in L-LTP present in 6-mth-old 3xTg mice. At this age we were able to detect low levels of Aβ in 3xTg mice, but phospho-tau was not detected until 12-mths-of-ages. This suggests that synaptic dysfunction is an early manifestation in AD and may be caused by low [Aβ]. However, exaggerated Ca^{2+} release may also directly or indirectly contribute to 3xTg L-LTP impairments independent of its possible effects on APP metabolism; 9-mth-old 3xTg;Opt mice did not demonstrate synaptic dysfunction despite having similar hippocampal Aβ loads as 6-mth-old 3xTg mice. Intracellular Ca^{2+} release is critical for proper synaptic plasticity. In fact, enhanced LTP is observed in mice lacking either RyR3 (Futatsugi et al., 1999) or $InsP_3R1$ (Fujii et al., 2000), suggesting that $[Ca^{2+}]_i$ signaling plays an opposing role to Ca^{2+} influx via the NMDA receptor in LTP induction. Additionally, Ca^{2+} has been found to enhance formation of Aβ oligomers (Itkin et al., 2011), the Aβ species thought responsible for impaired LTP maintenance *in vivo* (Walsh et al., 2002). This suggests that exaggerated $[Ca^{2+}]_i$ signaling may affect LTP both directly and indirectly.

The behavioral significance of the observed attenuation in 3xTg L-LTP deficits was determined by conducting hippocampal-dependent memory tests. We found that the Opt allele rescued 3xTg spatial, associative and contextual memory impairments. These findings provide significant support for a role of exaggerated $[Ca^{2+}]_i$ signaling in AD pathogenesis.

In the current study, we have shown that the $InsP_3R$ is necessary for exaggerated $[Ca^{2+}]_i$ signaling linked to the PS1M146V mutation. Additionally, we have implicated $InsP_3R$-dependent exaggerated $[Ca^{2+}]_i$ signaling as a proximal event *in vivo*, that contributes to the MCI-like phenotypes in M146V mice and AD-like phenotypes in 3xTg mice. These data suggest that early targeting of the $InsP_3R$ in patients at risk for developing AD may be a potential therapeutic strategy.

ACKNOWLEDGMENTS

We thank Dr. M. Mattson for providing the PS1M146V-KIN mice, Dr. H. Wei for providing the 3xTg mice and Dr. J. Chen for providing the Opt mice, Dr. R. Neumar for providing the anti-$InsP_3R1$ antibody, and the University of Pennsylvania Behavioral Core for providing assistance with the behavioral experiments conducted. We also thank M. Bridi, A. Park, S. Baratono and Drs. K. Cheung, E. Goldberg, M. Wimmer, W. O'Brien, A. Siebert and K. Kopil for technical assistance and stimulating discussions.

CONTRIBTUIONS

D.S. and J.K.F conceived of this research and contributed to experimental design. D.C. and H.T. helped to design and interpret the calcium imaging experiments. T.A. helped to design and interpret the hippocampal electrophysiology and behavioral experiments. M.M. carried out the biochemical and immunofluorescence experiments for activation of the CaMKIV-CREB pathway and D.S. conducted all other experiments. D.S. and D.M. contributed to data analysis. D.S., M.M. J.K.F. contributed to the writing of the paper, and all authors contributed to the final edits.

FIGURES AND LEGENDS

Figure 3.1

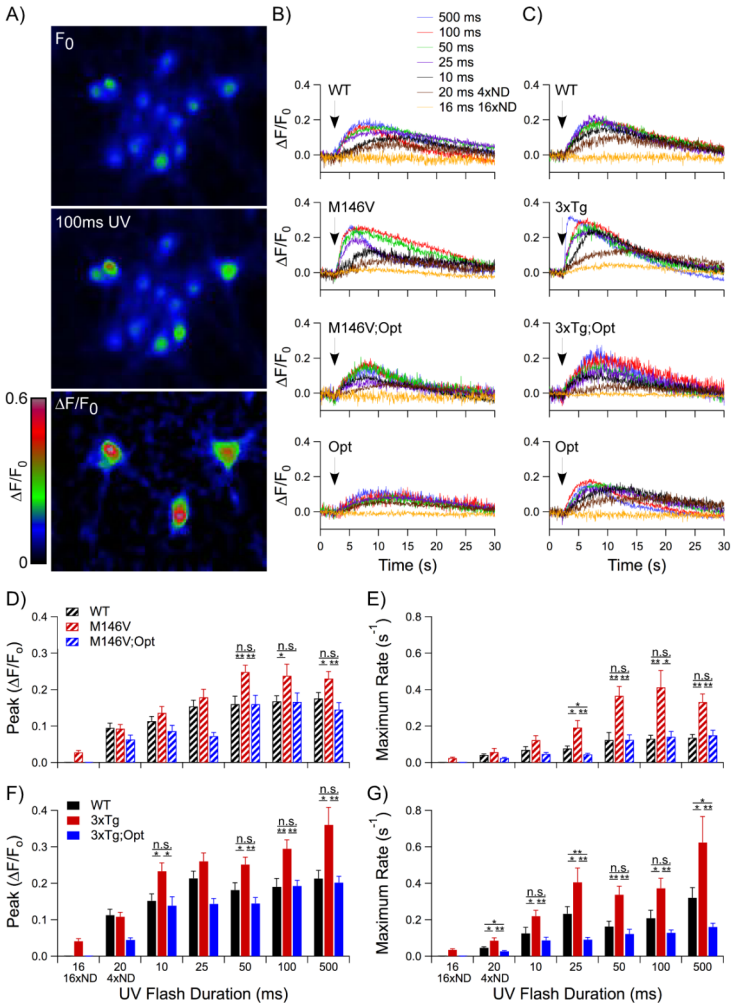

Figure 3.1 Oregon Green Ca^{2+} imaging in PCNs loaded with caged $InsP_3$.

PCN cultures were established from single embryonic day 14-16 mouse embryos and experiments were performed on 9-day-old cultures. Photolysis of caged $InsP_3$ was achieved by whole field illumination (350-400 nm; ~40 mW/mm^2) and stimulus strength was regulated by pulse duration and use of neutral density (ND) filters. Each cover slip was subjected to a single UV illumination, and experiments were performed on PCNs obtained from at least three different embryos for each genotype per UV illumination duration. *A*, Following a baseline recording (F_0), a 100 ms UV pulse was applied. *B & C*, Representative single cell traces for each genotype following UV illuminations (indicated by arrows) ranging from ~1 ms to 500 ms. *D-G*, Magnitudes (*D & F*), and rates (*E & G*) of Oregon Green fluorescence change following UV illumination. Data presented as mean ± SE *$p < 0.05$, **$p < 0.005$, (n.s.) not significant.

Figure 3.2

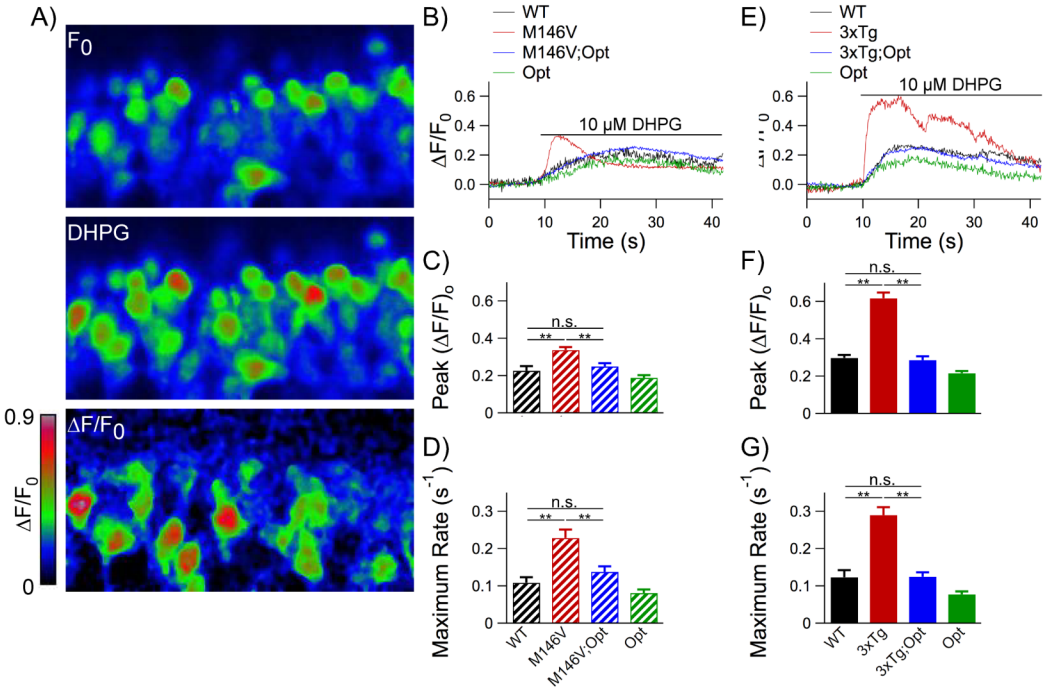

Figure 3.2 *Ex vivo* Oregon Green Ca^{2+} imaging in hippocampal dentate gyrus granular cell layer neurons.

300 μm thick brain slices containing hippocampal tissue were obtained from 10-12 day-old pups. *A*, Following a baseline recording (F_0), the solution was switched to aCSF containing 10 μM dihydroxyphenylglycine (DHPG) for the remainder of the recording period. *B & E*, Representative traces for (*B*) M146V lines and (*E*) 3xTg lines. *C & F*, Magnitudes of Oregon Green fluorescence change in (*C*) M146V lines and (*F*) 3xTg lines following DHPG perfusion. *D & G*, Rates of Oregon Green fluorescence change in (*D*) M146V lines and (*G*) 3xTg lines following DHPG perfusion. Experiments were conducted on slices obtained from at least three mice for each genotype. Data presented as mean ± SE **$p < 0.005$.

Figure 3.3

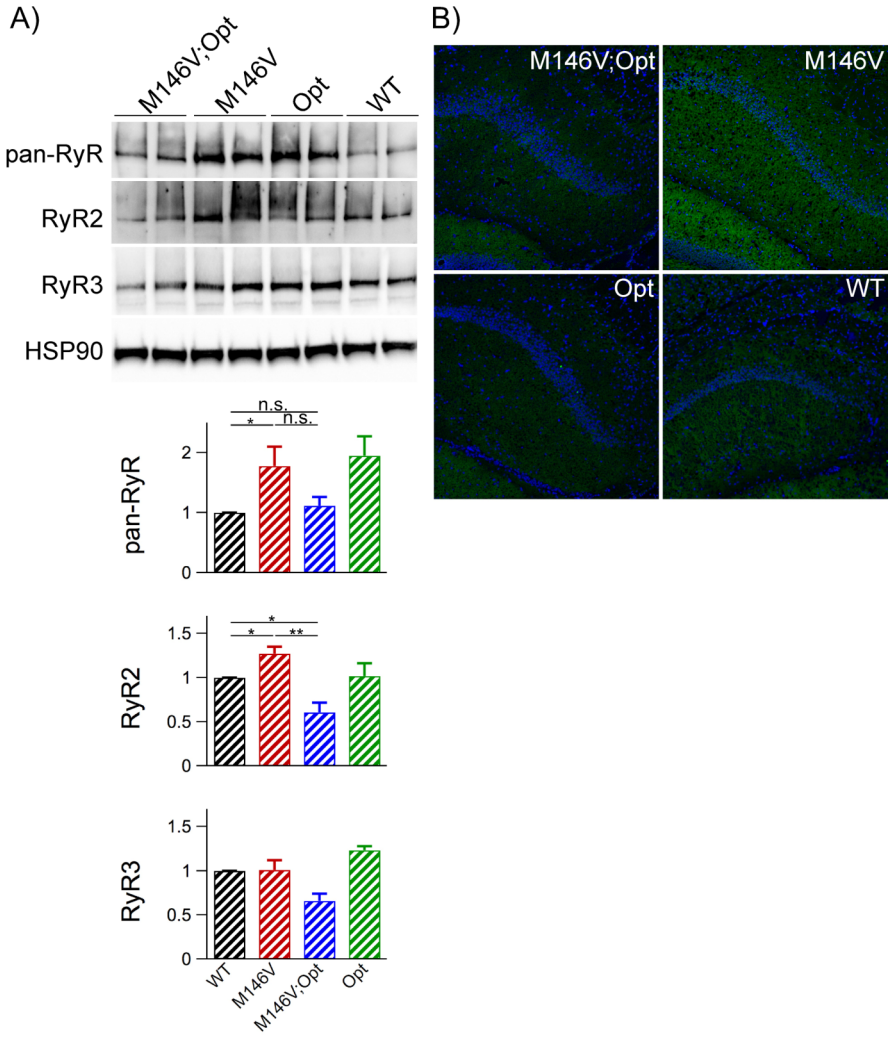

Figure 3.3 The Opt allele rescues elevated RyR protein level in M146V mice.

A, Western blot analysis of hippocampal lysates obtained from 5-wk-old animals using a pan-RyR antibody or antibodies specific to RyR2 or RyR3, and heat-shock protein 90 as a loading control ($n \geq 4$ of each genotype). *B*, Immunofluorescence on brain slices obtained from 5-wk-old animals using an antibody specific to RyR2. Hippocampal region CA1 is shown. Data presented as mean ± SE*$p \leq 0.05$, **$p \leq 0.005$.

Figure 3.4

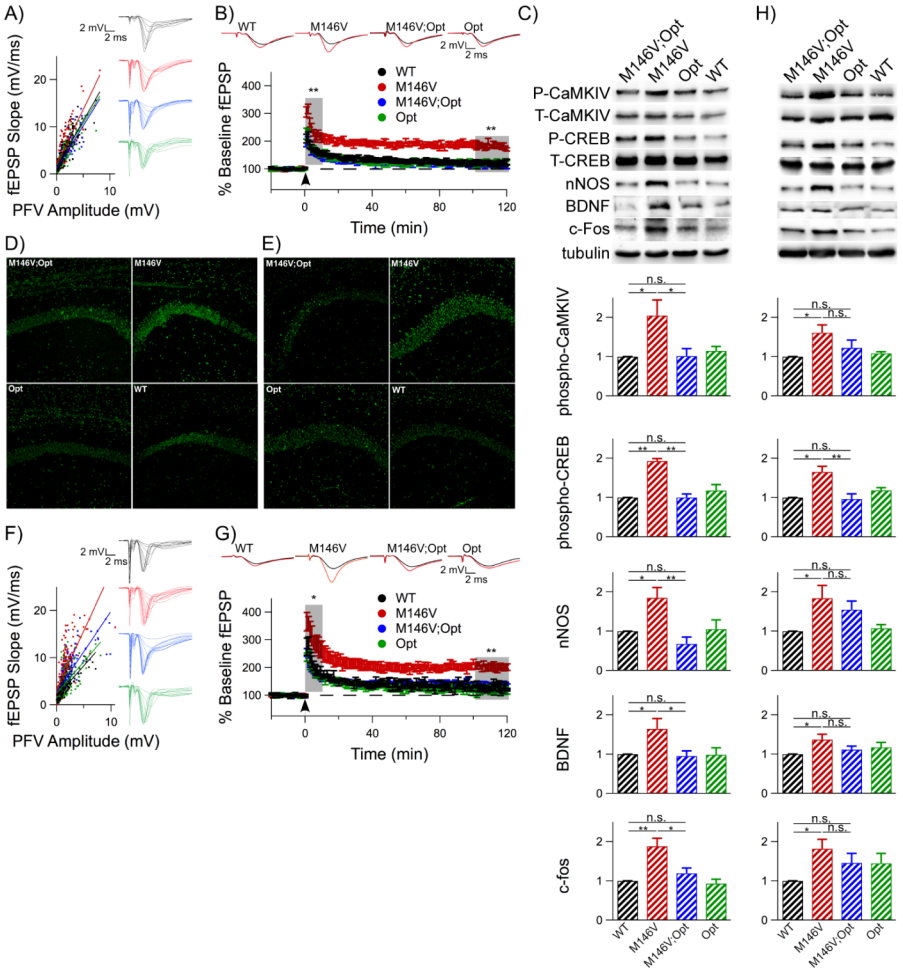

Figure 3.4 The Opt allele rescues enhanced hippocampal potentiation and aberrant activation of the CaMKIV-CREB transcriptional pathway in M146V mice.

A & *F*, Input (PFV)-output (fEPSP) curves obtained from electrophysiological experiments conducted in hippocampal region CA1 of (*A*) 5-wk-old mice (n ≥ 6 mice of each genotype) and (*F*) 3-mth-old mice (n ≥ 6 mice of each genotype). *B* & *G*, Hippocampal E-LTP resulting from a single 100 Hz, 1s tetanus applied at t = 0 in slices obtained from (*B*) 5-wk-old mice (n ≥ 5 mice of each genotype) and (*G*) 3-mth-old mice (n ≥ 5 mice of each genotype). The average of the baseline fEPSPs (black), and those recorded during the last 20 min (red) are presented. *C* & *H*, Western blot analysis of hippocampal lysates obtained from (*C*) 5-wk-old mice (n = 5 mice of each genotype) and (*H*) 3-mth-old mice (n = 6 mice of each genotype) for CaMKIV-CREB pathway activation and protein levels of CREB-dependent genes (phospho-CaMKIV (Thr-196) phospho-CREB (Ser-133)). *D* & *E*. Immunofluorescence in hippocampal sections from 5-wk-old mice for (*D*) phospho-CaMKIV (Thr-196) and (*E*) phospho-CREB (Ser-133). Data presented as mean ± SE *p < 0.05, **p < 0.005.

Figure 3.5

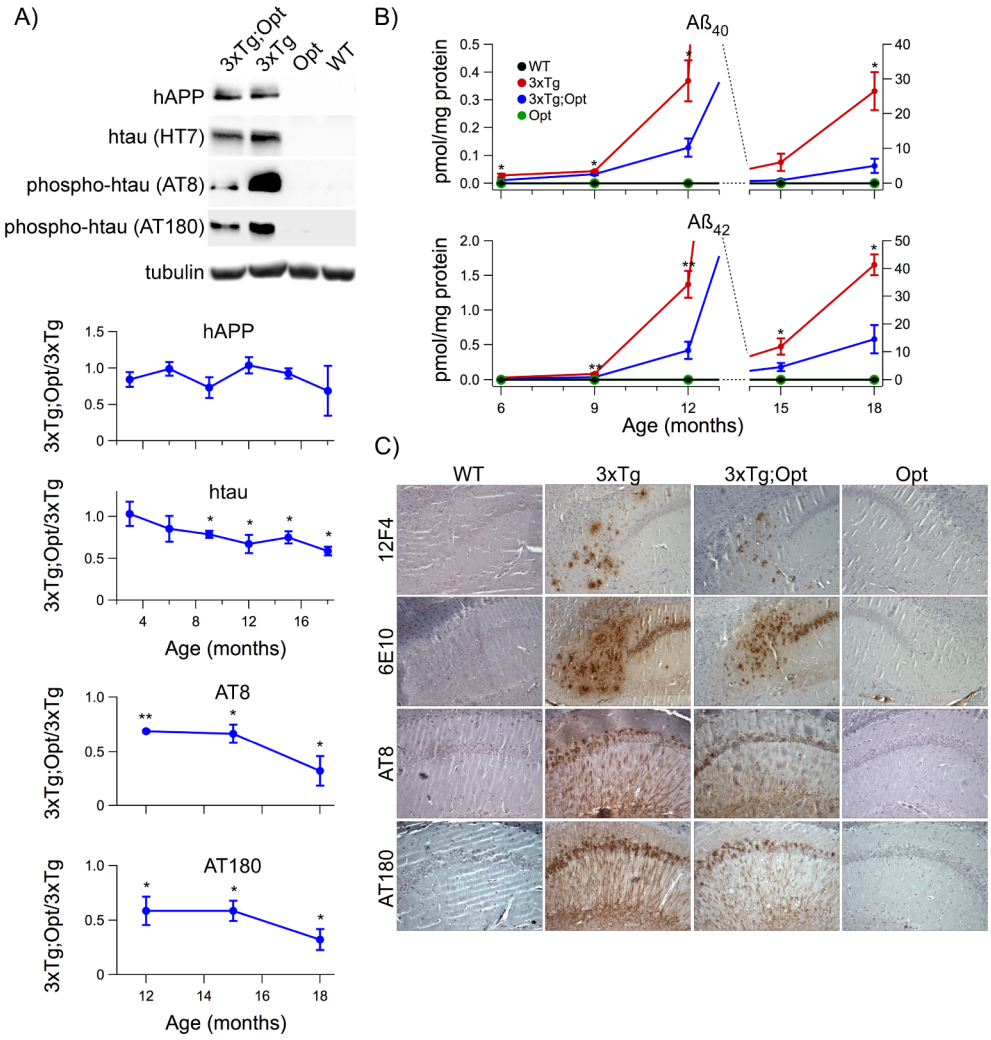

Figure 3.5 The Opt allele attenuates hippocampal Aβ and phospho-tau pathology in 3xTg mice.

A, Western blot analysis of hippocampal lysates obtained from mice 3- to 18-mths-of-age using antibodies specific for human APP (hAPP) (6E10), human tau (htau) (HT7), htau phosphorylated at Ser-202 (AT8) or Thr-231 (AT180), and tubulin as a loading control (n ≥ 3 for each genotype). Representative blots are from experiments conducted on 18-mth-old mice. *B*, ELISA analysis in hippocampal homogenates for $A\beta_{40}$ (top) and $A\beta_{42}$ (bottom) in mice ranging in age from 6- to 18-mths-old (n ≥ 5 for each genotype). Aβ content in homogenates obtained from WT and Opt animals were always below the detection limit of the ELISA. *C*, Immunohistochemistry on hippocampal slices obtained from 18-mth-old animals for Aβ and tau pathology. Data presented as mean ± SE *p ≤ 0.05, **p ≤ 0.005.

Figure 3.6

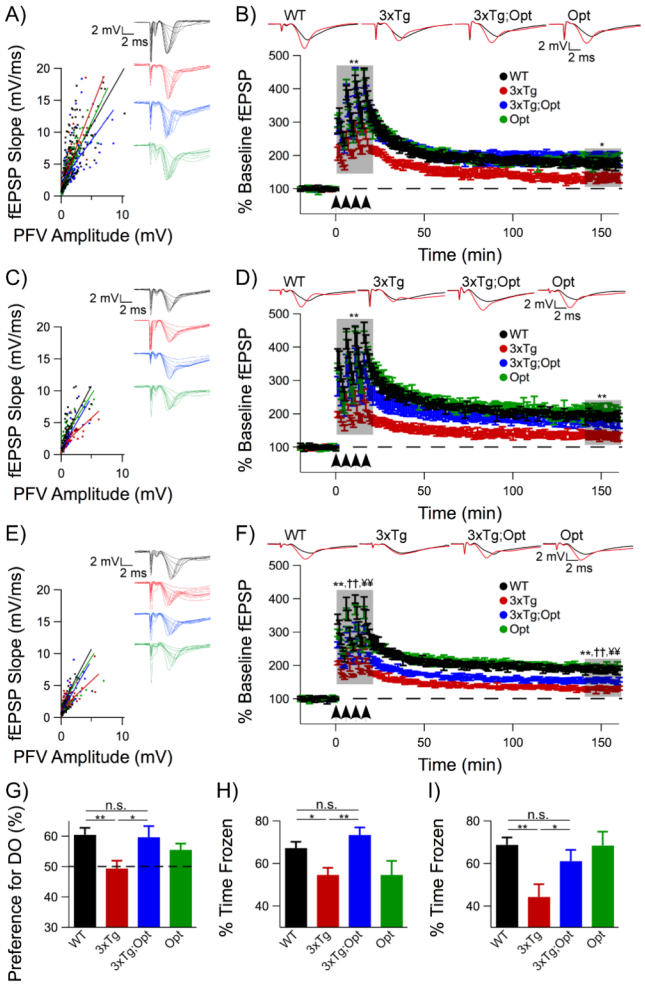

Figure 3.6 The Opt allele delays the onset and attenuates the severity of hippocampal deficits in 3xTg mice.

A, C & E, Input-output curves for each genotype at (*A*) 6- (n ≥ 7 mice for each genotype) (*C*) 9- (n ≥ 5 mice for each genotype) and (*E*) 12-mths-of-age (n ≥ 5 mice for each genotype). *B, D & F*, L-LTP in hippocampal region CA1 induced by application of four 100 Hz, 1s tetani with a 5 min inter-stimulus interval applied at t = 0. Experiments were conducted on slices obtained from mice (*B*) 6- (n ≥ 5 mice for each genotype) (*D*) 9- (n = 5 mice for each genotype) and (*F*) 12-mths-of-age (n = 5 mice for each genotype). The average of the baseline fEPSPs (black), and those recording during the last 20 min (red) are presented. Comparisons were made over the first 20 min post-tetani and over the last 20 min of the recording. *G*, Percentage preference for the displaced object (DO) during spatial object recognition testing on mice 12- to 13-mths-of-age (n ≥ 14 for WT, 3xTg and 3xTg;Opt; n = 7 for Opt). The dotted line indicates 50% (chance) preference. *H & I*, Percent of time spent frozen during a 3 min (*H*) contextual fear conditioning probe trial and (*I*) a 3 min cued fear conditioning probe trial (n ≥ 13 for WT, 3xTg and 3xTg;Opt; n = 7 for Opt). Data presented as mean ± SE *p ≤ 0.05, **,††,¥¥p ≤ 0.005.

Supplemental Figure 3.1

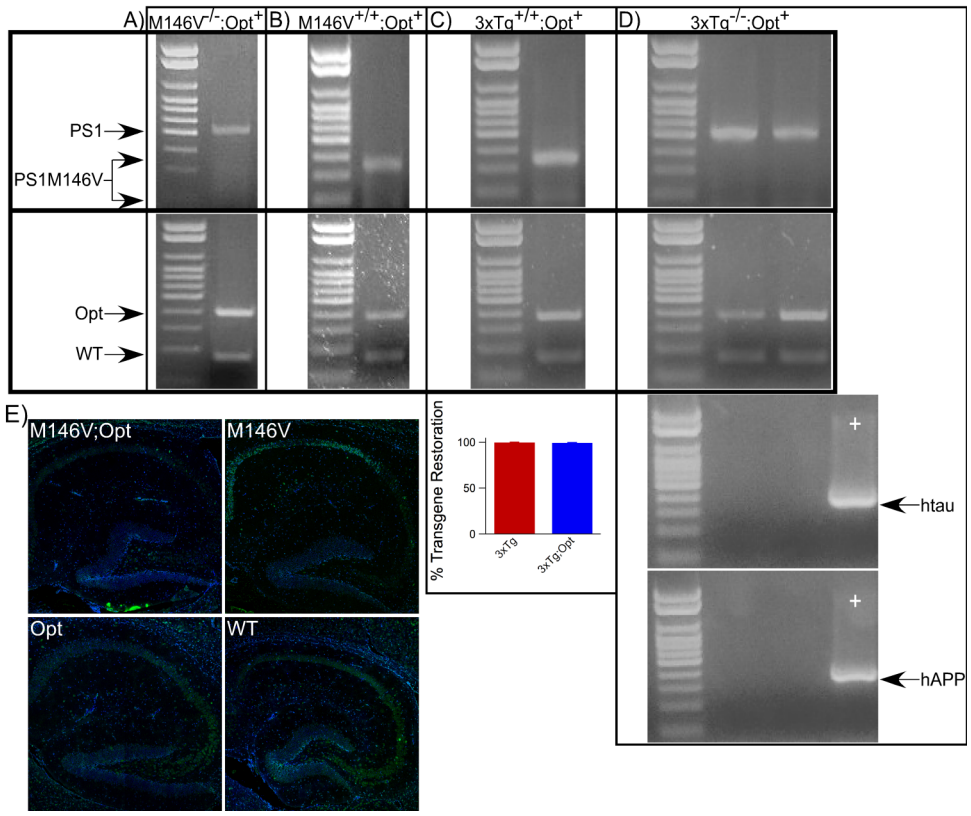

Supplemental Figure 3.1 Creation of the PS1M146V-KIN, $InsP_3R1^{Opt+/-}$ (M146V;Opt) and 3xTg, $InsP_3R1^{Opt+/-}$ (3xTg;Opt) mouse lines.

The Opisthotonos (Opt) allele is a spontaneously occurring in-frame deletion of exons 2 and 3 of the ITPR1 gene, which encodes the $InsP_3R1$ receptor, the major $InsP_3R$ expressed in the central nervous system. *A & B*, A C57BL/6 mouse carrying the Opt allele was crossed to a C57BL/6 mouse homozygote for the PS1M146V-KIN mutation. First generation $M146V^{+/-}$;$Opt^{+/-}$ mice were crossed to $M146V^{+/-}$ littermates without the Opt allele to (*A*) isolate the Opt allele on the WT background and (*B*) to generate the M146V;Opt line. *C & D*, A C57BL/6 mouse carrying the Opt allele was crossed to a C57BL/6/129S6 3xTg mouse (containing the PS1M146V-KIN mutation and the human APP_{SWE} and tau_{P301L} transgenes). *C*, First generation $3xTg^{+/-}$;$Opt^{+/-}$ mice were backcrossed to parental 3xTg mice to restore the PS1M146V-KIN mutation to homozygosity and the APP_{SWE} and tau_{P301L} transgenes' copy number. The bar graph presents data from real-time PCR experiments conducted on 3xTg;Opt genomic DNA for the APP_{SWE} and tau_{P301L} transgenes following six backcrosses to the 3xTg line. *D*, First generation $3xTg^{+/-}$;$Opt^{+/-}$ mice were crossed to littermates without the Opt allele to generate the control lines. *E*, Immunofluorescence analysis on hippocampal slices obtained from 5-wk-old mice using an antibody specific to $InsP_3R1$.

Supplemental Figure 3.2

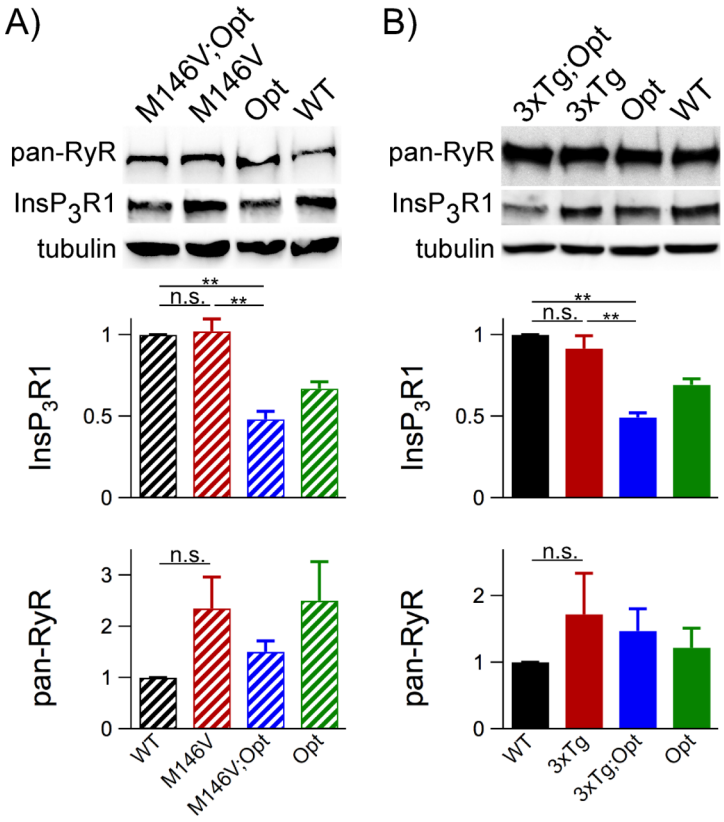

Supplemental Figure 3.2 $InsP_3R1$ and RyR protein levels in PCNs.

A & B, $InsP_3R1$ and RyR protein levels in PCNs obtained from (*A*) M146V (n = 4 of each genotype) and (*B*) 3xTg (n ≥ 5 of each genotype) lines, and tubulin as a loading control. Data presented as mean ± SE *p < 0.05; **p < 0.005.

Supplemental Figure 3.3

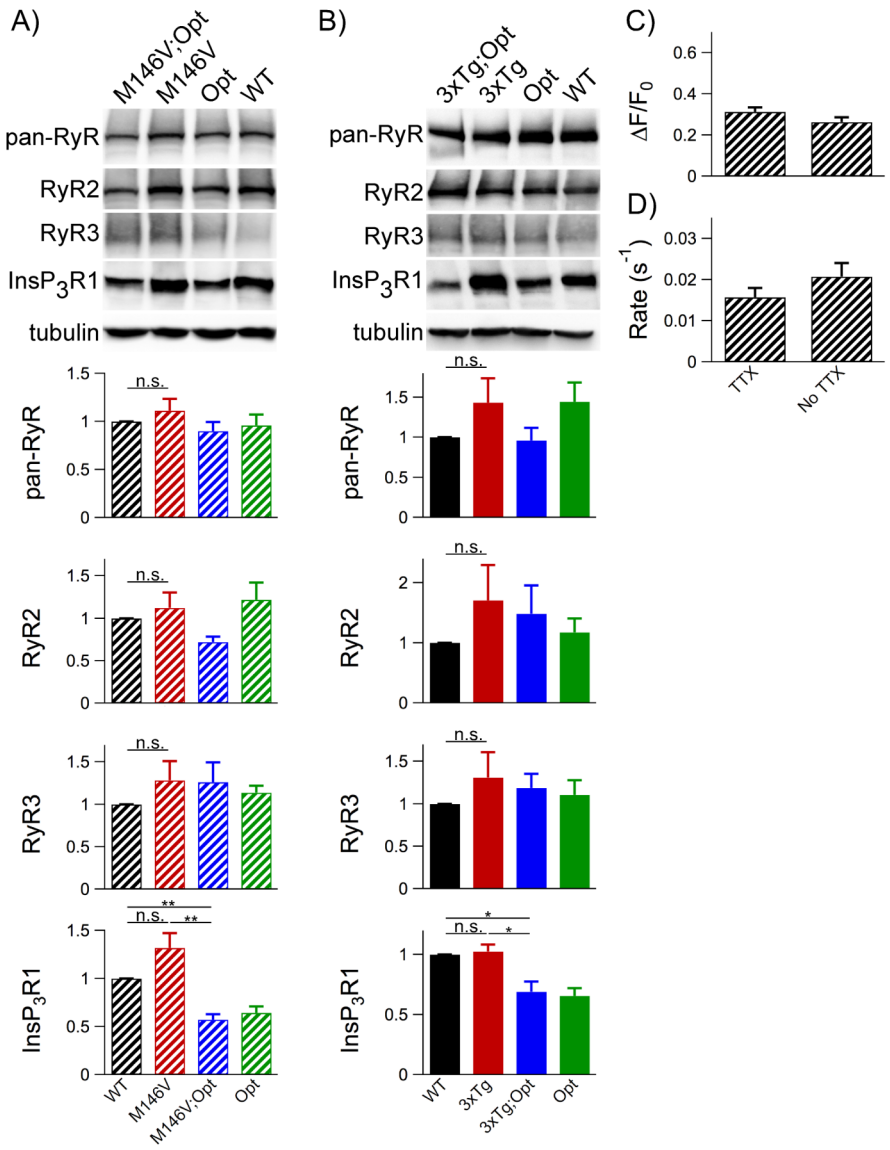

Supplemental Figure 3.3 *Ex vivo* Oregon Green Ca^{2+} imaging in hippocampal dentate gyrus granular cell layer neurons.

A & B, Western blot analysis of hippocampal lysates obtained from 10-12-day-old mice from (*A*) M146V lines (n = 6 for each genotype) and (*B*) 3xTg lines (n ≥ 6 for each genotype) using a pan-RyR antibody or antibodies specific to RyR2, RyR3 or $InsP_3R1$, and tubulin as a loading control. *C*, Magnitudes and (*D*) rates of Oregon Green fluorescence change in dentate gyrus granular cell layer neurons in WT mice (M146V control line) with and without tetrodotoxin present (n = 2 mice). Data presented as mean ± SE*p ≤ 0.05, **p ≤ 0.005.

Supplemental Figure 3.4

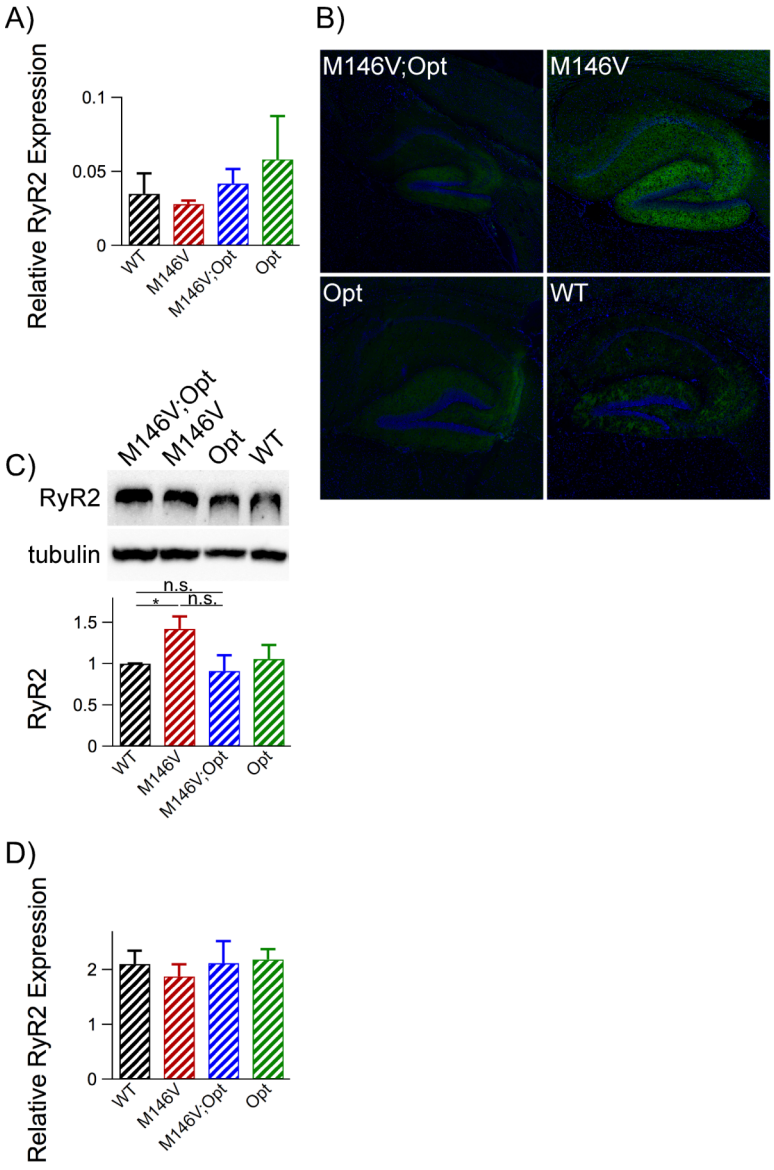

Supplemental Figure 3.4 The Opt allele rescues elevated RyR protein level in M146V mice.

A & D, RT-RTPCR on RNA isolate from hippocampal tissue of (*A*) 5-wk-old and (*D*) 3-mth-old animals using primers specific for RyR2 (n = 3 animals of each genotype). *B*, Immunofluorescence on brain slices obtained from 5-wk-old animals using an antibody specific for RyR2. *C*, Western blot analysis of hippocampal lysates obtained from 3-mth-old animals using a RyR2 specific antibody, and tubulin as a loading control (n =7 of each genotype). Data presented as mean ± SE*p ≤ 0.05.

Supplemental Figure 3.5

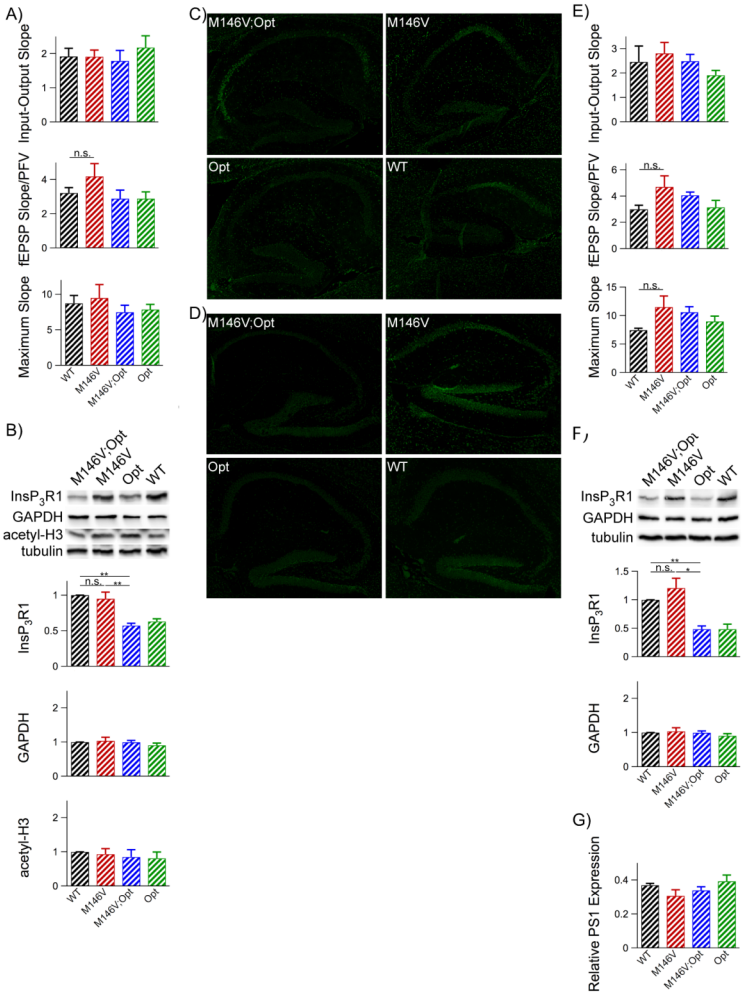

Supplemental Figure 3.5 The Opt allele rescues enhanced hippocampal potentiation and aberrant activation of the CaMKIV-CREB transcriptional pathway in M146V mice.

A & E, Basal synaptic transmission in hippocampal region CA1 as measured by the slope of the input-output curve, the ratio of the fEPSP slope to PFV amplitude at each applied voltage, and the maximum evoked fEPSP slope for slices obtained from (*A*) 5-wk-old mice ($n \geq 6$ mice of each genotype) and (*E*) 3-mth-old mice ($n \geq 6$ mice of each genotype). *B*, Hippocampal $InsP_3R1$, GAPDH and acetyl-H3 in 5-wk-old mice ($n \geq 5$ mice of each genotype). *C & D*, Immunofluorescence analysis on hippocampal slices obtained from 5-wk-old mice for (*C*) phospho-CaMKIV (Thr-196) and (*D*) phospho-CREB (Ser-133). *F*, Hippocampal $InsP_3R1$ and GAPDH protein levels in 3-mth-old mice ($n \geq 6$ mice of each genotype). *G*, RT-RTPCR on hippocampal RNA isolated from 3-mth old animals for PS1 expression ($n = 3$ mice of each genotype). Data presented as mean ± SE *$p < 0.05$, **$p < 0.005$.

Supplemental Figure 3.6

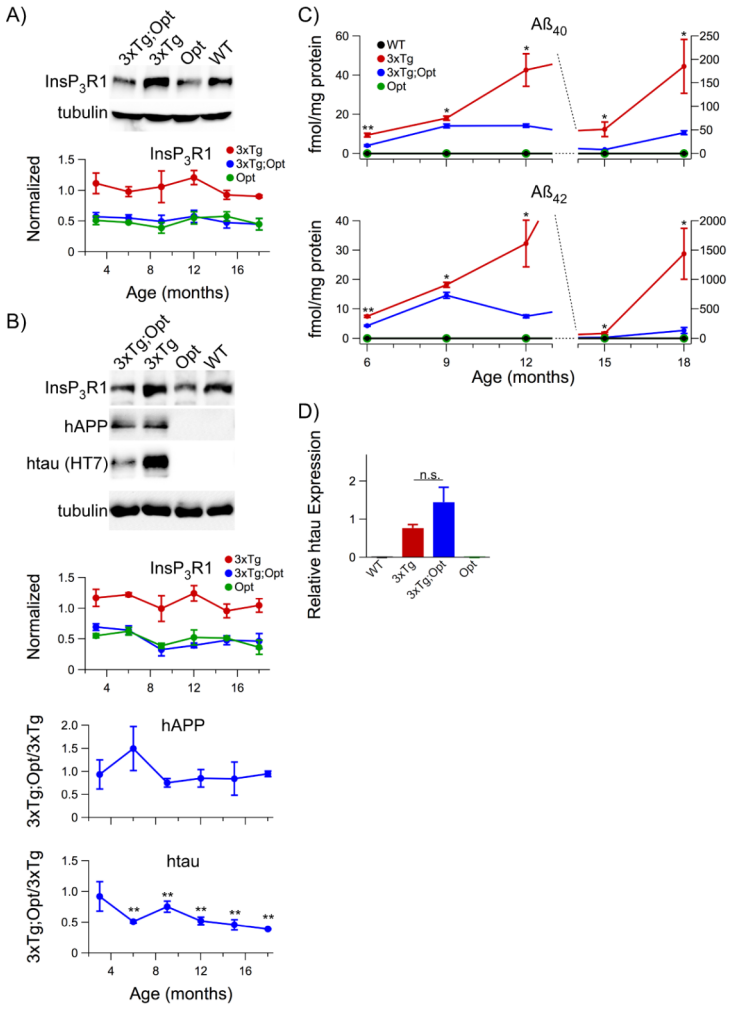

Supplemental Figure 3.6 The Opt allele attenuates hippocampal and cortical AD-like pathology in 3xTg mice.

A, Western blot analysis on hippocampal lysates obtained from mice 3- to 18-mths-of-age using an antibody specific for $InsP_3R1$, and tubulin as a loading control ($n \geq 3$ for each genotype). Data are normalized to WT. Representative blots are from experiments conducted on 18-mth-old mice. *B*, Western blot analysis of cortical lysates obtained from mice 3- to 18-mths-of-age, using antibodies specific for $InsP_3R1$ (data is normalized to WT), human APP (6E10), human tau (HT7), and tubulin as a loading control ($n \geq 3$ for each genotype). Representative blots are from experiments conducted on 18-mth-old mice. *C*, ELISA analysis of cortical homogenates for $A\beta_{40}$ (top) and $A\beta_{42}$ (bottom) in mice ranging in age from 6- to 18-mths ($n \geq 4$ for each genotype). Aβ content in homogenates obtained from WT and Opt animals were always below the detection limit of the ELISA. *D*, RT-RTPCR for htau expression conducted on cortical RNA isolated from 6-mth old animals (n = 3 mice of each genotype). Data presented as mean ± SE *$p \leq 0.05$, **$p \leq 0.005$.

Supplemental Figure 3.7

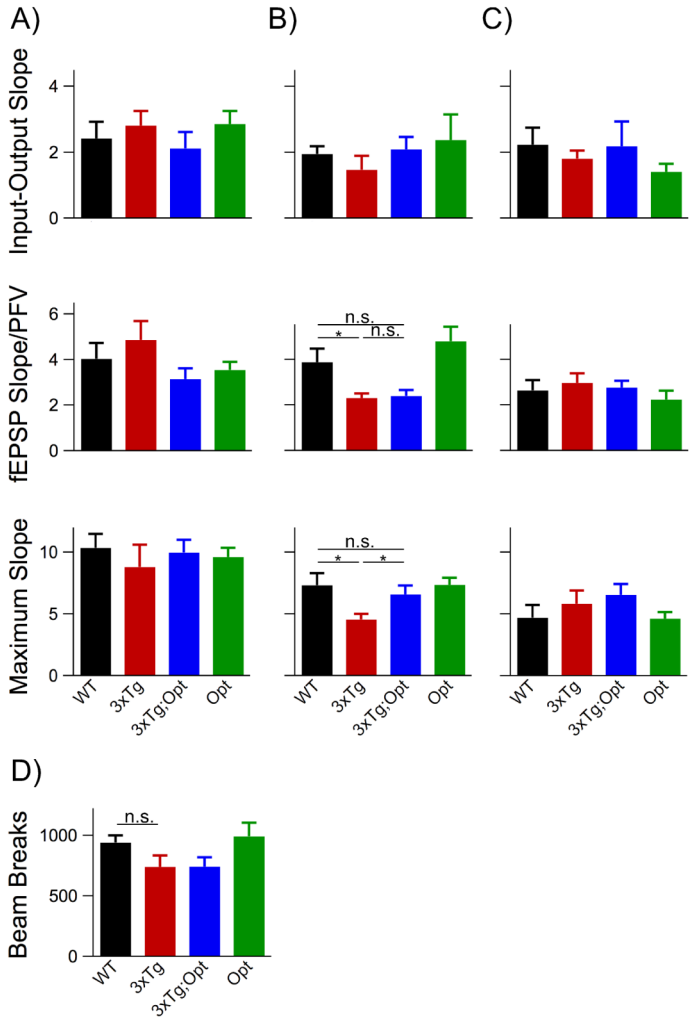

Supplemental Figure 3.7 The Opt allele delays the onset and attenuates the severity of hippocampal deficits in 3xTg mice.

A-C, Basal synaptic transmission in mice at (*A*) 6- (n ≥ 7 mice for each genotype) (*B*) 9- (n ≥ 5 mice for each genotype) and (*C*) 12-mths-of-age (n ≥ 5 mice for each genotype) as measured by the slope of the input-output curve, the ratio of the fEPSP slope to the PFV amplitude at each applied voltage, and the maximum evoked fEPSP slope. *D*, 10 min open-field test conducted on mice 12- to 13-mths-of-age to measure activity (n ≥ 16 for WT, 3xTg and 3xTg;Opt; n = 7 for Opt). Data presented as mean ± SE *p ≤ 0.05.

Chapter 4: Discussion

AD is the most prevalent form of dementia, resulting in cognitive decline and death. The aberrant molecular mechanisms responsible for the disease remain elusive. However, recent studies suggest that cellular changes occur decades prior to symptom onset (Jack et al., 2013). The work described in the previous chapters extends our understanding of the mechanisms and contributions of aberrant $[Ca^{2+}]_i$ signaling to AD pathogenesis. In this thesis, we present data supporting the hypothesis that FAD mutations in PSs cause exaggerated $[Ca^{2+}]_i$ signaling through an interaction with the $InsP_3R1$ that results in a gain-of-function enhancement of $InsP_3R1$ gating and ligand sensitivity. Additionally, we observed that exaggerated $[Ca^{2+}]_i$ signaling contributes to AD pathogenesis. Specifically, in Chapter 2, we test postulated mechanisms by which FAD mutant PS is hypothesized to cause exaggerated $[Ca^{2+}]_i$ signaling. However, we were unable to confirm the hypotheses that FAD mutations in PS disrupt its normal function as an ER Ca^{2+} leak channel (Tu et al., 2006) or that they provide a gain-of-function enhancement of SERCA pump activity, thereby resulting in enhanced filling of ER Ca^{2+} stores (Green et al., 2008). In Chapter 3, we show that decreasing the amount of $InsP_3R1$ protein present in hippocampal and cortical tissues rescues exaggerated $[Ca^{2+}]_i$ signaling. This allowed us to determine the *in vivo* contribution of exaggerated $[Ca^{2+}]_i$ signaling to AD pathogenesis. We found that $InsP_3R1$-dependent exaggerated $[Ca^{2+}]_i$ signaling contributes to MCI- and AD-like phenotypes present in AD mouse models. Together these findings support the idea that proximal changes in $[Ca^{2+}]_i$ signaling, due to

a gain-of-function enhancement of $InsP_3R1$ gating by FAD mutant PS, contribute to AD pathogenesis.

Exaggerated $[Ca^{2+}]_i$ Signaling is $InsP_3R1$-dependent

Our findings, consistent with the hypothesis that FAD mutations in PS result in exaggerated $[Ca^{2+}]_i$ signaling by a gain-of-function enhancement of $InsP_3R1$ gating, raise a very important question for future research - what regions of the PS and $InsP_3R$ proteins interact? Clues to the location come from the literature.

Previous studies employed co-immunoprecipitation to demonstrate an interaction between both WT and FAD PS1 or PS2 and $InsP_3R1$ or $InsP_3R3$ (Cheung et al., 2008). Although the effects of FAD mutant PS on $InsP_3R2$ gating have not been investigated, exaggerated $[Ca^{2+}]_i$ signaling is observed in FAD mutant PS expressing astrocytes, which predominantly express $InsP_3R2$ (Kuchibhotla et al., 2009). This suggests that a PS-$InsP_3R2$ interaction may also occur. These observations indicate that conserved elements between the two PS homologs and the three $InsP_3R$ homologs must be involved.

PSs are known to interact with many proteins. In fact, the N-terminus residues 1-87 of PS1 and PS2 interact with the RyR receptor, the other main ER Ca^{2+} release channel (Hayrapetyan et al., 2008; Rybalchenko et al., 2008). The PS2-RyR interaction is highly dependent upon $[Ca^{2+}]$ (Takeda et al., 2005), suggesting that PS2 binding might be dependent upon the conformation state of the RyR or that PSs might share an overlapping binding site with Ca^{2+} or a Ca^{2+}-activated RyR binding protein (Lanner et al., 2010). The possibility of a conformation state or context specific interaction should also be considered when investigating the PS-$InsP_3R$ interaction.

Recently, the first crystal structure of a PS family member was published (Li et al., 2012). Although the protein crystallized is a distant relative of human PS, the structure does identify a possible interaction site with the $InsP_3R$. This study observed a large membrane spanning hydrophobic pore surrounded by TM regions TM2, TM3, TM5 and TM7. The large diameter and hydrophobic nature of the residues lining the pore suggest that it may be a binding pocket for interacting proteins. Future studies mapping the PS-$InsP_3R$ interaction should focus on conserved regions of the PS and $InsP_3R$ homologs, consider conformation or context specific interactions, and the possibility that either the PS N-terminus and/or its hydrophobic pore are the sites of $InsP_3R$ binding. The fact that PS mutations tend to segregate to the TM regions suggest that the later may be the most likely location. In fact, PSs TM3 contains 11% of FAD mutations.

Mechanisms of Ca^{2+}-induced Alzheimer's Disease Pathogenesis

The work presented in this thesis supports a causative role for exaggerated $[Ca^{2+}]_i$ signaling in AD pathogenesis *in vivo*, and lays the groundwork for future studies investigating how Ca^{2+} activates pathological processes.

Amyloid precursor protein metabolism

Although the mechanisms are not well understood, elevations in cytosolic $[Ca^{2+}]$ clearly affect APP metabolism. To-date, mechanistic studies have largely focused on understanding how Ca^{2+} entry through NMDA receptors influences APP metabolism rather than Ca^{2+} released from intracellular stores. Although the source of a Ca^{2+} signal does play a large role in determining its effect, insights from studies on NMDA-mediated increases in cytosolic $[Ca^{2+}]$ may be applicable to $InsP_3R$-mediated elevations. Previous

groups have observed that NMDA-mediated Ca^{2+} entry can either activate (Lesne et al., 2005) or inhibit (Hoey et al., 2009) Aβ production depending on the duration of the increase in cytosolic [Ca^{2+}], with maintained elevations promoting Aβ production. A subsequent report suggested that this paradoxical effect of Ca^{2+} on APP metabolism is due to the population of NMDA receptors activated, with extra-synaptic NDMA receptor activation but not synaptic NMDA receptor activation, found to increase Aβ production (Bordji et al., 2010). The activation of extra-synaptic NDMA receptors resulted in a smaller rise in cytosolic [Ca^{2+}] compared to synaptic receptor activation, and favored APP pre-mRNA splicing towards amyloid favoring slice variants (Bordji et al., 2010).

However, this mechanism cannot account for the observed attenuation of Aβ accumulation in our studies because the 3xTg mouse transgenically expresses the neuronal isoform of the APP gene, which cannot be alternatively spliced. An explanation for our observations most likely comes from studies indicating that APP functions in synapse formation and function (Priller et al., 2006). In fact, synaptic activity appears to influence APP processing in a rapid manner, independent of *de novo* transcription. Synaptic activity influences Aβ levels directly (Kamenetz et al., 2003; Cirrito et al., 2005), and Aβ inhibits neuronal excitability (Kamenetz et al., 2003; Shankar et al., 2008). Recently it was found that interstitial fluid Aβ levels are affected in opposite directions depending on the dose of NMDA administered (Verges et al., 2011). Low NMDA doses increased synaptic transmission and lead to elevated Aβ production, whereas high doses diminished Aβ production (Verges et al., 2011). This difference was suggested to be due to differential phosphorylation of extracellular signal-regulated kinase (ERK), which in

its phospho-state can influence the activity of the secretases involved in APP metabolism (Verges et al., 2011).

The contradictory findings of these studies highlight one of the major pitfalls of using mice to study AD – they do not develop Alzheimer's disease. Transgenic expression of multiple mutant human genes is required to observe AD-like histopathology. This artificial system does not reflect the events occurring in the human disease and may give rise to histopathology through physiological irrelevant pathways. Therefore, better systems are needed to understand how increases in cytosolic [Ca^{2+}], arising from both extracellular and intracellular sources, influence APP metabolism. Future studies to address this issue should use FAD patients' fibroblasts in combination with induced pluripotent stem cell technology. This would allow for the study of APP metabolism in human "neuronal" cells with all genes under the control of endogenous promoters and post-translational modification mechanisms. Such a system would allow for the dissection of how FAD mutant PS associated exaggerated $[Ca^{2+}]_i$ signaling influences APP metabolism, either through pre-mRNA slicing, post-translational modification of APP, and/or modification of signal transduction pathways.

Tau hyperphosphorylation

Our studies revealed that exaggerated $[Ca^{2+}]_i$ signaling contributes to phospho-tau accumulation. Cytosolic [Ca^{2+}] clearly affects the kinases involved in tau phosphorylation, including GSK-3β and CDK5. However, questions still remain regarding the mechanisms by which this occurs.

GSK-3's role in AD pathogenesis is clearly demonstrated by a double-blind placebo-controlled clinical trail on MCI patients treated with lithium, a GSK-3β

antagonist. This study found a significant reduction in cerebrospinal fluid levels of phospho-tau in lithium treated individuals compared to placebo (Forlenza et al., 2011). Additionally, selective silencing of GSK-3α or -3β in AD mice diminished AD pathology accumulation (Hurtado et al., 2012). GSK-3β is constitutively active, but phosphorylation can inhibit or further activate is kinase activity. Both the insulin/PI3K/Atk and Wnt signaling pathways negatively regulate GSK-3 activity (Grimes and Jope, 2001), whereas Pyk2 phosphorylation enhances its activity (Sayas et al., 2006). Despite the observations that GSK-3β-dependent tau phosphorylation is induced by treatment of SH-SY5Y cells with low concentrations of a Ca^{2+} ionophore (Hartigan and Johnson, 1999) or in response to Ca^{2+} release from internal stores (Sayas et al., 2006), how Ca^{2+} affects GSK-3β activity is not established. Studies suggest that it may be through the Ca^{2+}-dependent activation of Pyk2 (Sayas et al., 2006). However, the effects of tyrosine phosphorylation on GSK-3β activity are not well studied. Future studies should investigate the contexts and effects of this phosphorylation on GSK-3β's activity and its contribution to phospho-tau accumulation.

Alternatively, FAD PS mutants could affect GSK-3β activity in a Ca^{2+}-independent manner by either inhibiting PS-dependent PI3K/Akt signaling, which normally acts to inhibit GSK-3β activity (Baki et al., 2004), or through promoting Aβ generation that also inhibits PI3K/Akt signaling (Takashima et al., 1996). Future studies are needed to determine the Ca^{2+}-dependence, and mechanism by which exaggerated $[Ca^{2+}]_i$ signaling contributes to GSK-3β activation.

In contrast, a mechanism for CDK5 activation by the Ca^{2+}-dependent calpain protease is well established. Calpain is aberrantly activated in the brains of AD patients

(Saito et al., 1993) and the level of calpain's endogenous inhibitor, calpastatin, is decreased (Nilsson et al., 1990). Treatment of AD mice with calpain inhibitors or over-expression of calpastatin decreased phospho-tau accumulation (Liang et al., 2010; Medeiros et al., 2012), restored normal synaptic function in hippocampal slices, and improved spatial-working memory and associative fear memory (Trinchese et al., 2008). These studies found that inhibition of calpain correlated with reduced levels of CDK5 activation (Liang et al., 2010; Medeiros et al., 2012), suggesting that calpain is a link between exaggerated $[Ca^{2+}]_i$ signaling and tau hyperphosphorylation. However, these studies are correlative rather than causative. Future studies should address the necessity of CDK5 activity for phospho-tau accumulation, perhaps by viral silencing, as was done for the GSK-3 isoforms (Hurtado et al., 2012).

Alternatively, or in addition to normalization of aberrantly activated tau kinases, decreasing $InsP_3R1$-mediated exaggerated $[Ca^{2+}]_i$ signaling may also decrease phospho-tau accumulation by activating the autophagy pathway. Autophagy is an intracellular pathway for degradation of abnormal proteins and prevents their accumulation. Inhibition of $InsP_3R$-mediated Ca^{2+} release induces autophagy (Cardenas et al., 2010), and enhancing autophagy provides rescue in animal models of neurodegenerative disease (Garcia-Arencibia et al., 2010). Future studies should investigate the effects of the Opt allele on the activity of the autophagy pathway.

Synaptic deficits

Ca^{2+} release from $[Ca^{2+}]_i$ stores plays an important role in hippocampal plasticity (Bashir et al., 1993; Futatsugi et al., 1999; Fujii et al., 2000; Raymond and Redman, 2006; Mellentin et al., 2007), and findings in this thesis indicate that FAD mutant PS-

associated exaggerated $[Ca^{2+}]_i$ signaling contributes directly to aberrant hippocampal synaptic plasticity. Our E-LTP studies revealed two distinct effects of exaggerated $[Ca^{2+}]_i$ signaling on E-LTP: (1) an enhancement in the induction phase (the change in synaptic strength directly following tetanus application, also known as post-tetanic potentiation (PTP)), and (2) maintenance (≥ 80 min post-tetanus application) of enhanced synaptic strength resulting from a single tetanus.

(1) *Enhanced PTP:* The mechanisms underlying PTP are mainly mediated by changes in the pre-synaptic terminal, through adjustments to the release probability (Pr) of synaptic vesicles and the size of the readily releasable pool (RRP) of synaptic vesicles. Changes in the Pr are mediated by tetanus-induced increases in pre-synaptic terminal $[Ca^{2+}]$. Normally, mitochondria act to buffer these increases in $[Ca^{2+}]$, and following termination of the tetanus the mitochondria leak the Ca^{2+} back into the pre-synaptic terminal. This results in a prolonged period of elevated pre-synaptic $[Ca^{2+}]$. Since the fusion of synaptic vesicles with the pre-synaptic membrane is Ca^{2+}-dependent, this long-lasting elevation in presynaptic $[Ca^{2+}]$ increases the Pr (Lee et al., 2007). FAD mutant PS-associated exaggerated $[Ca^{2+}]_i$ signaling may enhance PTP by causing further elevations in presynaptic $[Ca^{2+}]$ during tetanus application. This could increase the magnitude of the PTP.

In addition to changes in the Pr, exaggerated $[Ca^{2+}]_i$ signaling may influence the size of the RRP, which is dependent upon activation of the Ca^{2+}-dependent binding of calmodulin to myosin light chain kinase (MLCK). Active MLCK phosphorylates myosin light chain, thereby altering the trafficking of synaptic vesicles from the slowly releasing pool to locations where they can be readily released (Lee et al., 2010). Therefore, FAD

mutant PS-associated exaggerated $[Ca^{2+}]_i$ signaling may enhance PTP by increasing basal levels of calmodulin activation and/or causing enhanced activation of calmodulin following tetanus application. Future experiments should be conducted to investigate differences in pre-synaptic $[Ca^{2+}]$ dynamics between WT and M146V mice during PTP.

(2) *Maintenance of enhanced synaptic strength resulting from a single tetanus.* We believe that the association between exaggerated $[Ca^{2+}]_i$ signaling and long-lasting changes in synaptic strength induced by a single tetanus observed in hippocampal slices from M146V mice is indirect, mediated by constitutive activation of the CaMKIV-CREB transcriptional pathway. CREB transcription is important for the conversion of transient to long-lasting changes in synaptic strength (Yin and Tully, 1996). Mice over-expressing CaMKIV (Fukushima et al., 2008) or harboring constitutively active CREB (Barco et al., 2002) demonstrate a lowered threshold for eliciting long-lasting increases in synaptic strength independent of *de novo* transcription. Consistent with the idea that this effect is indirect, we observed elevated protein levels of CREB-dependent genes, including BDNF and nNOS, specifically in M146V mice. Both BDNF (Lu et al., 2008) and nNOS (Steinert et al., 2010) have significant roles in regulating synaptic plasticity. In fact, BDNF application can induce transformation of E-LTP to L-LTP in the presence of protein synthesis inhibitors (Pang and Lu, 2004). Future experiments should determine the contribution of these molecules to M146V-associated enhanced synaptic strength maintenance by using viral techniques to knock-down BDNF expression in M146V mice, crossing the M146V mouse to a $BDNF^{+/-}$ line (Chourbaji et al., 2004), or treatment with BDNF antibodies to deplete BDNF levels in the hippocampus (Mu et al., 1999).

Contributions of nNOS to enhanced LTP should be investigated using pharmacological inhibitors.

Interestingly, MCI patients demonstrate enhanced hippocampal activation during performance of memory tasks (Dickerson et al., 2005). Recently this observation was made in pre-symptomatic FAD mutant carriers (Quiroz et al., 2010; Reiman et al., 2012). Our findings suggest this may be due to constitutive activation of the CaMKIV-CREB pathway resulting from exaggerated $[Ca^{2+}]_i$ signaling. Further studies should investigate the activity of the CaMKIV-CREB transcriptional pathway in these patients as an early biomarker for AD.

Implications for Therapeutic Approaches

In the current study, we have shown that $InsP_3R$-dependent exaggerated $[Ca^{2+}]_i$ signaling is a proximal event *in vivo* that contributes to the MCI-like phenotypes in M146V mice and AD-like phenotypes in 3xTg mice. These data strongly suggest that early targeting of $InsP_3R$-mediated Ca^{2+} release might be a potential therapeutic strategy for treating patients at risk for developing AD.

Current therapeutic approaches

Currently there are four drugs approved to treat AD, three of which are acetylcholinesterase inhibitors. The other is memantine, an uncompetitive moderate-affinity NMDA receptor antagonist. Unfortunately, these current therapeutic approaches provide only symptomatic relief and do not appear to significantly alter the course of AD pathogenesis. This may in part be due to the fact that they are typically prescribed to patients suffering from advanced stages of the disease. Therefore, early biomarkers for

AD must be identified that allow for current therapies to be used more effectively. Our findings indicated that exaggerated $[Ca^{2+}]_i$ signaling may be one such biomarker, and assaying for CaMKIV-CREB pathway activation might be a potential indirect, but high-throughput assay to diagnose AD in its early stages.

Future therapeutic approaches

The findings in this thesis identify potential drug targets for treating AD including: (1) molecules upstream of the $InsP_3R$, (2) the $InsP_3R$, (3) molecules that disrupt the FAD mutant PS-$InsP_3R$ interaction or (4) molecules downstream of the $InsP_3R$.

(1) *Molecules upstream of the $InsP_3R$* – previous studies have found that lithium is beneficial in altering the course of AD if given early. Lithium has several targets, including GSK-3β and the inositol monophosphatase (IMPase) involved in $InsP_3$ generation. Studies have found that lithium's protective effects maybe due to IMPase inhibition (Teo et al., 2009). However, the multiple targets of lithium obscure the truth. Our studies suggest that inhibition of IMPase activity may be lithium's mechanism of action, and suggest that specific inhibitors of phosphatidylinositol metabolism should be identified and tested as AD therapeutics.

(2) *The $InsP_3R$* – Our studies specifically targeted the $InsP_3R1$, the predominant $InsP_3R$ expressed in the CNS. We found that reduction of $InsP_3R1$ protein by ~50% had no deleterious effects, indicating a potential therapeutic window. This suggests that $InsP_3R1$ specific inhibitors may prove beneficial in treating AD. Alternatively, siRNA, viral, or zinc finger exonuclease technology could be used to decrease expression of $InsP_3R1$.

However, decreasing $InsP_3R1$ expression might be technically challenging as too complete of a decrease in $InsP_3R1$ protein level results in motor discoordination, seizures and death in mice (Street et al., 1997).

(3) *Molecules that disrupt the FAD mutant PS-$InsP_3R$ interaction* – The WT PS-$InsP_3R$ interaction does have minor effects on $InsP_3R$ gating, however genetic ablation of both PS homologs does not result in significantly altered $InsP_3R$ gating properties (Cheung et al., 2010). This indicates that disruption of the PS-$InsP_3R$ interaction, with a small molecule or peptide, may be physiologically tolerable and a valid therapeutic approach.

(4) *Molecules downstream of the $InsP_3R$* – Our results suggest that $InsP_3R$-mediated exaggerated $[Ca^{2+}]_i$ signaling contributes to AD pathogenesis by modulating the activity of several downstream pathways. These pathways could be targeted in a multipronged approach, and would need to include inhibitors of APP metabolism and tau kinases and/or the molecules that activate tau kinases. This treatment strategy has the benefit that the developed molecules could be used individually to treat diseases in which only one of these pathways is aberrantly activated (e.g. frontotemporal dementia).

Regardless of which avenue provides success, our results lay the groundwork for future investigators to better understand early abnormalities in AD and identify and target disease-modifying processes in AD.

REFERENCES

Ahlijanian MK, Barrezueta NX, Williams RD, Jakowski A, Kowsz KP, McCarthy S, Coskran T, Carlo A, Seymour PA, Burkhardt JE, Nelson RB, McNeish JD (2000) Hyperphosphorylated tau and neurofilament and cytoskeletal disruptions in mice overexpressing human p25, an activator of cdk5. Proc Natl Acad Sci U S A 97:2910-2915.

Alves da Costa C, Sunyach C, Pardossi-Piquard R, Sevalle J, Vincent B, Boyer N, Kawarai T, Girardot N, St George-Hyslop P, Checler F (2006) Presenilin-dependent gamma-secretase-mediated control of p53-associated cell death in Alzheimer's disease. J Neurosci 26:6377-6385.

Alzheimer's Association T (2012) Alzheimer's Disease Facts and Figures. Alzheimer's & Dementia 8.

Angehagen M, Margineanu DG, Ben-Menachem E, Ronnback L, Hansson E, Klitgaard H (2003) Levetiracetam reduces caffeine-induced Ca2+ transients and epileptiform potentials in hippocampal neurons. Neuroreport 14:471-475.

Apelt J, Bigl M, Wunderlich P, Schliebs R (2004) Aging-related increase in oxidative stress correlates with developmental pattern of beta-secretase activity and beta-amyloid plaque formation in transgenic Tg2576 mice with Alzheimer-like pathology. Int J Dev Neurosci 22:475-484.

Auffret A, Gautheron V, Mattson MP, Mariani J, Rovira C (2010) Progressive age-related impairment of the late long-term potentiation in Alzheimer's disease presenilin-1 mutant knock-in mice. J Alzheimers Dis 19:1021-1033.

Auffret A, Gautheron V, Repici M, Kraftsik R, Mount HT, Mariani J, Rovira C (2009) Age-dependent impairment of spine morphology and synaptic plasticity in hippocampal CA1 neurons of a presenilin 1 transgenic mouse model of Alzheimer's disease. J Neurosci 29:10144-10152.

Baek SH, Ohgi KA, Rose DW, Koo EH, Glass CK, Rosenfeld MG (2002) Exchange of N-CoR corepressor and Tip60 coactivator complexes links gene expression by NF-kappaB and beta-amyloid precursor protein. Cell 110:55-67.

Baki L, Shioi J, Wen P, Shao Z, Schwarzman A, Gama-Sosa M, Neve R, Robakis NK (2004) PS1 activates PI3K thus inhibiting GSK-3 activity and tau overphosphorylation: effects of FAD mutations. Embo J 23:2586-2596.

Bakker A, Krauss GL, Albert MS, Speck CL, Jones LR, Stark CE, Yassa MA, Bassett SS, Shelton AL, Gallagher M (2012) Reduction of hippocampal hyperactivity improves cognition in amnestic mild cognitive impairment. Neuron 74:467-474.

Barco A, Alarcon JM, Kandel ER (2002) Expression of constitutively active CREB protein facilitates the late phase of long-term potentiation by enhancing synaptic capture. Cell 108:689-703.

Barco A, Patterson SL, Alarcon JM, Gromova P, Mata-Roig M, Morozov A, Kandel ER (2005) Gene expression profiling of facilitated L-LTP in VP16-CREB mice reveals that BDNF is critical for the maintenance of LTP and its synaptic capture. Neuron 48:123-137.

Barrow PA, Empson RM, Gladwell SJ, Anderson CM, Killick R, Yu X, Jefferys JG, Duff K (2000) Functional phenotype in transgenic mice expressing mutant human presenilin-1. Neurobiol Dis 7:119-126.

Bashir ZI, Bortolotto ZA, Davies CH, Berretta N, Irving AJ, Seal AJ, Henley JM, Jane DE, Watkins JC, Collingridge GL (1993) Induction of LTP in the hippocampus needs synaptic activation of glutamate metabotropic receptors. Nature 363:347-350.

Bero AW, Yan P, Roh JH, Cirrito JR, Stewart FR, Raichle ME, Lee JM, Holtzman DM (2011) Neuronal activity regulates the regional vulnerability to amyloid-beta deposition. Nat Neurosci 14:750-756.

Berridge MJ (1998) Neuronal calcium signaling. Neuron 21:13-26.

Berridge MJ (2010) Calcium hypothesis of Alzheimer's disease. Pflugers Arch 459:441-449.

Berridge MJ, Lipp P, Bootman MD (2000) The versatility and universality of calcium signalling. Nat Rev Mol Cell Biol 1:11-21.

Bettens K, Sleegers K, Van Broeckhoven C (2010) Current status on Alzheimer disease molecular genetics: from past, to present, to future. Hum Mol Genet 19:R4-R11.

Bezprozvanny I, Mattson MP (2008) Neuronal calcium mishandling and the pathogenesis of Alzheimer's disease. Trends Neurosci 31:454-463.

Bordji K, Becerril-Ortega J, Nicole O, Buisson A (2010) Activation of extrasynaptic, but not synaptic, NMDA receptors modifies amyloid precursor protein expression pattern and increases amyloid-ss production. J Neurosci 30:15927-15942.

Boyle JP, Hettiarachchi NT, Wilkinson JA, Pearson HA, Scragg JL, Lendon C, Al-Owais MM, Kim CB, Myers DM, Warburton P, Peers C (2012) Cellular consequences of the expression of Alzheimer's disease-causing presenilin 1 mutations in human neuroblastoma (SH-SY5Y) cells. Brain Res 1443:75-88.

Brunello L, Zampese E, Florean C, Pozzan T, Pizzo P, Fasolato C (2009) Presenilin-2 dampens intracellular Ca2+ stores by increasing Ca2+ leakage and reducing Ca2+ uptake. J Cell Mol Med 13:3358-3369.

Bruno AM, Huang JY, Bennett DA, Marr RA, Hastings ML, Stutzmann GE (2012) Altered ryanodine receptor expression in mild cognitive impairment and Alzheimer's disease. Neurobiol Aging 33:1001 e1001-1006.

Buxbaum JD, Ruefli AA, Parker CA, Cypess AM, Greengard P (1994) Calcium regulates processing of the Alzheimer amyloid protein precursor in a protein kinase C-independent manner. Proc Natl Acad Sci U S A 91:4489-4493.

Campion D, Dumanchin C, Hannequin D, Dubois B, Belliard S, Puel M, Thomas-Anterion C, Michon A, Martin C, Charbonnier F, Raux G, Camuzat A, Penet C, Mesnage V, Martinez M, Clerget-Darpoux F, Brice A, Frebourg T (1999) Early-onset autosomal dominant Alzheimer disease: prevalence, genetic heterogeneity, and mutation spectrum. Am J Hum Genet 65:664-670.

Cao X, Sudhof TC (2004) Dissection of amyloid-beta precursor protein-dependent transcriptional transactivation. J Biol Chem 279:24601-24611.

Cardenas C, Miller RA, Smith I, Bui T, Molgo J, Muller M, Vais H, Cheung KH, Yang J, Parker I, Thompson CB, Birnbaum MJ, Hallows KR, Foskett JK (2010) Essential regulation of cell bioenergetics by constitutive InsP3 receptor Ca2+ transfer to mitochondria. Cell 142:270-283.

Chakroborty S, Goussakov I, Miller MB, Stutzmann GE (2009) Deviant ryanodine receptor-mediated calcium release resets synaptic homeostasis in presymptomatic 3xTg-AD mice. J Neurosci 29:9458-9470.

Chan SL, Mayne M, Holden CP, Geiger JD, Mattson MP (2000) Presenilin-1 mutations increase levels of ryanodine receptors and calcium release in PC12 cells and cortical neurons. J Biol Chem 275:18195-18200.

Chavez-Gutierrez L, Bammens L, Benilova I, Vandersteen A, Benurwar M, Borgers M, Lismont S, Zhou L, Van Cleynenbreugel S, Esselmann H, Wiltfang J, Serneels L, Karran E, Gijsen H, Schymkowitz J, Rousseau F, Broersen K, De Strooper B (2012) The mechanism of gamma-Secretase dysfunction in familial Alzheimer disease. Embo J 31:2261-2274.

Chen X, Huang T, Zhang J, Song J, Chen L, Zhu Y (2008) Involvement of calpain and p25 of CDK5 pathway in ginsenoside Rb1's attenuation of beta-amyloid peptide25-35-induced tau hyperphosphorylation in cortical neurons. Brain Res 1200:99-106.

Cheung KH, Mei L, Mak DO, Hayashi I, Iwatsubo T, Kang DE, Foskett JK (2010) Gain-of-function enhancement of IP3 receptor modal gating by familial Alzheimer's disease-linked presenilin mutants in human cells and mouse neurons. Sci Signal 3:ra22.

Cheung KH, Shineman D, Muller M, Cardenas C, Mei L, Yang J, Tomita T, Iwatsubo T, Lee VM, Foskett JK (2008) Mechanism of Ca2+ disruption in Alzheimer's disease by presenilin regulation of InsP3 receptor channel gating. Neuron 58:871-883.

Cho HJ, Jin SM, Youn HD, Huh K, Mook-Jung I (2008) Disrupted intracellular calcium regulates BACE1 gene expression via nuclear factor of activated T cells 1 (NFAT 1) signaling. Aging Cell 7:137-147.

Chourbaji S, Hellweg R, Brandis D, Zorner B, Zacher C, Lang UE, Henn FA, Hortnagl H, Gass P (2004) Mice with reduced brain-derived neurotrophic factor expression show decreased choline acetyltransferase activity, but regular brain monoamine levels and unaltered emotional behavior. Brain Res Mol Brain Res 121:28-36.

Cirrito JR, Yamada KA, Finn MB, Sloviter RS, Bales KR, May PC, Schoepp DD, Paul SM, Mennerick S, Holtzman DM (2005) Synaptic activity regulates interstitial fluid amyloid-beta levels in vivo. Neuron 48:913-922.

Clinton LK, Billings LM, Green KN, Caccamo A, Ngo J, Oddo S, McGaugh JL, LaFerla FM (2007) Age-dependent sexual dimorphism in cognition and stress response in the 3xTg-AD mice. Neurobiol Dis 28:76-82.

Dahms SO, Hoefgen S, Roeser D, Schlott B, Guhrs KH, Than ME (2010) Structure and biochemical analysis of the heparin-induced E1 dimer of the amyloid precursor protein. Proc Natl Acad Sci U S A 107:5381-5386.

Dal Forno G, Carson KA, Brookmeyer R, Troncoso J, Kawas CH, Brandt J (2002) APOE genotype and survival in men and women with Alzheimer's disease. Neurology 58:1045-1050.

De Strooper B, Saftig P, Craessaerts K, Vanderstichele H, Guhde G, Annaert W, Von Figura K, Van Leuven F (1998) Deficiency of presenilin-1 inhibits the normal cleavage of amyloid precursor protein. Nature 391:387-390.

Dickerson BC, Salat DH, Greve DN, Chua EF, Rand-Giovannetti E, Rentz DM, Bertram L, Mullin K, Tanzi RE, Blacker D, Albert MS, Sperling RA (2005) Increased hippocampal activation in mild cognitive impairment compared to normal aging and AD. Neurology 65:404-411.

Dries DR, Yu G (2008) Assembly, maturation, and trafficking of the gamma-secretase complex in Alzheimer's disease. Curr Alzheimer Res 5:132-146.

Drzezga A, Grimmer T, Henriksen G, Muhlau M, Perneczky R, Miederer I, Praus C, Sorg C, Wohlschlager A, Riemenschneider M, Wester HJ, Foerstl H, Schwaiger M, Kurz A (2009) Effect of APOE genotype on amyloid plaque load and gray matter volume in Alzheimer disease. Neurology 72:1487-1494.

Eckman CB, Mehta ND, Crook R, Perez-tur J, Prihar G, Pfeiffer E, Graff-Radford N, Hinder P, Yager D, Zenk B, Refolo LM, Prada CM, Younkin SG, Hutton M, Hardy J (1997) A new pathogenic mutation in the APP gene (I716V) increases the relative proportion of A beta 42(43). Hum Mol Genet 6:2087-2089.

Ertekin-Taner N (2010) Genetics of Alzheimer disease in the pre- and post-GWAS era. Alzheimers Res Ther 2:3.

Etcheberrigaray R, Hirashima N, Nee L, Prince J, Govoni S, Racchi M, Tanzi RE, Alkon DL (1998) Calcium responses in fibroblasts from asymptomatic members of Alzheimer's disease families. Neurobiol Dis 5:37-45.

Fasolato C, Zottini M, Clementi E, Zacchetti D, Meldolesi J, Pozzan T (1991) Intracellular Ca2+ pools in PC12 cells. Three intracellular pools are distinguished by their turnover and mechanisms of Ca2+ accumulation, storage, and release. J Biol Chem 266:20159-20167.

Fassler M, Zocher M, Klare S, de la Fuente AG, Scheuermann J, Capell A, Haass C, Valkova C, Veerappan A, Schneider D, Kaether C (2010) Masking of transmembrane-based retention signals controls ER export of gamma-secretase. Traffic 11:250-258.

Feng R, Wang H, Wang J, Shrom D, Zeng X, Tsien JZ (2004) Forebrain degeneration and ventricle enlargement caused by double knockout of Alzheimer's presenilin-1 and presenilin-2. Proc Natl Acad Sci U S A 101:8162-8167.

Finckh U, Alberici A, Antoniazzi M, Benussi L, Fedi V, Giannini C, Gal A, Nitsch RM, Binetti G (2000) Variable expression of familial Alzheimer disease associated with presenilin 2 mutation M239I. Neurology 54:2006-2008.

Forlenza OV, Diniz BS, Radanovic M, Santos FS, Talib LL, Gattaz WF (2011) Disease-modifying properties of long-term lithium treatment for amnestic mild cognitive impairment: randomised controlled trial. Br J Psychiatry 198:351-356.

Fujii S, Matsumoto M, Igarashi K, Kato H, Mikoshiba K (2000) Synaptic plasticity in hippocampal CA1 neurons of mice lacking type 1 inositol-1,4,5-trisphosphate receptors. Learn Mem 7:312-320.

Fukumoto H, Cheung BS, Hyman BT, Irizarry MC (2002) Beta-secretase protein and activity are increased in the neocortex in Alzheimer disease. Arch Neurol 59:1381-1389.

Fukushima H, Maeda R, Suzuki R, Suzuki A, Nomoto M, Toyoda H, Wu LJ, Xu H, Zhao MG, Ueda K, Kitamoto A, Mamiya N, Yoshida T, Homma S, Masushige S, Zhuo M, Kida S (2008) Upregulation of calcium/calmodulin-dependent protein kinase

IV improves memory formation and rescues memory loss with aging. J Neurosci 28:9910-9919.

Furuichi T, Simon-Chazottes D, Fujino I, Yamada N, Hasegawa M, Miyawaki A, Yoshikawa S, Guenet JL, Mikoshiba K (1993) Widespread expression of inositol 1,4,5-trisphosphate receptor type 1 gene (Insp3r1) in the mouse central nervous system. Receptors Channels 1:11-24.

Furukawa K, Barger SW, Blalock EM, Mattson MP (1996a) Activation of K+ channels and suppression of neuronal activity by secreted beta-amyloid-precursor protein. Nature 379:74-78.

Furukawa K, Sopher BL, Rydel RE, Begley JG, Pham DG, Martin GM, Fox M, Mattson MP (1996b) Increased activity-regulating and neuroprotective efficacy of alpha-secretase-derived secreted amyloid precursor protein conferred by a C-terminal heparin-binding domain. J Neurochem 67:1882-1896.

Futatsugi A, Kato K, Ogura H, Li ST, Nagata E, Kuwajima G, Tanaka K, Itohara S, Mikoshiba K (1999) Facilitation of NMDAR-independent LTP and spatial learning in mutant mice lacking ryanodine receptor type 3. Neuron 24:701-713.

Gakhar-Koppole N, Hundeshagen P, Mandl C, Weyer SW, Allinquant B, Muller U, Ciccolini F (2008) Activity requires soluble amyloid precursor protein alpha to promote neurite outgrowth in neural stem cell-derived neurons via activation of the MAPK pathway. Eur J Neurosci 28:871-882.

Galvan V, Gorostiza OF, Banwait S, Ataie M, Logvinova AV, Sitaraman S, Carlson E, Sagi SA, Chevallier N, Jin K, Greenberg DA, Bredesen DE (2006) Reversal of Alzheimer's-like pathology and behavior in human APP transgenic mice by mutation of Asp664. Proc Natl Acad Sci U S A 103:7130-7135.

Gandy S, Doeven MK, Poolman B (2006) Alzheimer disease: presenilin springs a leak. Nat Med 12:1121-1123.

Garcia-Arencibia M, Hochfeld WE, Toh PP, Rubinsztein DC (2010) Autophagy, a guardian against neurodegeneration. Semin Cell Dev Biol 21:691-698.

Geroldi C, Laakso MP, DeCarli C, Beltramello A, Bianchetti A, Soininen H, Trabucchi M, Frisoni GB (2000) Apolipoprotein E genotype and hippocampal asymmetry in Alzheimer's disease: a volumetric MRI study. J Neurol Neurosurg Psychiatry 68:93-96.

Giacomello M, Barbiero L, Zatti G, Squitti R, Binetti G, Pozzan T, Fasolato C, Ghidoni R, Pizzo P (2005) Reduction of Ca2+ stores and capacitative Ca2+ entry is associated with the familial Alzheimer's disease presenilin-2 T122R mutation and anticipates the onset of dementia. Neurobiol Dis 18:638-648.

Goate A, Chartier-Harlin MC, Mullan M, Brown J, Crawford F, Fidani L, Giuffra L, Haynes A, Irving N, James L, et al. (1991) Segregation of a missense mutation in the amyloid precursor protein gene with familial Alzheimer's disease. Nature 349:704-706.

Goldstein FC, Ashley AV, Gearing M, Hanfelt J, Penix L, Freedman LJ, Levey AI (2001) Apolipoprotein E and age at onset of Alzheimer's disease in African American patients. Neurology 57:1923-1925.

Gonzalez GA, Montminy MR (1989) Cyclic AMP stimulates somatostatin gene transcription by phosphorylation of CREB at serine 133. Cell 59:675-680.

Goussakov I, Chakroborty S, Stutzmann GE (2010a) Generation of dendritic Ca2+ oscillations as a consequence of altered ryanodine receptor function in AD neurons. Channels (Austin) 5:9-13.

Goussakov I, Miller MB, Stutzmann GE (2010b) NMDA-mediated Ca(2+) influx drives aberrant ryanodine receptor activation in dendrites of young Alzheimer's disease mice. J Neurosci 30:12128-12137.

Green KN, Demuro A, Akbari Y, Hitt BD, Smith IF, Parker I, LaFerla FM (2008) SERCA pump activity is physiologically regulated by presenilin and regulates amyloid beta production. J Cell Biol 181:1107-1116.

Grimes CA, Jope RS (2001) The multifaceted roles of glycogen synthase kinase 3beta in cellular signaling. Prog Neurobiol 65:391-426.

Grynkiewicz G, Poenie M, Tsien RY (1985) A new generation of Ca2+ indicators with greatly improved fluorescence properties. J Biol Chem 260:3440-3450.

Guo Q, Fu W, Sopher BL, Miller MW, Ware CB, Martin GM, Mattson MP (1999) Increased vulnerability of hippocampal neurons to excitotoxic necrosis in presenilin-1 mutant knock-in mice. Nat Med 5:101-106.

Guo Q, Furukawa K, Sopher BL, Pham DG, Xie J, Robinson N, Martin GM, Mattson MP (1996) Alzheimer's PS-1 mutation perturbs calcium homeostasis and sensitizes PC12 cells to death induced by amyloid beta-peptide. Neuroreport 8:379-383.

Hanger DP, Seereeram A, Noble W (2009) Mediators of tau phosphorylation in the pathogenesis of Alzheimer's disease. Expert Rev Neurother 9:1647-1666.

Hanger DP, Byers HL, Wray S, Leung KY, Saxton MJ, Seereeram A, Reynolds CH, Ward MA, Anderton BH (2007) Novel phosphorylation sites in tau from Alzheimer brain support a role for casein kinase 1 in disease pathogenesis. J Biol Chem 282:23645-23654.

Hardingham GE, Bading H (1999) Calcium as a versatile second messenger in the control of gene expression. Microsc Res Tech 46:348-355.

Hardy J, Selkoe DJ (2002) The amyloid hypothesis of Alzheimer's disease: progress and problems on the road to therapeutics. Science 297:353-356.

Harold D, Abraham R, Hollingworth P, Sims R, Gerrish A, Hamshere ML, Pahwa JS, Moskvina V, Dowzell K, Williams A, Jones N, Thomas C, Stretton A, Morgan AR, Lovestone S, Powell J, Proitsi P, Lupton MK, Brayne C, Rubinsztein DC, Gill M, Lawlor B, Lynch A, Morgan K, Brown KS, Passmore PA, Craig D, McGuinness B, Todd S, Holmes C, Mann D, Smith AD, Love S, Kehoe PG, Hardy J, Mead S, Fox N, Rossor M, Collinge J, Maier W, Jessen F, Schurmann B, van den Bussche H, Heuser I, Kornhuber J, Wiltfang J, Dichgans M, Frolich L, Hampel H, Hull M, Rujescu D, Goate AM, Kauwe JS, Cruchaga C, Nowotny P, Morris JC, Mayo K, Sleegers K, Bettens K, Engelborghs S, De Deyn PP, Van Broeckhoven C, Livingston G, Bass NJ, Gurling H, McQuillin A, Gwilliam R, Deloukas P, Al-Chalabi A, Shaw CE, Tsolaki M, Singleton AB, Guerreiro R, Muhleisen TW, Nothen MM, Moebus S, Jockel KH, Klopp N, Wichmann HE, Carrasquillo MM, Pankratz VS, Younkin SG, Holmans PA, O'Donovan M, Owen MJ, Williams J (2009) Genome-wide association study identifies variants at CLU and PICALM associated with Alzheimer's disease. Nat Genet 41:1088-1093.

Hartigan JA, Johnson GV (1999) Transient increases in intracellular calcium result in prolonged site-selective increases in Tau phosphorylation through a glycogen synthase kinase 3beta-dependent pathway. J Biol Chem 274:21395-21401.

Hayrapetyan V, Rybalchenko V, Rybalchenko N, Koulen P (2008) The N-terminus of presenilin-2 increases single channel activity of brain ryanodine receptors through direct protein-protein interaction. Cell Calcium 44:507-518.

Heber S, Herms J, Gajic V, Hainfellner J, Aguzzi A, Rulicke T, von Kretzschmar H, von Koch C, Sisodia S, Tremml P, Lipp HP, Wolfer DP, Muller U (2000) Mice with combined gene knock-outs reveal essential and partially redundant functions of amyloid precursor protein family members. J Neurosci 20:7951-7963.

Herreman A, Serneels L, Annaert W, Collen D, Schoonjans L, De Strooper B (2000) Total inactivation of gamma-secretase activity in presenilin-deficient embryonic stem cells. Nat Cell Biol 2:461-462.

Herreman A, Hartmann D, Annaert W, Saftig P, Craessaerts K, Serneels L, Umans L, Schrijvers V, Checler F, Vanderstichele H, Baekelandt V, Dressel R, Cupers P, Huylebroeck D, Zwijsen A, Van Leuven F, De Strooper B (1999) Presenilin 2 deficiency causes a mild pulmonary phenotype and no changes in amyloid precursor protein processing but enhances the embryonic lethal phenotype of presenilin 1 deficiency. Proc Natl Acad Sci U S A 96:11872-11877.

Hertle DN, Yeckel MF (2007) Distribution of inositol-1,4,5-trisphosphate receptor isotypes and ryanodine receptor isotypes during maturation of the rat hippocampus. Neuroscience 150:625-638.

Hirashima N, Etcheberrigaray R, Bergamaschi S, Racchi M, Battaini F, Binetti G, Govoni S, Alkon DL (1996) Calcium responses in human fibroblasts: a diagnostic molecular profile for Alzheimer's disease. Neurobiol Aging 17:549-555.

Ho N, Liauw JA, Blaeser F, Wei F, Hanissian S, Muglia LM, Wozniak DF, Nardi A, Arvin KL, Holtzman DM, Linden DJ, Zhuo M, Muglia LJ, Chatila TA (2000) Impaired synaptic plasticity and cAMP response element-binding protein activation in Ca2+/calmodulin-dependent protein kinase type IV/Gr-deficient mice. J Neurosci 20:6459-6472.

Hoey SE, Williams RJ, Perkinton MS (2009) Synaptic NMDA receptor activation stimulates alpha-secretase amyloid precursor protein processing and inhibits amyloid-beta production. J Neurosci 29:4442-4460.

Hollingworth P, Harold D, Sims R, Gerrish A, Lambert JC, Carrasquillo MM, Abraham R, Hamshere ML, Pahwa JS, Moskvina V, Dowzell K, Jones N, Stretton A, Thomas C, Richards A, Ivanov D, Widdowson C, Chapman J, Lovestone S, Powell J, Proitsi P, Lupton MK, Brayne C, Rubinsztein DC, Gill M, Lawlor B, Lynch A, Brown KS, Passmore PA, Craig D, McGuinness B, Todd S, Holmes C, Mann D, Smith AD, Beaumont H, Warden D, Wilcock G, Love S, Kehoe PG, Hooper NM, Vardy ER, Hardy J, Mead S, Fox NC, Rossor M, Collinge J, Maier W, Jessen F, Ruther E, Schurmann B, Heun R, Kolsch H, van den Bussche H, Heuser I, Kornhuber J, Wiltfang J, Dichgans M, Frolich L, Hampel H, Gallacher J, Hull M, Rujescu D, Giegling I, Goate AM, Kauwe JS, Cruchaga C, Nowotny P, Morris JC, Mayo K, Sleegers K, Bettens K, Engelborghs S, De Deyn PP, Van Broeckhoven C, Livingston G, Bass NJ, Gurling H, McQuillin A, Gwilliam R, Deloukas P, Al-Chalabi A, Shaw CE, Tsolaki M, Singleton AB, Guerreiro R,

Muhleisen TW, Nothen MM, Moebus S, Jockel KH, Klopp N, Wichmann HE, Pankratz VS, Sando SB, Aasly JO, Barcikowska M, Wszolek ZK, Dickson DW, Graff-Radford NR, Petersen RC, et al. (2011) Common variants at ABCA7, MS4A6A/MS4A4E, EPHA1, CD33 and CD2AP are associated with Alzheimer's disease. Nat Genet 43:429-435.

Honarnejad K, Jung CK, Lammich S, Arzberger T, Kretzschmar H, Herms J (2013) Involvement of presenilin holoprotein upregulation in calcium dyshomeostasis of Alzheimer's disease. J Cell Mol Med.

Hsiung GY, Sadovnick AD, Feldman H (2004) Apolipoprotein E epsilon4 genotype as a risk factor for cognitive decline and dementia: data from the Canadian Study of Health and Aging. Cmaj 171:863-867.

Huang XG, Yee BK, Nag S, Chan ST, Tang F (2003) Behavioral and neurochemical characterization of transgenic mice carrying the human presenilin-1 gene with or without the leucine-to-proline mutation at codon 235. Exp Neurol 183:673-681.

Hurtado DE, Molina-Porcel L, Carroll JC, Macdonald C, Aboagye AK, Trojanowski JQ, Lee VM (2012) Selectively silencing GSK-3 isoforms reduces plaques and tangles in mouse models of Alzheimer's disease. J Neurosci 32:7392-7402.

Hye A, Kerr F, Archer N, Foy C, Poppe M, Brown R, Hamilton G, Powell J, Anderton B, Lovestone S (2005) Glycogen synthase kinase-3 is increased in white cells early in Alzheimer's disease. Neurosci Lett 373:1-4.

Itkin A, Dupres V, Dufrene YF, Bechinger B, Ruysschaert JM, Raussens V (2011) Calcium ions promote formation of amyloid beta-peptide (1-40) oligomers causally implicated in neuronal toxicity of Alzheimer's disease. PLoS One 6:e18250.

Ito E, Oka K, Etcheberrigaray R, Nelson TJ, McPhie DL, Tofel-Grehl B, Gibson GE, Alkon DL (1994) Internal Ca2+ mobilization is altered in fibroblasts from patients with Alzheimer disease. Proc Natl Acad Sci U S A 91:534-538.

Jack CR, Jr., Knopman DS, Jagust WJ, Petersen RC, Weiner MW, Aisen PS, Shaw LM, Vemuri P, Wiste HJ, Weigand SD, Lesnick TG, Pankratz VS, Donohue MC, Trojanowski JQ (2013) Tracking pathophysiological processes in Alzheimer's disease: an updated hypothetical model of dynamic biomarkers. Lancet Neurol 12:207-216.

Janssen JC, Beck JA, Campbell TA, Dickinson A, Fox NC, Harvey RJ, Houlden H, Rossor MN, Collinge J (2003) Early onset familial Alzheimer's disease: Mutation frequency in 31 families. Neurology 60:235-239.

Jin H, Sanjo N, Uchihara T, Watabe K, St George-Hyslop P, Fraser PE, Mizusawa H (2010) Presenilin-1 holoprotein is an interacting partner of sarco endoplasmic reticulum calcium-ATPase and confers resistance to endoplasmic reticulum stress. J Alzheimers Dis 20:261-273.

Kamal A, Stokin GB, Yang Z, Xia CH, Goldstein LS (2000) Axonal transport of amyloid precursor protein is mediated by direct binding to the kinesin light chain subunit of kinesin-I. Neuron 28:449-459.

Kamenetz F, Tomita T, Hsieh H, Seabrook G, Borchelt D, Iwatsubo T, Sisodia S, Malinow R (2003) APP processing and synaptic function. Neuron 37:925-937.

Kang DE, Soriano S, Xia X, Eberhart CG, De Strooper B, Zheng H, Koo EH (2002) Presenilin couples the paired phosphorylation of beta-catenin independent of axin: implications for beta-catenin activation in tumorigenesis. Cell 110:751-762.

Kang DE, Yoon IS, Repetto E, Busse T, Yermian N, Ie L, Koo EH (2005) Presenilins mediate phosphatidylinositol 3-kinase/AKT and ERK activation via select signaling receptors. Selectivity of PS2 in platelet-derived growth factor signaling. J Biol Chem 280:31537-31547.

Kang H, Sun LD, Atkins CM, Soderling TR, Wilson MA, Tonegawa S (2001) An important role of neural activity-dependent CaMKIV signaling in the consolidation of long-term memory. Cell 106:771-783.

Kasri NN, Kocks SL, Verbert L, Hebert SS, Callewaert G, Parys JB, Missiaen L, De Smedt H (2006) Up-regulation of inositol 1,4,5-trisphosphate receptor type 1 is responsible for a decreased endoplasmic-reticulum Ca2+ content in presenilin double knock-out cells. Cell Calcium 40:41-51.

Khachaturian ZS (1994) Calcium hypothesis of Alzheimer's disease and brain aging. Ann N Y Acad Sci 747:1-11.

Kim HS, Kim EM, Lee JP, Park CH, Kim S, Seo JH, Chang KA, Yu E, Jeong SJ, Chong YH, Suh YH (2003) C-terminal fragments of amyloid precursor protein exert neurotoxicity by inducing glycogen synthase kinase-3beta expression. Faseb J 17:1951-1953.

Kuchibhotla KV, Lattarulo CR, Hyman BT, Bacskai BJ (2009) Synchronous hyperactivity and intercellular calcium waves in astrocytes in Alzheimer mice. Science 323:1211-1215.

LaFerla FM (2002) Calcium dyshomeostasis and intracellular signalling in Alzheimer's disease. Nat Rev Neurosci 3:862-872.

Lambert JC, Heath S, Even G, Campion D, Sleegers K, Hiltunen M, Combarros O, Zelenika D, Bullido MJ, Tavernier B, Letenneur L, Bettens K, Berr C, Pasquier F, Fievet N, Barberger-Gateau P, Engelborghs S, De Deyn P, Mateo I, Franck A, Helisalmi S, Porcellini E, Hanon O, de Pancorbo MM, Lendon C, Dufouil C, Jaillard C, Leveillard T, Alvarez V, Bosco P, Mancuso M, Panza F, Nacmias B, Bossu P, Piccardi P, Annoni G, Seripa D, Galimberti D, Hannequin D, Licastro F, Soininen H, Ritchie K, Blanche H, Dartigues JF, Tzourio C, Gut I, Van Broeckhoven C, Alperovitch A, Lathrop M, Amouyel P (2009) Genome-wide association study identifies variants at CLU and CR1 associated with Alzheimer's disease. Nat Genet 41:1094-1099.

Lanner JT, Georgiou DK, Joshi AD, Hamilton SL (2010) Ryanodine receptors: structure, expression, molecular details, and function in calcium release. Cold Spring Harb Perspect Biol 2:a003996.

Laudon H, Hansson EM, Melen K, Bergman A, Farmery MR, Winblad B, Lendahl U, von Heijne G, Naslund J (2005) A nine-transmembrane domain topology for presenilin 1. J Biol Chem 280:35352-35360.

Lee D, Lee KH, Ho WK, Lee SH (2007) Target cell-specific involvement of presynaptic mitochondria in post-tetanic potentiation at hippocampal mossy fiber synapses. J Neurosci 27:13603-13613.

Lee JS, Ho WK, Lee SH (2010) Post-tetanic increase in the fast-releasing synaptic vesicle pool at the expense of the slowly releasing pool. J Gen Physiol 136:259-272.

Lee MS, Kwon YT, Li M, Peng J, Friedlander RM, Tsai LH (2000) Neurotoxicity induces cleavage of p35 to p25 by calpain. Nature 405:360-364.

Lee SY, Hwang DY, Kim YK, Lee JW, Shin IC, Oh KW, Lee MK, Lim JS, Yoon DY, Hwang SJ, Hong JT (2006) PS2 mutation increases neuronal cell vulnerability to neurotoxicants through activation of caspase-3 by enhancing of ryanodine receptor-mediated calcium release. Faseb J 20:151-153.

Leissring MA, Parker I, LaFerla FM (1999a) Presenilin-2 mutations modulate amplitude and kinetics of inositol 1, 4,5-trisphosphate-mediated calcium signals. J Biol Chem 274:32535-32538.

Leissring MA, Paul BA, Parker I, Cotman CW, LaFerla FM (1999b) Alzheimer's presenilin-1 mutation potentiates inositol 1,4,5-trisphosphate-mediated calcium signaling in Xenopus oocytes. J Neurochem 72:1061-1068.

Leissring MA, Akbari Y, Fanger CM, Cahalan MD, Mattson MP, LaFerla FM (2000) Capacitative calcium entry deficits and elevated luminal calcium content in mutant presenilin-1 knockin mice. J Cell Biol 149:793-798.

Lesne S, Ali C, Gabriel C, Croci N, MacKenzie ET, Glabe CG, Plotkine M, Marchand-Verrecchia C, Vivien D, Buisson A (2005) NMDA receptor activation inhibits alpha-secretase and promotes neuronal amyloid-beta production. J Neurosci 25:9367-9377.

Levy-Lahad E, Wasco W, Poorkaj P, Romano DM, Oshima J, Pettingell WH, Yu CE, Jondro PD, Schmidt SD, Wang K, et al. (1995) Candidate gene for the chromosome 1 familial Alzheimer's disease locus. Science 269:973-977.

Li X, Dang S, Yan C, Gong X, Wang J, Shi Y (2012) Structure of a presenilin family intramembrane aspartate protease. Nature 493:56-61.

Liang B, Duan BY, Zhou XP, Gong JX, Luo ZG (2010) Calpain activation promotes BACE1 expression, amyloid precursor protein processing, and amyloid plaque formation in a transgenic mouse model of Alzheimer disease. J Biol Chem 285:27737-27744.

Lissandron V, Podini P, Pizzo P, Pozzan T (2010) Unique characteristics of Ca2+ homeostasis of the trans-Golgi compartment. Proc Natl Acad Sci U S A 107:9198-9203.

Liu C, Hermann TE (1978) Characterization of ionomycin as a calcium ionophore. J Biol Chem 253:5892-5894.

Lopez JR, Lyckman A, Oddo S, Laferla FM, Querfurth HW, Shtifman A (2008) Increased intraneuronal resting [Ca2+] in adult Alzheimer's disease mice. J Neurochem 105:262-271.

Lu DC, Soriano S, Bredesen DE, Koo EH (2003) Caspase cleavage of the amyloid precursor protein modulates amyloid beta-protein toxicity. J Neurochem 87:733-741.

Lu DC, Rabizadeh S, Chandra S, Shayya RF, Ellerby LM, Ye X, Salvesen GS, Koo EH, Bredesen DE (2000) A second cytotoxic proteolytic peptide derived from amyloid beta-protein precursor. Nat Med 6:397-404.

Lu Y, Christian K, Lu B (2008) BDNF: a key regulator for protein synthesis-dependent LTP and long-term memory? Neurobiol Learn Mem 89:312-323.

Lucas JJ, Hernandez F, Gomez-Ramos P, Moran MA, Hen R, Avila J (2001) Decreased nuclear beta-catenin, tau hyperphosphorylation and neurodegeneration in GSK-3beta conditional transgenic mice. Embo J 20:27-39.

Ma T, Zhao Y, Kwak YD, Yang Z, Thompson R, Luo Z, Xu H, Liao FF (2009) Statin's excitoprotection is mediated by sAPP and the subsequent attenuation of calpain-induced truncation events, likely via rho-ROCK signaling. J Neurosci 29:11226-11236.

Martinez-Coria H, Green KN, Billings LM, Kitazawa M, Albrecht M, Rammes G, Parsons CG, Gupta S, Banerjee P, LaFerla FM (2010) Memantine improves cognition and reduces Alzheimer's-like neuropathology in transgenic mice. Am J Pathol 176:870-880.

Martins CA, Oulhaj A, de Jager CA, Williams JH (2005) APOE alleles predict the rate of cognitive decline in Alzheimer disease: a nonlinear model. Neurology 65:1888-1893.

Marx J (2007) Alzheimer's disease. Fresh evidence points to an old suspect: calcium. Science 318:384-385.

Matsumoto M, Nakagawa T, Inoue T, Nagata E, Tanaka K, Takano H, Minowa O, Kuno J, Sakakibara S, Yamada M, Yoneshima H, Miyawaki A, Fukuuchi Y, Furuichi T, Okano H, Mikoshiba K, Noda T (1996) Ataxia and epileptic seizures in mice lacking type 1 inositol 1,4,5-trisphosphate receptor. Nature 379:168-171.

Matthews RP, Guthrie CR, Wailes LM, Zhao X, Means AR, McKnight GS (1994) Calcium/calmodulin-dependent protein kinase types II and IV differentially regulate CREB-dependent gene expression. Mol Cell Biol 14:6107-6116.

Mattson MP (1997) Cellular actions of beta-amyloid precursor protein and its soluble and fibrillogenic derivatives. Physiol Rev 77:1081-1132.

Mattson MP (2007) Calcium and neurodegeneration. Aging Cell 6:337-350.

Mattson MP (2010) ER calcium and Alzheimer's disease: in a state of flux. Sci Signal 3:pe10.

Mattson MP, Cheng B, Culwell AR, Esch FS, Lieberburg I, Rydel RE (1993) Evidence for excitoprotective and intraneuronal calcium-regulating roles for secreted forms of the beta-amyloid precursor protein. Neuron 10:243-254.

Mbebi C, See V, Mercken L, Pradier L, Muller U, Loeffler JP (2002) Amyloid precursor protein family-induced neuronal death is mediated by impairment of the neuroprotective calcium/calmodulin protein kinase IV-dependent signaling pathway. J Biol Chem 277:20979-20990.

McCombs JE, Gibson EA, Palmer AE (2010) Using a genetically targeted sensor to investigate the role of presenilin-1 in ER Ca2+ levels and dynamics. Mol Biosyst 6:1640-1649.

Medeiros R, Kitazawa M, Chabrier MA, Cheng D, Baglietto-Vargas D, Kling A, Moeller A, Green KN, LaFerla FM (2012) Calpain inhibitor A-705253 mitigates Alzheimer's disease-like pathology and cognitive decline in aged 3xTgAD mice. Am J Pathol 181:616-625.

Mellentin C, Jahnsen H, Abraham WC (2007) Priming of long-term potentiation mediated by ryanodine receptor activation in rat hippocampal slices. Neuropharmacology 52:118-125.
Meziane H, Dodart JC, Mathis C, Little S, Clemens J, Paul SM, Ungerer A (1998) Memory-enhancing effects of secreted forms of the beta-amyloid precursor protein in normal and amnestic mice. Proc Natl Acad Sci U S A 95:12683-12688.
Miller PJMaMW (2003) Culturing Hippocampal and Cortical Neurons. Methods in Cell Biology 71:111.
Molsa PK, Marttila RJ, Rinne UK (1986) Survival and cause of death in Alzheimer's disease and multi-infarct dementia. Acta Neurol Scand 74:103-107.
Morfini G, Pigino G, Beffert U, Busciglio J, Brady ST (2002) Fast axonal transport misregulation and Alzheimer's disease. Neuromolecular Med 2:89-99.
Mori E, Lee K, Yasuda M, Hashimoto M, Kazui H, Hirono N, Matsui M (2002) Accelerated hippocampal atrophy in Alzheimer's disease with apolipoprotein E epsilon4 allele. Ann Neurol 51:209-214.
Mori F, Fukaya M, Abe H, Wakabayashi K, Watanabe M (2000) Developmental changes in expression of the three ryanodine receptor mRNAs in the mouse brain. Neurosci Lett 285:57-60.
Morishima-Kawashima M, Hasegawa M, Takio K, Suzuki M, Yoshida H, Titani K, Ihara Y (1995a) Proline-directed and non-proline-directed phosphorylation of PHF-tau. J Biol Chem 270:823-829.
Morishima-Kawashima M, Hasegawa M, Takio K, Suzuki M, Yoshida H, Watanabe A, Titani K, Ihara Y (1995b) Hyperphosphorylation of tau in PHF. Neurobiol Aging 16:365-371; discussion 371-380.
Mu JS, Li WP, Yao ZB, Zhou XF (1999) Deprivation of endogenous brain-derived neurotrophic factor results in impairment of spatial learning and memory in adult rats. Brain Res 835:259-265.
Muller M, Cardenas C, Mei L, Cheung KH, Foskett JK (2011) Constitutive cAMP response element binding protein (CREB) activation by Alzheimer's disease presenilin-driven inositol trisphosphate receptor (InsP3R) Ca2+ signaling. Proc Natl Acad Sci U S A 108:13293-13298.
Myers RH, Schaefer EJ, Wilson PW, D'Agostino R, Ordovas JM, Espino A, Au R, White RF, Knoefel JE, Cobb JL, McNulty KA, Beiser A, Wolf PA (1996) Apolipoprotein E epsilon4 association with dementia in a population-based study: The Framingham study. Neurology 46:673-677.
Nelson O, Supnet C, Liu H, Bezprozvanny I (2010) Familial Alzheimer's disease mutations in presenilins: effects on endoplasmic reticulum calcium homeostasis and correlation with clinical phenotypes. J Alzheimers Dis 21:781-793.
Nelson O, Tu H, Lei T, Bentahir M, de Strooper B, Bezprozvanny I (2007) Familial Alzheimer disease-linked mutations specifically disrupt Ca2+ leak function of presenilin 1. J Clin Invest 117:1230-1239.
Nelson O, Supnet C, Tolia A, Horre K, De Strooper B, Bezprozvanny I (2011) Mutagenesis mapping of the presenilin 1 calcium leak conductance pore. J Biol Chem 286:22339-22347.
Nikolaev A, McLaughlin T, O'Leary DD, Tessier-Lavigne M (2009) APP binds DR6 to trigger axon pruning and neuron death via distinct caspases. Nature 457:981-989.

Nilsson E, Alafuzoff I, Blennow K, Blomgren K, Hall CM, Janson I, Karlsson I, Wallin A, Gottfries CG, Karlsson JO (1990) Calpain and calpastatin in normal and Alzheimer-degenerated human brain tissue. Neurobiol Aging 11:425-431.

Nishimoto I, Okamoto T, Matsuura Y, Takahashi S, Okamoto T, Murayama Y, Ogata E (1993) Alzheimer amyloid protein precursor complexes with brain GTP-binding protein G(o). Nature 362:75-79.

Nixon RA, Yang DS (2011) Autophagy failure in Alzheimer's disease--locating the primary defect. Neurobiol Dis 43:38-45.

Noble W, Olm V, Takata K, Casey E, Mary O, Meyerson J, Gaynor K, LaFrancois J, Wang L, Kondo T, Davies P, Burns M, Veeranna, Nixon R, Dickson D, Matsuoka Y, Ahlijanian M, Lau LF, Duff K (2003) Cdk5 is a key factor in tau aggregation and tangle formation in vivo. Neuron 38:555-565.

O'Brien JL, O'Keefe KM, LaViolette PS, DeLuca AN, Blacker D, Dickerson BC, Sperling RA (2010) Longitudinal fMRI in elderly reveals loss of hippocampal activation with clinical decline. Neurology 74:1969-1976.

Oddo S, Caccamo A, Shepherd JD, Murphy MP, Golde TE, Kayed R, Metherate R, Mattson MP, Akbari Y, LaFerla FM (2003) Triple-transgenic model of Alzheimer's disease with plaques and tangles: intracellular Abeta and synaptic dysfunction. Neuron 39:409-421.

Odero GL, Oikawa K, Glazner KA, Schapansky J, Grossman D, Thiessen JD, Motnenko A, Ge N, Martin M, Glazner GW, Albensi BC (2007) Evidence for the involvement of calbindin D28k in the presenilin 1 model of Alzheimer's disease. Neuroscience 169:532-543.

Ogura H, Matsumoto M, Mikoshiba K (2001) Motor discoordination in mutant mice heterozygous for the type 1 inositol 1,4,5-trisphosphate receptor. Behav Brain Res 122:215-219.

Okamoto T, Takeda S, Giambarella U, Murayama Y, Matsui T, Katada T, Matsuura Y, Nishimoto I (1996) Intrinsic signaling function of APP as a novel target of three V642 mutations linked to familial Alzheimer's disease. Embo J 15:3769-3777.

Olarte L, Schupf N, Lee JH, Tang MX, Santana V, Williamson J, Maramreddy P, Tycko B, Mayeux R (2006) Apolipoprotein E epsilon4 and age at onset of sporadic and familial Alzheimer disease in Caribbean Hispanics. Arch Neurol 63:1586-1590.

Oules B, Del Prete D, Greco B, Zhang X, Lauritzen I, Sevalle J, Moreno S, Paterlini-Brechot P, Trebak M, Checler F, Benfenati F, Chami M (2012) Ryanodine receptor blockade reduces amyloid-beta load and memory impairments in Tg2576 mouse model of Alzheimer disease. J Neurosci 32:11820-11834.

Palmer AE, Tsien RY (2006) Measuring calcium signaling using genetically targetable fluorescent indicators. Nat Protoc 1:1057-1065.

Palmer AE, Jin C, Reed JC, Tsien RY (2004) Bcl-2-mediated alterations in endoplasmic reticulum Ca2+ analyzed with an improved genetically encoded fluorescent sensor. Proc Natl Acad Sci U S A 101:17404-17409.

Pang PT, Lu B (2004) Regulation of late-phase LTP and long-term memory in normal and aging hippocampus: role of secreted proteins tPA and BDNF. Ageing Res Rev 3:407-430.

Pardossi-Piquard R, Petit A, Kawarai T, Sunyach C, Alves da Costa C, Vincent B, Ring S, D'Adamio L, Shen J, Muller U, St George Hyslop P, Checler F (2005)

Presenilin-dependent transcriptional control of the Abeta-degrading enzyme neprilysin by intracellular domains of betaAPP and APLP. Neuron 46:541-554.
Parent A, Linden DJ, Sisodia SS, Borchelt DR (1999) Synaptic transmission and hippocampal long-term potentiation in transgenic mice expressing FAD-linked presenilin 1. Neurobiol Dis 6:56-62.
Passer B, Pellegrini L, Russo C, Siegel RM, Lenardo MJ, Schettini G, Bachmann M, Tabaton M, D'Adamio L (2000) Generation of an apoptotic intracellular peptide by gamma-secretase cleavage of Alzheimer's amyloid beta protein precursor. J Alzheimers Dis 2:289-301.
Patrick GN, Zukerberg L, Nikolic M, de la Monte S, Dikkes P, Tsai LH (1999) Conversion of p35 to p25 deregulates Cdk5 activity and promotes neurodegeneration. Nature 402:615-622.
Pei JJ, Tanaka T, Tung YC, Braak E, Iqbal K, Grundke-Iqbal I (1997) Distribution, levels, and activity of glycogen synthase kinase-3 in the Alzheimer disease brain. J Neuropathol Exp Neurol 56:70-78.
Peng J, Liang G, Inan S, Wu Z, Joseph DJ, Meng Q, Peng Y, Eckenhoff MF, Wei H (2012) Dantrolene ameliorates cognitive decline and neuropathology in Alzheimer triple transgenic mice. Neurosci Lett 516:274-279.
Pierrot N, Ghisdal P, Caumont AS, Octave JN (2004) Intraneuronal amyloid-beta1-42 production triggered by sustained increase of cytosolic calcium concentration induces neuronal death. J Neurochem 88:1140-1150.
Pierrot N, Santos SF, Feyt C, Morel M, Brion JP, Octave JN (2006) Calcium-mediated transient phosphorylation of tau and amyloid precursor protein followed by intraneuronal amyloid-beta accumulation. J Biol Chem 281:39907-39914.
Pigino G, Morfini G, Pelsman A, Mattson MP, Brady ST, Busciglio J (2003) Alzheimer's presenilin 1 mutations impair kinesin-based axonal transport. J Neurosci 23:4499-4508.
Pratt KG, Zimmerman EC, Cook DG, Sullivan JM (2011) Presenilin 1 regulates homeostatic synaptic scaling through Akt signaling. Nat Neurosci 14:1112-1114.
Priller C, Bauer T, Mitteregger G, Krebs B, Kretzschmar HA, Herms J (2006) Synapse formation and function is modulated by the amyloid precursor protein. J Neurosci 26:7212-7221.
Prox J, Rittger A, Saftig P (2012) Physiological functions of the amyloid precursor protein secretases ADAM10, BACE1, and presenilin. Exp Brain Res 217:331-341.
Querfurth HW, Selkoe DJ (1994) Calcium ionophore increases amyloid beta peptide production by cultured cells. Biochemistry 33:4550-4561.
Querfurth HW, Jiang J, Geiger JD, Selkoe DJ (1997) Caffeine stimulates amyloid beta-peptide release from beta-amyloid precursor protein-transfected HEK293 cells. J Neurochem 69:1580-1591.
Quiroz YT, Budson AE, Celone K, Ruiz A, Newmark R, Castrillon G, Lopera F, Stern CE (2010) Hippocampal hyperactivation in presymptomatic familial Alzheimer's disease. Ann Neurol 68:865-875.
Raymond CR, Redman SJ (2006) Spatial segregation of neuronal calcium signals encodes different forms of LTP in rat hippocampus. J Physiol 570:97-111.

Reiman EM, Quiroz YT, Fleisher AS, Chen K, Velez-Pardo C, Jimenez-Del-Rio M, Fagan AM, Shah AR, Alvarez S, Arbelaez A, Giraldo M, Acosta-Baena N, Sperling RA, Dickerson B, Stern CE, Tirado V, Munoz C, Reiman RA, Huentelman MJ, Alexander GE, Langbaum JB, Kosik KS, Tariot PN, Lopera F (2012) Brain imaging and fluid biomarker analysis in young adults at genetic risk for autosomal dominant Alzheimer's disease in the presenilin 1 E280A kindred: a case-control study. Lancet Neurol 11:1048-1056.

Repetto E, Yoon IS, Zheng H, Kang DE (2007) Presenilin 1 regulates epidermal growth factor receptor turnover and signaling in the endosomal-lysosomal pathway. J Biol Chem 282:31504-31516.

Resende R, Ferreiro E, Pereira C, Oliveira CR (2008) ER stress is involved in Abeta-induced GSK-3beta activation and tau phosphorylation. J Neurosci Res 86:2091-2099.

Rickert RC, Rajewsky K, Roes J (1995) Impairment of T-cell-dependent B-cell responses and B-1 cell development in CD19-deficient mice. Nature 376:352-355.

Rovelet-Lecrux A, Hannequin D, Raux G, Le Meur N, Laquerriere A, Vital A, Dumanchin C, Feuillette S, Brice A, Vercelletto M, Dubas F, Frebourg T, Campion D (2006) APP locus duplication causes autosomal dominant early-onset Alzheimer disease with cerebral amyloid angiopathy. Nat Genet 38:24-26.

Rybalchenko V, Hwang SY, Rybalchenko N, Koulen P (2008) The cytosolic N-terminus of presenilin-1 potentiates mouse ryanodine receptor single channel activity. Int J Biochem Cell Biol 40:84-97.

Sahlin C, Lord A, Magnusson K, Englund H, Almeida CG, Greengard P, Nyberg F, Gouras GK, Lannfelt L, Nilsson LN (2007) The Arctic Alzheimer mutation favors intracellular amyloid-beta production by making amyloid precursor protein less available to alpha-secretase. J Neurochem 101:854-862.

Saito K, Elce JS, Hamos JE, Nixon RA (1993) Widespread activation of calcium-activated neutral proteinase (calpain) in the brain in Alzheimer disease: a potential molecular basis for neuronal degeneration. Proc Natl Acad Sci U S A 90:2628-2632.

Sanchez PE, Zhu L, Verret L, Vossel KA, Orr AG, Cirrito JR, Devidze N, Ho K, Yu GQ, Palop JJ, Mucke L (2012) Levetiracetam suppresses neuronal network dysfunction and reverses synaptic and cognitive deficits in an Alzheimer's disease model. Proc Natl Acad Sci U S A 109:E2895-2903.

Sastre M, Steiner H, Fuchs K, Capell A, Multhaup G, Condron MM, Teplow DB, Haass C (2001) Presenilin-dependent gamma-secretase processing of beta-amyloid precursor protein at a site corresponding to the S3 cleavage of Notch. EMBO Rep 2:835-841.

Saura CA, Choi SY, Beglopoulos V, Malkani S, Zhang D, Shankaranarayana Rao BS, Chattarji S, Kelleher RJ, 3rd, Kandel ER, Duff K, Kirkwood A, Shen J (2004) Loss of presenilin function causes impairments of memory and synaptic plasticity followed by age-dependent neurodegeneration. Neuron 42:23-36.

Sayas CL, Ariaens A, Ponsioen B, Moolenaar WH (2006) GSK-3 is activated by the tyrosine kinase Pyk2 during LPA1-mediated neurite retraction. Mol Biol Cell 17:1834-1844.

Schneider I, Reverse D, Dewachter I, Ris L, Caluwaerts N, Kuiperi C, Gilis M, Geerts H, Kretzschmar H, Godaux E, Moechars D, Van Leuven F, Herms J (2001) Mutant presenilins disturb neuronal calcium homeostasis in the brain of transgenic mice, decreasing the threshold for excitotoxicity and facilitating long-term potentiation. J Biol Chem 276:11539-11544.

Selbert MA, Anderson KA, Huang QH, Goldstein EG, Means AR, Edelman AM (1995) Phosphorylation and activation of Ca(2+)-calmodulin-dependent protein kinase IV by Ca(2+)-calmodulin-dependent protein kinase Ia kinase. Phosphorylation of threonine 196 is essential for activation. J Biol Chem 270:17616-17621.

Seshadri S, Fitzpatrick AL, Ikram MA, DeStefano AL, Gudnason V, Boada M, Bis JC, Smith AV, Carassquillo MM, Lambert JC, Harold D, Schrijvers EM, Ramirez-Lorca R, Debette S, Longstreth WT, Jr., Janssens AC, Pankratz VS, Dartigues JF, Hollingworth P, Aspelund T, Hernandez I, Beiser A, Kuller LH, Koudstaal PJ, Dickson DW, Tzourio C, Abraham R, Antunez C, Du Y, Rotter JI, Aulchenko YS, Harris TB, Petersen RC, Berr C, Owen MJ, Lopez-Arrieta J, Varadarajan BN, Becker JT, Rivadeneira F, Nalls MA, Graff-Radford NR, Campion D, Auerbach S, Rice K, Hofman A, Jonsson PV, Schmidt H, Lathrop M, Mosley TH, Au R, Psaty BM, Uitterlinden AG, Farrer LA, Lumley T, Ruiz A, Williams J, Amouyel P, Younkin SG, Wolf PA, Launer LJ, Lopez OL, van Duijn CM, Breteler MM (2010) Genome-wide analysis of genetic loci associated with Alzheimer disease. Jama 303:1832-1840.

Shankar GM, Li S, Mehta TH, Garcia-Munoz A, Shepardson NE, Smith I, Brett FM, Farrell MA, Rowan MJ, Lemere CA, Regan CM, Walsh DM, Sabatini BL, Selkoe DJ (2008) Amyloid-beta protein dimers isolated directly from Alzheimer's brains impair synaptic plasticity and memory. Nat Med 14:837-842.

Shen J, Bronson RT, Chen DF, Xia W, Selkoe DJ, Tonegawa S (1997) Skeletal and CNS defects in Presenilin-1-deficient mice. Cell 89:629-639.

Sherrington R, Froelich S, Sorbi S, Campion D, Chi H, Rogaeva EA, Levesque G, Rogaev EI, Lin C, Liang Y, Ikeda M, Mar L, Brice A, Agid Y, Percy ME, Clerget-Darpoux F, Piacentini S, Marcon G, Nacmias B, Amaducci L, Frebourg T, Lannfelt L, Rommens JM, St George-Hyslop PH (1996) Alzheimer's disease associated with mutations in presenilin 2 is rare and variably penetrant. Hum Mol Genet 5:985-988.

Sherrington R, Rogaev EI, Liang Y, Rogaeva EA, Levesque G, Ikeda M, Chi H, Lin C, Li G, Holman K, Tsuda T, Mar L, Foncin JF, Bruni AC, Montesi MP, Sorbi S, Rainero I, Pinessi L, Nee L, Chumakov I, Pollen D, Brookes A, Sanseau P, Polinsky RJ, Wasco W, Da Silva HA, Haines JL, Perkicak-Vance MA, Tanzi RE, Roses AD, Fraser PE, Rommens JM, St George-Hyslop PH (1995) Cloning of a gene bearing missense mutations in early-onset familial Alzheimer's disease. Nature 375:754-760.

Shilling D, Mak DO, Kang DE, Foskett JK (2012) Lack of evidence for presenilins as endoplasmic reticulum Ca2+ leak channels. J Biol Chem 287:10933-10944.

Sleegers K, Brouwers N, Gijselinck I, Theuns J, Goossens D, Wauters J, Del-Favero J, Cruts M, van Duijn CM, Van Broeckhoven C (2006) APP duplication is sufficient to cause early onset Alzheimer's dementia with cerebral amyloid angiopathy. Brain 129:2977-2983.

Slooter AJ, Cruts M, Hofman A, Koudstaal PJ, van der Kuip D, de Ridder MA, Witteman JC, Breteler MM, Van Broeckhoven C, van Duijn CM (2004) The impact of APOE on myocardial infarction, stroke, and dementia: the Rotterdam Study. Neurology 62:1196-1198.

Smith IF, Hitt B, Green KN, Oddo S, LaFerla FM (2005) Enhanced caffeine-induced Ca2+ release in the 3xTg-AD mouse model of Alzheimer's disease. J Neurochem 94:1711-1718.

Smith IF, Boyle JP, Vaughan PF, Pearson HA, Cowburn RF, Peers CS (2002) Ca(2+) stores and capacitative Ca(2+) entry in human neuroblastoma (SH-SY5Y) cells expressing a familial Alzheimer's disease presenilin-1 mutation. Brain Res 949:105-111.

Soba P, Eggert S, Wagner K, Zentgraf H, Siehl K, Kreger S, Lower A, Langer A, Merdes G, Paro R, Masters CL, Muller U, Kins S, Beyreuther K (2005) Homo- and heterodimerization of APP family members promotes intercellular adhesion. Embo J 24:3624-3634.

Spasic D, Tolia A, Dillen K, Baert V, De Strooper B, Vrijens S, Annaert W (2006) Presenilin-1 maintains a nine-transmembrane topology throughout the secretory pathway. J Biol Chem 281:26569-26577.

Steinert JR, Chernova T, Forsythe ID (2010) Nitric oxide signaling in brain function, dysfunction, and dementia. Neuroscientist 16:435-452.

Street VA, Bosma MM, Demas VP, Regan MR, Lin DD, Robinson LC, Agnew WS, Tempel BL (1997) The type 1 inositol 1,4,5-trisphosphate receptor gene is altered in the opisthotonos mouse. J Neurosci 17:635-645.

Stutzmann GE (2005) Calcium dysregulation, IP3 signaling, and Alzheimer's disease. Neuroscientist 11:110-115.

Stutzmann GE, Caccamo A, LaFerla FM, Parker I (2004) Dysregulated IP3 signaling in cortical neurons of knock-in mice expressing an Alzheimer's-linked mutation in presenilin1 results in exaggerated Ca2+ signals and altered membrane excitability. J Neurosci 24:508-513.

Stutzmann GE, Smith I, Caccamo A, Oddo S, Laferla FM, Parker I (2006) Enhanced ryanodine receptor recruitment contributes to Ca2+ disruptions in young, adult, and aged Alzheimer's disease mice. J Neurosci 26:5180-5189.

Stutzmann GE, Smith I, Caccamo A, Oddo S, Parker I, Laferla F (2007) Enhanced ryanodine-mediated calcium release in mutant PS1-expressing Alzheimer's mouse models. Ann N Y Acad Sci 1097:265-277.

Sun P, Enslen H, Myung PS, Maurer RA (1994) Differential activation of CREB by Ca2+/calmodulin-dependent protein kinases type II and type IV involves phosphorylation of a site that negatively regulates activity. Genes Dev 8:2527-2539.

Sun X, Beglopoulos V, Mattson MP, Shen J (2005) Hippocampal spatial memory impairments caused by the familial Alzheimer's disease-linked presenilin 1 M146V mutation. Neurodegener Dis 2:6-15.

Supnet C, Grant J, Kong H, Westaway D, Mayne M (2006) Amyloid-beta-(1-42) increases ryanodine receptor-3 expression and function in neurons of TgCRND8 mice. J Biol Chem 281:38440-38447.

Supnet C, Noonan C, Richard K, Bradley J, Mayne M (2010) Up-regulation of the type 3 ryanodine receptor is neuroprotective in the TgCRND8 mouse model of Alzheimer's disease. J Neurochem 112:356-365.

Takashima A, Noguchi K, Michel G, Mercken M, Hoshi M, Ishiguro K, Imahori K (1996) Exposure of rat hippocampal neurons to amyloid beta peptide (25-35) induces the inactivation of phosphatidyl inositol-3 kinase and the activation of tau protein kinase I/glycogen synthase kinase-3 beta. Neurosci Lett 203:33-36.

Takeda T, Asahi M, Yamaguchi O, Hikoso S, Nakayama H, Kusakari Y, Kawai M, Hongo K, Higuchi Y, Kashiwase K, Watanabe T, Taniike M, Nakai A, Nishida K, Kurihara S, Donoviel DB, Bernstein A, Tomita T, Iwatsubo T, Hori M, Otsu K (2005) Presenilin 2 regulates the systolic function of heart by modulating Ca2+ signaling. Faseb J 19:2069-2071.

Taru H, Kirino Y, Suzuki T (2002) Differential roles of JIP scaffold proteins in the modulation of amyloid precursor protein metabolism. J Biol Chem 277:27567-27574.

Taylor CJ, Ireland DR, Ballagh I, Bourne K, Marechal NM, Turner PR, Bilkey DK, Tate WP, Abraham WC (2008) Endogenous secreted amyloid precursor protein-alpha regulates hippocampal NMDA receptor function, long-term potentiation and spatial memory. Neurobiol Dis 31:250-260.

Tedde A, Nacmias B, Ciantelli M, Forleo P, Cellini E, Bagnoli S, Piccini C, Caffarra P, Ghidoni E, Paganini M, Bracco L, Sorbi S (2003) Identification of new presenilin gene mutations in early-onset familial Alzheimer disease. Arch Neurol 60:1541-1544.

Teo R, King J, Dalton E, Ryves J, Williams RS, Harwood AJ (2009) PtdIns(3,4,5)P(3) and inositol depletion as a cellular target of mood stabilizers. Biochem Soc Trans 37:1110-1114.

Thinakaran G, Sisodia SS (2006) Presenilins and Alzheimer disease: the calcium conspiracy. Nat Neurosci 9:1354-1355.

Thinakaran G, Borchelt DR, Lee MK, Slunt HH, Spitzer L, Kim G, Ratovitsky T, Davenport F, Nordstedt C, Seeger M, Hardy J, Levey AI, Gandy SE, Jenkins NA, Copeland NG, Price DL, Sisodia SS (1996) Endoproteolysis of presenilin 1 and accumulation of processed derivatives in vivo. Neuron 17:181-190.

Tiraboschi P, Hansen LA, Masliah E, Alford M, Thal LJ, Corey-Bloom J (2004) Impact of APOE genotype on neuropathologic and neurochemical markers of Alzheimer disease. Neurology 62:1977-1983.

Trinchese F, Fa M, Liu S, Zhang H, Hidalgo A, Schmidt SD, Yamaguchi H, Yoshii N, Mathews PM, Nixon RA, Arancio O (2008) Inhibition of calpains improves memory and synaptic transmission in a mouse model of Alzheimer disease. J Clin Invest 118:2796-2807.

Tseng BP, Green KN, Chan JL, Blurton-Jones M, LaFerla FM (2008) Abeta inhibits the proteasome and enhances amyloid and tau accumulation. Neurobiol Aging 29:1607-1618.

Tsubuki S, Takaki Y, Saido TC (2003) Dutch, Flemish, Italian, and Arctic mutations of APP and resistance of Abeta to physiologically relevant proteolytic degradation. Lancet 361:1957-1958.

Tu H, Nelson O, Bezprozvanny A, Wang Z, Lee SF, Hao YH, Serneels L, De Strooper B, Yu G, Bezprozvanny I (2006) Presenilins form ER Ca2+ leak channels, a function disrupted by familial Alzheimer's disease-linked mutations. Cell 126:981-993.

Turner BM (1998) Histone acetylation as an epigenetic determinant of long-term transcriptional competence. Cell Mol Life Sci 54:21-31.

Verges DK, Restivo JL, Goebel WD, Holtzman DM, Cirrito JR (2011) Opposing synaptic regulation of amyloid-beta metabolism by NMDA receptors in vivo. J Neurosci 31:11328-11337.

Walsh DM, Klyubin I, Fadeeva JV, Cullen WK, Anwyl R, Wolfe MS, Rowan MJ, Selkoe DJ (2002) Naturally secreted oligomers of amyloid beta protein potently inhibit hippocampal long-term potentiation in vivo. Nature 416:535-539.

Wang Z, Wang B, Yang L, Guo Q, Aithmitti N, Songyang Z, Zheng H (2009) Presynaptic and postsynaptic interaction of the amyloid precursor protein promotes peripheral and central synaptogenesis. J Neurosci 29:10788-10801.

Weihl CC, Ghadge GD, Kennedy SG, Hay N, Miller RJ, Roos RP (1999) Mutant presenilin-1 induces apoptosis and downregulates Akt/PKB. J Neurosci 19:5360-5369.

Wimmer ME, Hernandez PJ, Blackwell J, Abel T (2011) Aging impairs hippocampus-dependent long-term memory for object location in mice. Neurobiol Aging 33:2220-2224.

Winton MJ, Lee EB, Sun E, Wong MM, Leight S, Zhang B, Trojanowski JQ, Lee VM (2011) Intraneuronal APP, not free Abeta peptides in 3xTg-AD mice: implications for tau versus Abeta-mediated Alzheimer neurodegeneration. J Neurosci 31:7691-7699.

Wong PC, Zheng H, Chen H, Becher MW, Sirinathsinghji DJ, Trumbauer ME, Chen HY, Price DL, Van der Ploeg LH, Sisodia SS (1997) Presenilin 1 is required for Notch1 and DII1 expression in the paraxial mesoderm. Nature 387:288-292.

Woods NK, Padmanabhan J (2012) Neuronal calcium signaling and Alzheimer's disease. Adv Exp Med Biol 740:1193-1217.

Wu HY, Hudry E, Hashimoto T, Kuchibhotla K, Rozkalne A, Fan Z, Spires-Jones T, Xie H, Arbel-Ornath M, Grosskreutz CL, Bacskai BJ, Hyman BT (2010) Amyloid beta induces the morphological neurodegenerative triad of spine loss, dendritic simplification, and neuritic dystrophies through calcineurin activation. J Neurosci 30:2636-2649.

Xu Y, Kim HS, Joo Y, Choi Y, Chang KA, Park CH, Shin KY, Kim S, Cheon YH, Baik TK, Kim JH, Suh YH (2007) Intracellular domains of amyloid precursor-like protein 2 interact with CP2 transcription factor in the nucleus and induce glycogen synthase kinase-3beta expression. Cell Death Differ 14:79-91.

Yin JC, Tully T (1996) CREB and the formation of long-term memory. Curr Opin Neurobiol 6:264-268.

Yoo AS, Cheng I, Chung S, Grenfell TZ, Lee H, Pack-Chung E, Handler M, Shen J, Xia W, Tesco G, Saunders AJ, Ding K, Frosch MP, Tanzi RE, Kim TW (2000) Presenilin-mediated modulation of capacitative calcium entry. Neuron 27:561-572.

Young-Pearse TL, Bai J, Chang R, Zheng JB, LoTurco JJ, Selkoe DJ (2007) A critical function for beta-amyloid precursor protein in neuronal migration revealed by in utero RNA interference. J Neurosci 27:14459-14469.

Yu C, Kim SH, Ikeuchi T, Xu H, Gasparini L, Wang R, Sisodia SS (2001) Characterization of a presenilin-mediated amyloid precursor protein carboxyl-terminal fragment gamma. Evidence for distinct mechanisms involved in gamma -secretase processing of the APP and Notch1 transmembrane domains. J Biol Chem 276:43756-43760.

Zaman SH, Parent A, Laskey A, Lee MK, Borchelt DR, Sisodia SS, Malinow R (2000) Enhanced synaptic potentiation in transgenic mice expressing presenilin 1 familial Alzheimer's disease mutation is normalized with a benzodiazepine. Neurobiol Dis 7:54-63.

Zatti G, Ghidoni R, Barbiero L, Binetti G, Pozzan T, Fasolato C, Pizzo P (2004) The presenilin 2 M239I mutation associated with familial Alzheimer's disease reduces Ca2+ release from intracellular stores. Neurobiol Dis 15:269-278.

Zatti G, Burgo A, Giacomello M, Barbiero L, Ghidoni R, Sinigaglia G, Florean C, Bagnoli S, Binetti G, Sorbi S, Pizzo P, Fasolato C (2006) Presenilin mutations linked to familial Alzheimer's disease reduce endoplasmic reticulum and Golgi apparatus calcium levels. Cell Calcium 39:539-550.

Zhang C, Wu B, Beglopoulos V, Wines-Samuelson M, Zhang D, Dragatsis I, Sudhof TC, Shen J (2009) Presenilins are essential for regulating neurotransmitter release. Nature 460:632-636.

Zhang H, Sun S, Herreman A, De Strooper B, Bezprozvanny I (2010) Role of presenilins in neuronal calcium homeostasis. J Neurosci 30:8566-8580.

Zhang YW, Wang R, Liu Q, Zhang H, Liao FF, Xu H (2007) Presenilin/gamma-secretase-dependent processing of beta-amyloid precursor protein regulates EGF receptor expression. Proc Natl Acad Sci U S A 104:10613-10618.

Zheng H, Koo EH (2011) Biology and pathophysiology of the amyloid precursor protein. Mol Neurodegener 6:27.

Zheng H, Jiang M, Trumbauer ME, Hopkins R, Sirinathsinghji DJ, Stevens KA, Conner MW, Slunt HH, Sisodia SS, Chen HY, Van der Ploeg LH (1996) Mice deficient for the amyloid precursor protein gene. Ann N Y Acad Sci 777:421-426.